DYNAMIC CHARACTERISATION OF HUMAN NECK FOR IMPACT APPLICATIONS

ÇARPIŞMA UYGULAMALARI İÇİN İNSAN BOYNUNUN DİNAMİK ÖZELLİKLERİNİN BELİRLENMESİ

BURAK EMRE ÖZCAN

ASST. PROF. DR. SELÇUK HİMMETOĞLU

Supervisor

Submitted to

Graduate School of Science and Engineering of Hacettepe University

As a Partial Fulfillment to the Requirements for the Award of the Degree of Master of

Science in Mechanical Engineering.

2023

ABSTRACT

DYNAMIC CHARACTERISATION OF HUMAN NECK FOR IMPACT APPLICATIONS

Burak Emre ÖZCAN

The neck is the part of the spine and has highest risk of injury in traffic accidents. Neck trauma can occur in several types of collisions, but rear-end collisions have the highest risk of trauma. Human neck models are needed to quantify the risk of neck trauma and to develop protective systems for it. For human neck models to behave like real human beings, the passive mechanical properties of the neck as well as the active muscle contractions need to be accurately modelled. In this thesis, active muscle behaviour will be modelled just before, during and just after the collision. Thus, static equilibrium will be achieved in the neck model and reflex muscle contractions will be modelled accurately. Volunteer test data will be used to validate and dynamically characterize the neck model. Among these data, muscle electromyography signals are of foremost importance. The results obtained in this thesis can be used in future active crash-test-manikin designs.

Keywords: Neck Trauma, Neck Model, Active Muscle Behavior, Dynamic Characterisation, Multibody Model

ÖZET

ÇARPIŞMA UYGULAMALARI İÇİN İNSAN BOYNUNUN DİNAMİK ÖZELLİKLERİNİN BELİRLENMESİ

Burak Emre ÖZCAN

Yüksek Lisans, Makina Mühendisliği Bölümü
Tez Danışmanı: Dr. Selçuk HİMMETOĞLU
Ocak 2023, 98 sayfa

Trafik kazalarında omurga bölgesinin en çok yaralanma riski taşıyan kısmı boyundur. Boyun travması farklı çarpışma şekillerinde kendini gösterebilir ancak travma riskinin en yüksek olduğu çarpışmalar arkadan çarpmalardır. Boyun travma riskini ölçmek ve bunun için koruyucu sistemleri geliştirmek için insan boyun modellerine ihtiyaç vardır. İnsan boyun modellerinin gerçek insandaki gibi davranması için boynun pasif mekanik özellikleriyle birlikte aktif kas kasılmalarının da doğru bir şekilde modellenmesi gerekmektedir. Bu tezde çarpışmanın hemen öncesinde, çarpışma anında ve çarpışmanın hemen sonrasında aktif kas davranışları modellenecektir. Böylelikle boyun modelinde statik denge sağlanacak ve refleks kas kasılmaları doğru bir şekilde modellenecektir. Oluşturulan boyun modelini doğrulamak ve dinamik karakterizasyonunu yapmak için gönüllü test verileri kullanılacaktır. Bu veriler arasında olan kas elektromyografi sinyalleri büyük önem taşımaktadır. Bu tezde elde edilecek sonuçlar gelecekte görülmesi umulan aktif çarpışma-test-mankeni tasarımlarında kullanılabilecektir.

Anahtar Kelimeler: Boyun Travması, Boyun Modeli, Aktif Kas Davranışı, Dinamik Karakterizasyon, Çoklu Gövde Modeli

TABLE OF CONTENTS

LIST OF FIGURES

LIST OF TABLES

LIST OF SYMBOLS & ABBREVIATIONS

List of Symbols

T	Kinetic Energy
U	Potential Energy
L	Lagrangian Equation
q_i	Generalized Coordinates
m	Mass
g	Gravitational Acceleration
C_i	Center of Gravity of body i
C_8	Center of Gravity of T1
r_0	Length between O.C. and Co
C_0	Center of Gravity of Head
Ts_i	Static Torque Applied to Body i
Tr_i	Resistive Torque Applied to Body i
Ts_j	Static Torque Applied to Body j
Tr_j	Resistive Torque Applied to Body j
b_i	Height of Neck Segment
θ_{hT}	Head Rotation with respect to T1
θ_T	T1 Rotation with respect to Inertial Coordinate Frame
θ_h	Head Angle with respect to Inertial Coordinate Frame

List of Abbreviations

MRI	Magnetic Resonance Imaging
CT	Computed Tomography
ATD	Anthropomorphic Test Device
FE	Finite Element
2D	2 Dimensional
JARI	Japan Automobile Research Institute
U.K	United Kingdom
VS.	Versus

1. INTRODUCTION

1.1. Problem Definition

The main function of the spine in humans is to support the body and, in addition, to protect the spinal cord. For this reason, damage to the spine, regardless of its origin, is serious. Millions of traffic accidents occur every year in countries. The most common type of accident among these traffic accidents is spinal injuries [1]. 85% of these spinal injuries occur in rear-end accidents [2]. Spinal injuries also bring a heavy economic burden for countries in terms of financial terms. In the U.K., spinal injuries cost insurance companies more than £1 billion a year. In the United States, it is estimated that approximately 88 billion dollars is spent annually on spinal injuries, more than is spent on the treatment of most critical illnesses. [3]. The subject of this thesis is Dynamic Characterisation of Human Neck for Impact Applications, but it should not be limited to traffic accidents. In addition to traffic accidents, spinal injuries can also be caused by heavy workloads and non-ergonomic sitting positions of office workers. Considering all these details, the study of spinal injuries has become a critical issue.

The presence of soft tissues and nerves in the spine, head and neck region and the complex behavior of soft tissues and nerves make the detection of damage in these regions inadequate. The detection and examination of damage to the spine, head and neck [4] is usually performed using X-ray, MRI and CT scanning techniques, which, although modern, can be inadequate.
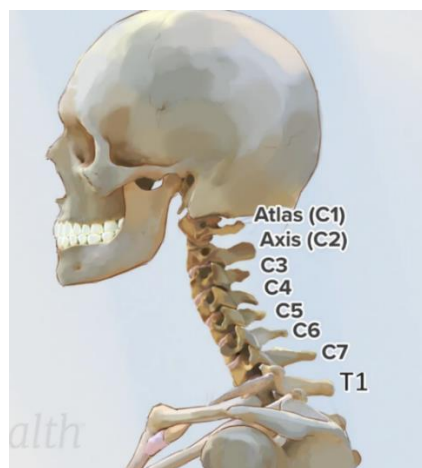
Figure 1.1 Head, neck and spines [4].

At this point, new tools are needed for the detection and examination of damage to the head, neck and spine.

When a vehicle crashes into another vehicle from rear-end, the head and neck of the person who will be affected by this crash, move backwards and forwards, creating a phenomenon that is called the S-Shape [5].
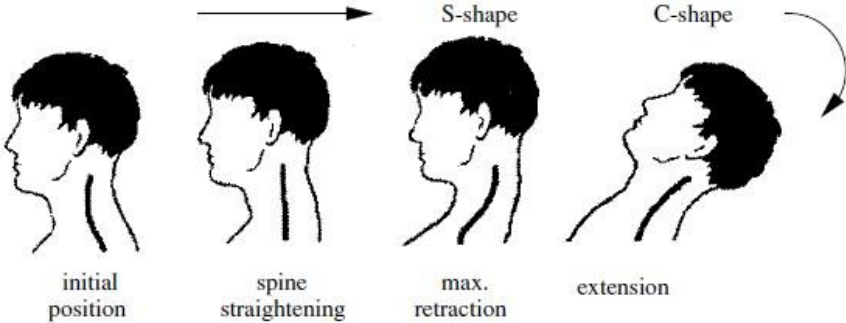
Figure 1.2 S-Shape during rear end impact [5].

It is believed that the spinal injuries mentioned above are caused by the whiplash effect caused by the S-Shape. Therefore, it is necessary to develop simulations and models that can simulate the human-like S-Shape and detect the damage it can cause. In this way, it is thought that the material damage caused by spinal injuries will be prevented and the treatment will be faster and more exact as the detection and examination processes are more sensitive. Simulations and models are usually head and neck models and crash test dummies. There are many studies on head and neck models in the literature, but one of the most well-known crash test dummies is BioRID-II [6].

Figure 1.3 BioRID-II Crash test dummy [6].

Crash test dummies are referred to in the literature as anthropomorphic test devices (ATD), which can be used not only for rear impact but also for frontal and side impact. Anthropomorphic test dummies have been developed to represent the human head, neck, and vertebrae in the most realistic way since the initial models did not perform well experimentally in whiplash. These improvements consisted of; adding muscles in the head, neck and spine system, or ensuring that the vertebrae or implemented muscles are made as close to reality as possible according to the data obtained from human experiments, cadaver experiments [7].
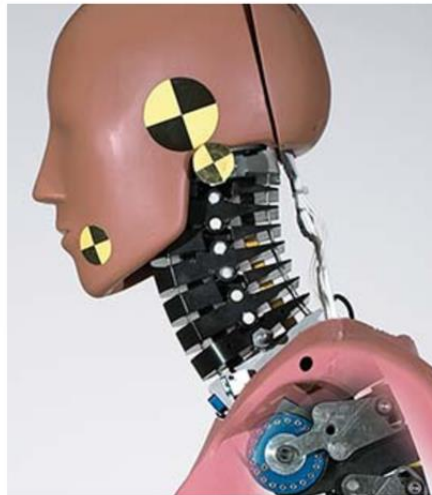
Figure 1.4 Head and neck of BioRID-II Crash test dummy which has a cable at rear as extensor muscle [7].

In addition to anthropomorphic testing devices, there are computer-based head and neck models [8] that can be used to study head and neck and spine injuries. A properly developed neck model can help to model the neck as a test device and to assess the damage that may occur in the event of a rear impact. Neck models can be developed by two methods: multibody dynamics and finite element (FE) methods. Multibody models have fewer parts than finite element models and the models developed with this technique reduce simulation times and provide advantages in long-term crash simulations including pre- and post-crash. In addition, the finite-element method [9] is more detailed in terms of model geometry, material properties and contact definitions; thus, local stresses and crushes can be measured, and injury mechanisms can be investigated, and stress analysis of vertebrae can be done in finite element models. Multi-body models can successfully and inexpensively simulate human motion, estimate component forces and moments,

perform parameter variation and optimization analyses quickly, and are a highly effective method for the development of control system designs.
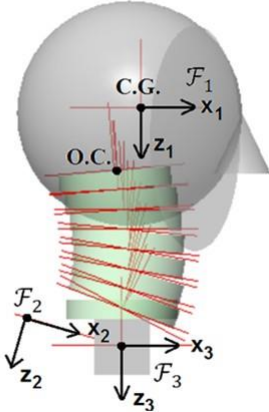
Figure 1.5 S. Himmetoglu multi-body head and neck model [8].
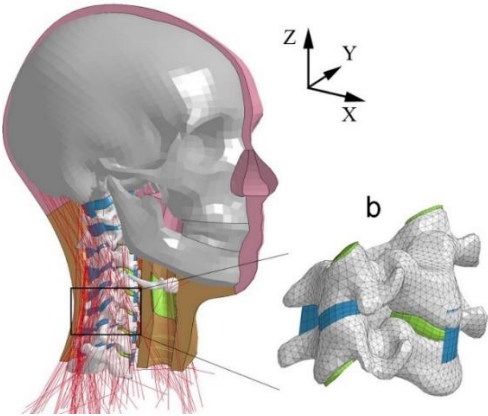
Figure 1.6 Finite element head and neck model [9].

When acceleration or velocity values of rear impact are given as input to these models developed with multibody model or finite element analysis, acceleration and velocity values in the head, neck and vertebrae are obtained as output and information about the behavior of the head, neck and vertebrae is obtained. This information can be verified by comparing it with human rear impact experiments.

As with anthropomorphic test devices, the features added when developing head and neck models are the modeled muscles and nerves in the head and neck and vertebrae regions, and these are added to model them in a way that is closest to the real head and neck structure.

Among the actively used crash-test manikins, the lack of a crash-test manikin with elements that can adjust the damping coefficient in line with the electromyography signals of the behavior of the elements that perform muscle contraction is a problem and this thesis finds a solution to this problem. While solving this problem, multi-body modeling to design of model was performed using the MSC VisualNastran 4D program. Voluntary test results were used to validation of model. The movements of the head and vertebrae obtained from the volunteer tests were given as input to model and muscle forces needed to perform these movements were determined by the inverse dynamics method. The behavior of the elements that will perform muscle contractions in the model has elements that can adjust the damping coefficient in line with muscle electromyography signals, and these are physical dampers. As a result, a multi-body model has been developed that will be a reference for systems that can measure the risk of neck trauma and prevent these risks, reduce the money spent by countries on head, neck and spine traumas and take place for the first time in the literature.

1.2. Scope of the Thesis

In this thesis, the dynamic behavior of a male neck of average height and weight will be characterized before, during and immediately after a collision. Active muscle contractions will be modelled, and static equilibrium of the neck will be achieved. Muscle substitutes will be used in the neck model. The neck model will be validated with data obtained from volunteer tests. The volunteer tests to be used will include rear impact and frontal impact situations. With a more accurate modeled neck, the risk of neck trauma can be predicted more accurately, so that protective systems such as seats and head restraints can be designed in a better way. This study is intended to pioneer the development of an active test-manikin that can replace the passive crash-test-manikins used today.

For the neck model design, multi-body modeling will be performed using Visual Nastran program. Volunteer test results will be used to validation of model. The movements of the head and vertebrae obtained from volunteer tests will be given as input to model and muscle forces needed to perform these movements will be determined by inverse dynamics method.

The neck model to be obtained at the end of this study will enable the design of better protective systems and will reduce whiplash injuries that occur in rear and frontal impacts in vehicles today. The loss of labor, resources and time due to these traumas will also be reduced. The data of this study can be used in active crash-test-manikin designs.

1.3. Thesis Outline

This thesis study consists of 5 chapters. The studies within the chapters are listed below.

First chapter explains problem definition and general information about head and neck trauma, rear impact collision, multibody and finite element model, anthropomorphic test dummies, s-shape, the aim of thesis study and the general explanation of the thesis study.

In the following chapter, which is the literature survey, the previous research about multibody head and neck models, differences between these researches, rear impact tests, and validation of head and neck models.

In the third chapter, Lagrange mechanics and inverse dynamics theories are explained. Since the first aim of this study is to provide static equilibrium of model, the method used at this point is Lagrange mechanics. As a secondary aim, when we give the results of volunteer experiments as input to the head and neck models, inverse dynamics was used as a theory to obtain the neck movement. For this reason, Lagrange mechanics and inverse dynamics theories are explained in this chapter.

In the fourth chapter the static equilibrium of model, the application of the data obtained from the rear impact volunteer tests to model, and the addition of flexor, extensor and sternocleidomastoid muscles to be implemented to model are shown.

In the fifth chapter, a simulation matrix was constructed to compare the results of simulation of model with the literature data.

In the sixth chapter includes discussion of the results of the developed and validated model.

2. LITERATURE SURVEY

2.1. Multibody Head and Neck Models

In literature, different multibody head size models with various levels of complexity for frontal and rear impacts. Some of them have contributed to literature by making improvements to previous studies and some models have reached a level that can be used in advanced anthropomorphic test devices. The head and neck models have been validated with different test methods.

The multibody head and neck model developed by Jakobsson et al [10] on Madymo includes the cervical part of the entire spine. This model is a sagittal plane model that can work on the left and right sides of the body. Model have revolute joints, which could apply resistance according to the torque set against the rotation functions. The shortcomings of this model were that the muscle reflexes were not time dependent, and the validation method was based only on the single impact speed condition.
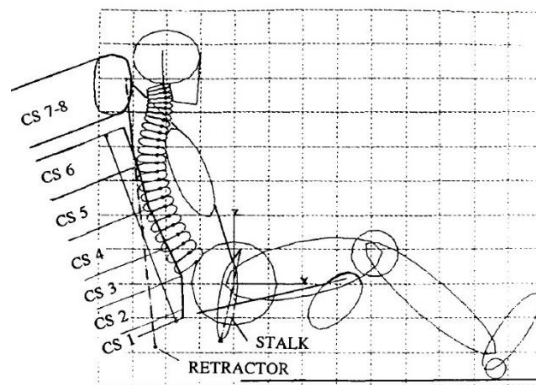
Figure 2.1 2D rear-end collision model created in Madymo program by Jakobbson et al. [10].

One of the most important models contributing to literature is the "global model" developed by De Jager [11], in the initial version all the mechanical behaviors of soft tissues are collected in the intervertebral joints. The second model he developed is more advanced and more detailed than the first model and includes linear and non-linear intervertebral discs, active muscles and frictionless facet joints. Another reason, why this model is an advanced model, is that it includes muscles as straight-line elements. As a

7

result of this complexity, it has shown acceptable response to frontal and side impacts, and these have been verified. This model was also developed through Madymo.
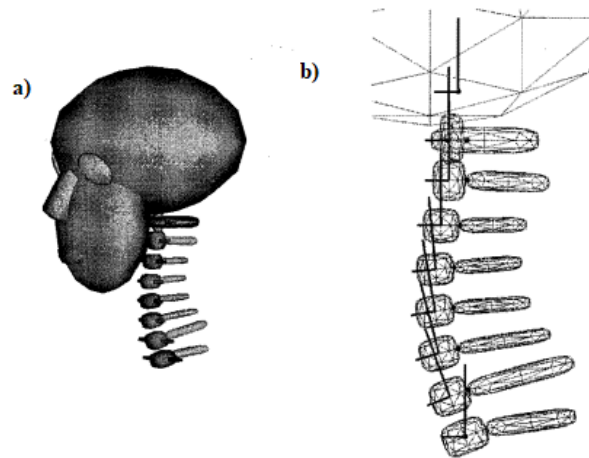
Figure 2.2 a) General view of "the global model" of De Jager b) : Lateral view of "the global model" shown are the vertebrae and base of the skull with their body local coordinate systems [11].

van Kroonenberg et al. [12] used De Jager [11] global model in the head and neck part of the rear impact human body model and compared it with data from rear sled tests and human cadaver tests for low and high intensity impacts, but this model could not be validated due to insufficient data. Yamazaki et al. [13] developed De Jager's global model and optimized the model with data from one of the JARI volunteer tests.

Especially in the case of rear-end collisions multibody head and neck models, improvements have also been made at this point. The mathematical model of the rear impact dummy neck developed by Linder [14] has been used in the development of anthropometric testing devices. In this model, cable-shaped muscles were implemented in the front and back of the neck. The addition of the muscles led to the conclusion that if a model has only revolute joints, the neck cannot give biofidelic responses. The model was developed for low-speed rear impact and Madymo was used in its development.
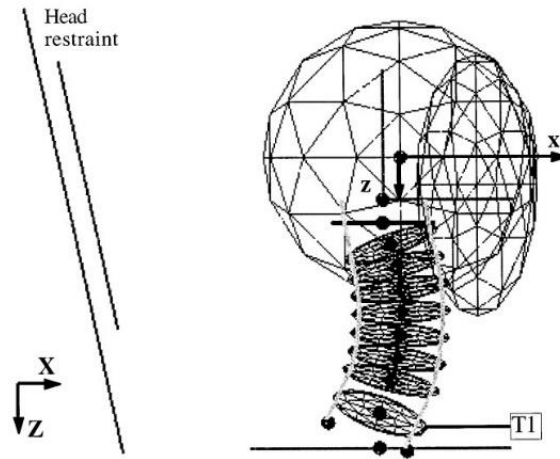
Figure 2.3 Linder head and neck model [14].

van der Horst [15] also improved on De Jager [11] global model. In the model, the muscles have been implemented in detail so that they can follow the curvature of the neck. This model was also compared with data from volunteer test experiments and showed acceptable to poor validation. Once this model was developed and validated, it was used in Madymo as the head and neck in a model of the human body.
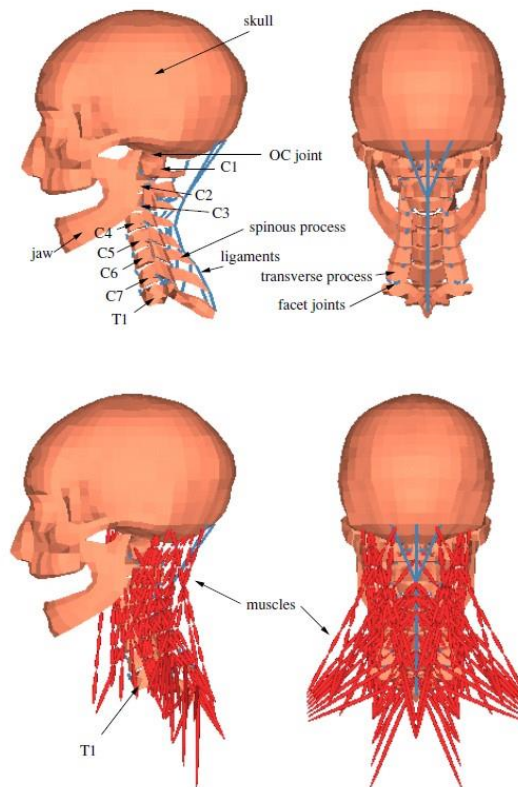
Figure 2.4 van der Horst detailed head and neck model [15].

Similar to this study, van Lopik [16]'s head and neck model, modeled in MSC VisualNastran 4D, is also a detailed model and includes active and passive muscles. In addition, linear actuators manage the curving motion around the vertebrae when the neck is bent, and validation of model is for only frontal and side impacts. As a result of the validation, this model showed the closest result according to comparison with experimental data.

Among the multibody models explained in this section, model in Van der Horst [15] thesis study become prominent because it is more complete in the validation phase than the others, but Linder [14] model has also become a very important model as it has given satisfactory results after validation with volunteer data and led to the development of the BioRID II P3 dummy. Because the BioRID II P3 dummy showed responses close to the volunteer in rear impact sled tests [7].
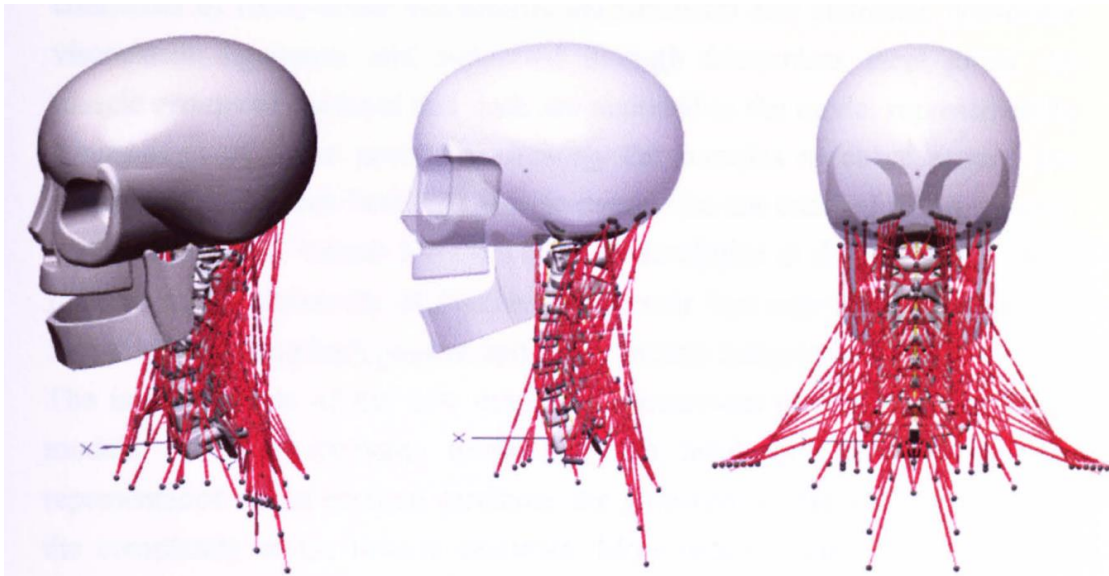
Figure 2.5 van Lopik head and neck model isometric, lateral and rear view with all muscles [16].

Finally, the most important model for this thesis, the biofidelic model with the simple architecture developed by Himmetoglu et al [8]. This model is developed for rear impact. The details of the model are explained in the model development section in chapter four.

2.2. Test Methods

Since rear-end impact is a common type of traffic accident, there are many studies on this subject in the literature. There are many volunteer or cadaver tests, but the proper studies are limited or incomplete for validation of rear impact multibody or finite element models. These deficiencies can be stated as the lack of sufficient information about the test setups or the lack of information or documentation about the exact time of the reactions of the volunteers during the test.

There are differences between volunteer tests and sled tests. In volunteer testing, the test speed is typically low because it is necessary to provide safety to volunteer during test. In cadaveric tests, cadavers are used in relatively high speed tests compared to volunteer tests, but at this point, although they seem to have an advantage over volunteer tests, the disadvantages are that there are not many cadaveric tests that can be considered suitable, or that cadaveric tests are characterized as elderly subjects in terms of age and that the muscles do not have muscle tone and reflexes in response to the reaction.

In one of the steps in this thesis, flexor, extensor and sternocleidomastoid muscles were implemented to model. To find the exact positions such as the start and end points of these muscles on the head, neck and vertebrae, data from a cadaver test [17] found in the literature were used.

Figure 2.6 An example of a cadaver test setup [17].

There are different cadaveric and volunteer tests to validate rear impact models. Among these, the JARI and Pendulum tests have been characterized as suitable for validating rear-end impact models. 50th percentile male human is used in tests. The 50th percentile male is a standardized measure of the average human being based on physical characteristics such as height and weight.

In the Pendulum [18] cadaver test, seven males and one female cadaver were used. Accelerometers were placed in the head pelvis and spine to perform the test. In addition, a triaxle accelerometer was placed on some of the vertebrae for visualization and photography. A power-assisted pendulum was used for the impact, which was suspended by wires and could move freely. The pendulum was accelerated by a pneumatic piston and the rear impact experiment was performed first at low speeds for T1 and T6 vertebra and then at high speeds for T6. In between these tests, the injury was detected by x-ray. In the pendulum test, the cadaver was placed on an adjustable platform. By performing the pendulum test with the cadaver in this way, it contributed to the literature in validating the rear impact models.
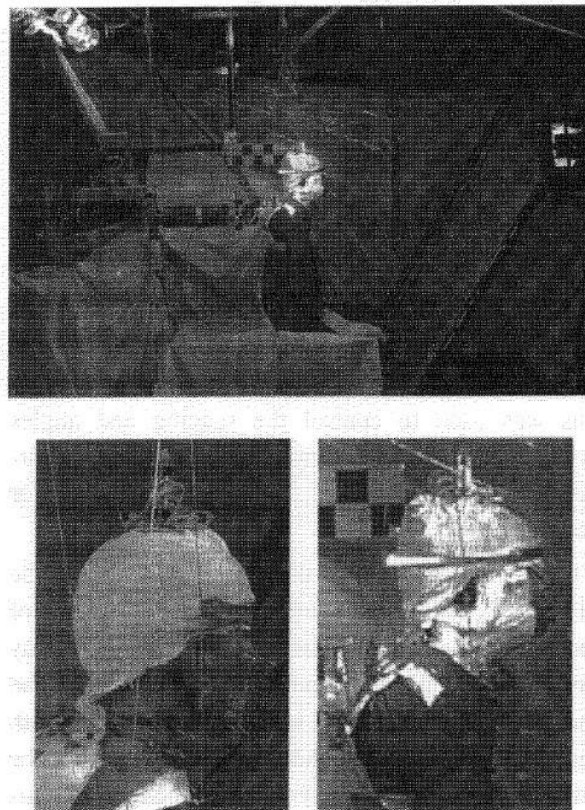
Figure 2.7 Pendulum cadaver test setup [18].

The JARI [8] test is a voluntary rear-end impact test. The volunteers are seated on a seat assembly and this seat has no head restraint. The seat is placed on a sliding sled with a 10° angle to the horizontal axis. The volunteers were seated on the seat with the Frankfort plane [8] of the head horizontal.
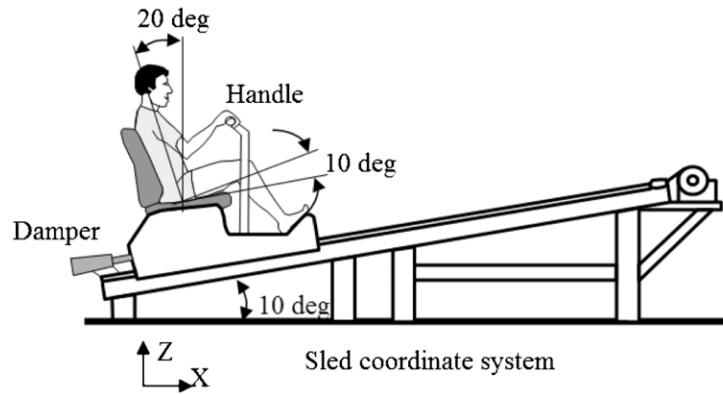
Figure 2.8 JARI volunteer test setup [8].
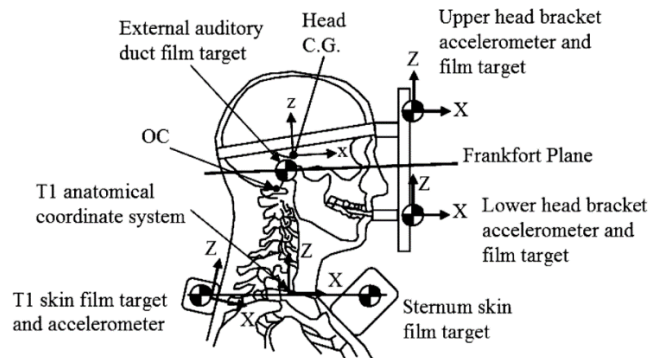
Figure 2.9 JARI Frankfort plane and head and upper torso instrumentation [8].

The JARI test rig simulated a low speed rear-end impact event. In Figure 2.7, film targets and accelerometers were placed on the volunteer's head to obtain post-test data, which was also used to find the center of gravity of the volunteer's head. The pre-impact state of the volunteers was checked by electromyography, and it was stated that the volunteers were comfortable.

In conclusion, the most relevant and important rear impact multibody models in literature and the most appropriate validation methods for these models are presented in the sections above.

3. THEORY OF MULTIBODY HEAD AND NECK MODEL

3.1. Lagrange Mechanics

To provide static equilibrium of head and neck model, it is necessary to define motion and dynamics. The most basic approach that can be used at this point is Newton's laws. Using Lagrangian mechanics, which is a more fundamental and energy-based formulation that can be used before Newton's laws, is a more helpful method to achieve static equilibrium. First, it should be noted that Lagrangian mechanics is basically based on the principle of stationary action and the equations of motion to be obtained at the same time are obtained by the Euler-Lagrange equations, which impose the condition that the stationary motion is stationary. Lagrangian mechanics is expressed as a formulation based on energy, and this energy is defined by the kinetic and potential energy of the state of a moving object.

Motion is the result of the different forces we apply to an object. In addition to that change in position when the force acts are motion. The change of position can give us velocity and acceleration. In other words, if the motion of an object is to be defined, its position and velocity at the point where it is located are sufficient. Since the kinetic and potential energy of the object ultimately provides the position and velocity of the object, it can explain where it will be at the next moment of its motion. The position or velocity of a ball free-falling from a certain height [19] to the ground or a ball thrown from the ground at a certain angle [20] can be calculated from the transformations between kinetic energy and potential energy.
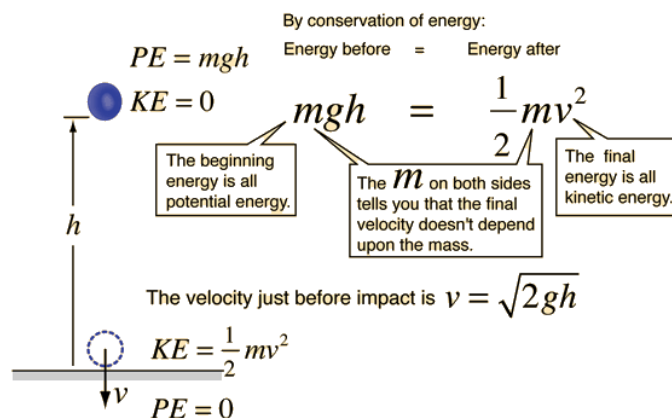
Figure 3.1 Explaining kinetic and potential energy conservation in free fall [19].
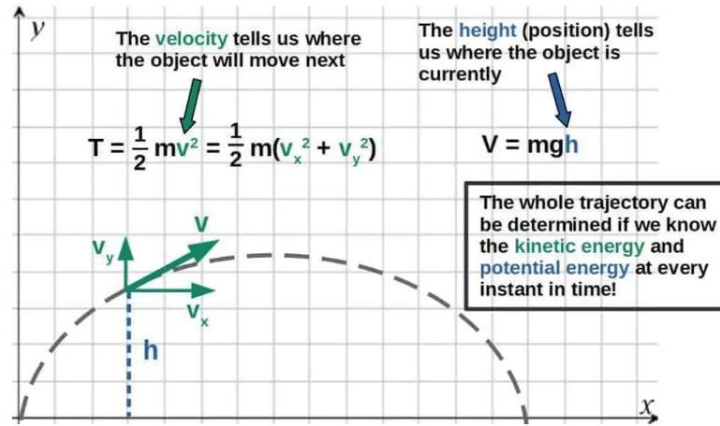
Figure 3.2 Explaining kinetic energy and potential energy conservation in thrown ball [20].

$$L = L\,(T, U) \tag{3.1}$$

In the equation (3.1), T is the kinetic energy and U is the potential energy because Lagrange is a function of energies. When an object is moving from one point to another and the kinetic and potential energy of each point between these points is known, a trajectory can be drawn between the starting and end points. The energy that is meant to be described here is a process, and the mathematical equivalent of the process is defined with the integral, because in Lagrangian mechanics, the sum of the kinetic and potential energies in the process is considered, not the sum of them separately.

$$A = \int_{t1}^{t2} L\,(T, U)\,dt \tag{3.2}$$

In equation (3.2), A is defined as action and is the sum of kinetic and potential energy between the beginning and the end of the process. The classically defined Lagrange is given in equation (3.3).

$$L = T - U \tag{3.3}$$

There is a reason for T - U instead of T + U in the equation (3.3). In Lagrangian mechanics, there is no such thing as the sum of energy, the total energy of the object or the position of energies. Since Lagrange is based on the principle of stationary action and

since kinetic and potential energies have velocity and position in the process of motion, kinetic and potential energies can transform into each other, so it is more logical to have T-U in the Lagrange equation. Also, potential energy alone does not define a motion, the change in potential energy into kinetic energy defines a motion. The change here also makes it T-U instead of T+U. While T+U is time-invariant, T-U is time-varying and better describes the motion of an object.
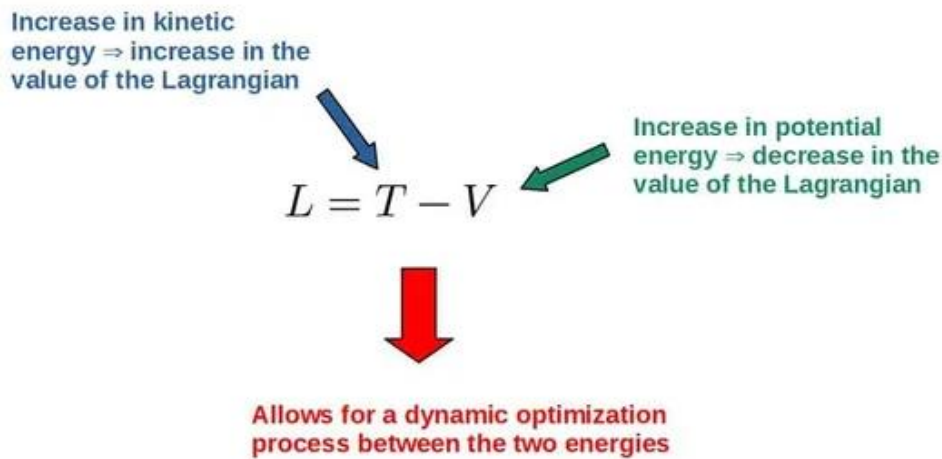
Figure 3.3 Explaining Lagrange equation [20].

Equation (3.2) corresponds to the Euler-Lagrange equation when solved mathematically. The Euler-Lagrange equation is given below.

$$\frac{d}{dt}\frac{\partial L}{\dot{x}} = \frac{\partial L}{x} \tag{3.4}$$

Equation (3.4) is a necessary condition for the principle of stationary action on which the Lagrangian is based. Consequently, the Euler-Lagrange equation is a derivation of the Lagrangian with respect to position and velocity, and the Lagrangian must satisfy the Euler-Lagrange equation. When the Lagrangian is added to equation (3.4), the following equation is obtained.

$$\frac{d}{dt}\frac{\partial (T-U)}{\dot{x}} = \frac{\partial (T-U)}{x} \tag{3.5}$$

In equation (3.5), potential energy is eliminated on the left side of the equation and kinetic energy is eliminated on the right side of the equation. The new equation according to this situation is given below.

$$\frac{d}{dt}\frac{\partial T}{\dot{x}} = -\frac{\partial(U)}{x} \tag{3.6}$$

The minus sign on the right-hand side of Equation (3.6) comes from the Lagrangian as mentioned before and is due to the trade-off between kinetic and potential energy. The velocity of a free-falling body increases as the potential energy decreases, or the velocity of an upwardly thrown body decreases as the potential energy increases, and this is one of the best explanations for the Lagrangian equation being T-U.

3.1.1. Solving Problems Using Lagrangian Equation

Basically, the equation that will be used to solve motion problems is L=T-U. From here, there are some detailed steps that need to be done to elaborate and create the equation. First, it is necessary to create a suitable generalized coordinate system for the problem. This coordinate system can be a cartesian coordinate system such as x, y, z or a spherical coordinate system. The definition of the Euler-Lagrange equation in generalized coordinates is given below.

$$\frac{d}{dt}\frac{\partial T}{\partial q_i} = \frac{\partial(U)}{\partial q_i} \tag{3.7}$$

The second step is to define the Lagrange equation with the help of the selected generalized coordinate system, at this point, if there is more than one object in the system, it is necessary to define the Lagrangian equation for each object.

As a third step, once the Lagrangian equations are defined, it is necessary to apply the Euler-Lagrange equations to the Lagrangian equations, and this must be done for each coordinate system we have chosen in the first step. As a result, there will be a Euler-Lagrange equation for each coordinate system.

In some cases, the system in question may not only consist of kinetic and potential energies. Forces can also act on systems. These forces acting on the systems are Newtonian forces, but when it is necessary to use them in Lagrangian mechanics, just as kinetic and potential energy are adapted to generalized coordinates, the forces must also be adapted to generalized coordinates. Although the Lagrangian depends on energies, forces can also add the equation because, for example, the frictional force can also cause an energy change and can therefore be included in the Lagrangian equation. As a result, the forces in the Lagrangian equation are called generalized forces and their equation is given in Figure 3.4.
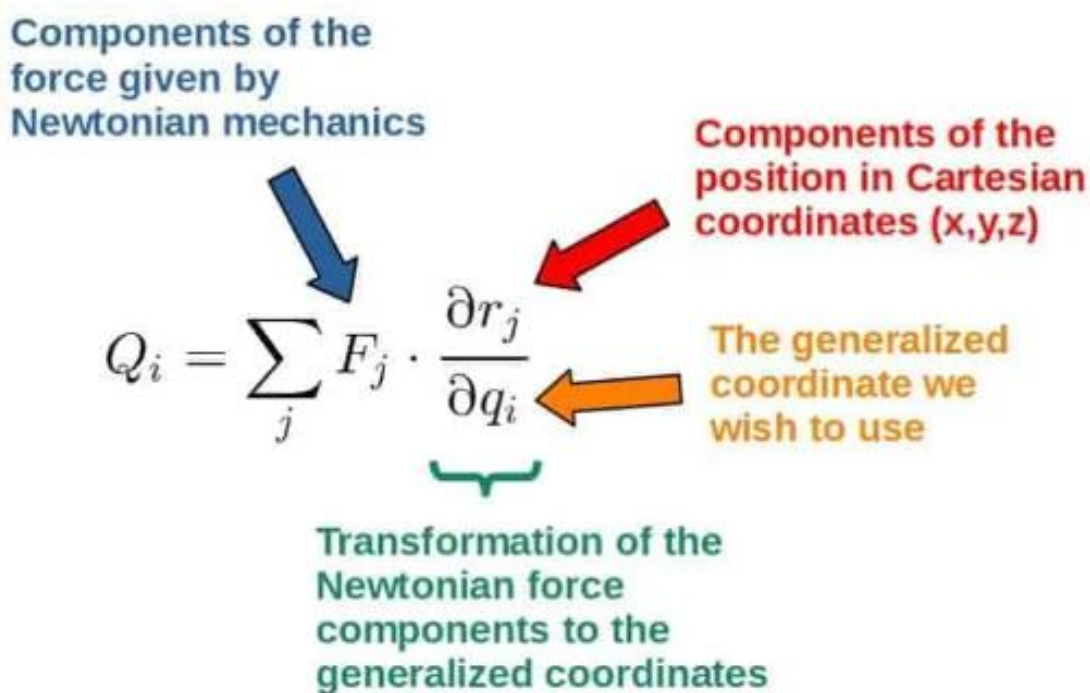
Figure 3.4 Generalized forces in Lagrange equation [20].

If non-conservative forces such as frictional forces are present in the system, these forces are added directly to the Euler-Lagrange equation as in the equation (3.8).

$$\frac{d}{dt}\frac{\partial T}{\partial q_i} = \frac{\partial(U)}{\partial q_i} + Q_i^f \tag{3.8}$$

After all this information about Lagrangian mechanics, let us solve a spring pendulum system with Lagrangian. First, as shown in the Figure 3.5, there is a body at end of the

spring in the system. The mass of the body is m. The normal length of the spring is l. As a first step, generalized coordinates x and θ can be chosen for this system. As a second step, the kinetic energy and potential energy of the system is given in the following equations.
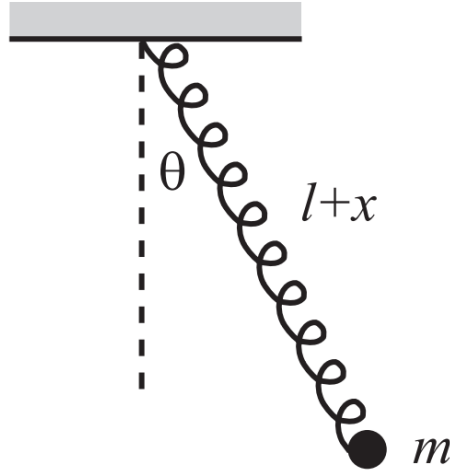
Figure 3.5 Spring pendulum system [21].

$$T = \frac{1}{2} m(\dot{x}^2 + (l + x)^2 \dot{\theta}^2)$$

(3.9)

$$U(x, \theta) = -mg(l + x)cos\theta + \frac{1}{2} kx^2$$

(3.10)

Then Lagrangian is

$$L = T - V = \frac{1}{2} m(\dot{x}^2 + (l + x)^2 \dot{\theta}^2) + mg(l + x)cos\theta - \frac{1}{2} kx^2$$

(3.11)

The system has two generalized coordinates, x and θ. When the Euler-Lagrange equation is written for each coordinate

$$\frac{d}{dt} \frac{\partial L}{\partial \dot{x}} = \frac{\partial L}{\partial x} \rightarrow m\ddot{x} = m + (l + x)\dot{\theta}^2 + mgcos\theta - kx$$

(3.12)

$$\frac{d}{dt}\frac{\partial L}{\partial \dot{\theta}} = \frac{\partial L}{\partial \theta} \rightarrow m(l+x)\ddot{\theta} + 2m\dot{x}\dot{\theta} = -mgsin\theta \qquad (3.13)$$

This is the solution of the spring pendulum system according to Lagrange and Euler-Lagrange. Equation (3.12) corresponds simply to the equation F=m.a and its similarity to the Newtonian solution can be stated in this way.

3.2. Inverse Dynamics

As mentioned before, the model in Himmetoglu et al. [8] was used in this thesis study. In this multibody model, the connections between the vertebrae are provided by revolute joints. After the implementation of muscles to model as stated in the aim of the thesis section, the movements of the head and vertebrae obtained from the volunteer tests described in the literature research section will be given as input to model and the values of the muscle forces that will perform these movements will be found by the inverse dynamics method.

To explain inverse dynamics, it may not be enough to talk only about the multibody model. Inverse dynamics comes into play in robotics or when you want to find the force needed to move an arm, leg or other limb of a human or an animal from one point to another. For this reason, inverse dynamics applications are widely used in biomechanics and robotics. The connections in these application areas are usually joints. As in this thesis, if the angular velocity or angular acceleration affecting these joints is known or obtained from any volunteer experiments, forces can be obtained with inverse dynamics. Inverse dynamics can find these forces by running the formula force = mass times acceleration in reverse.

In inverse dynamics there is no direct formula or method as in Lagrangian Mechanics. In general, a problem-specific method, algorithm or method is developed.
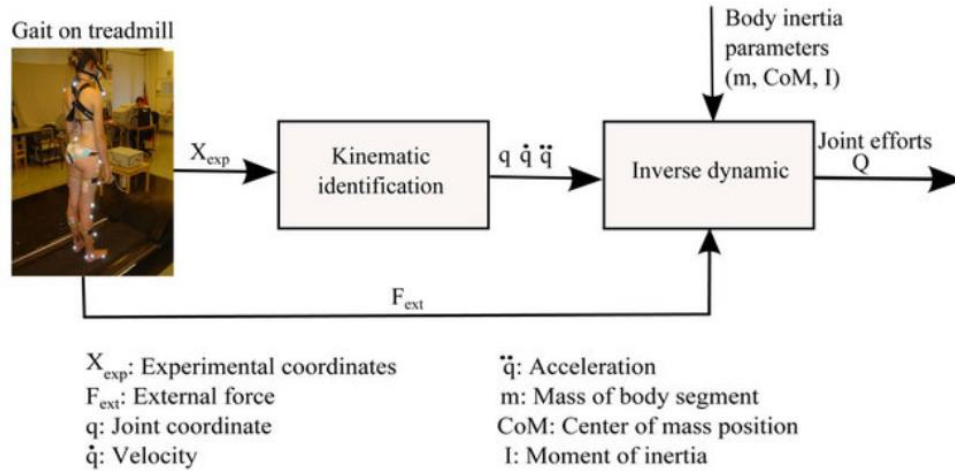
Figure 3.6 Generalized forces in Lagrangian equation [22].

As shown as an example in Figure 3.6, first a kinematic definition is made, and in the model used in this thesis, a kinematic definition is made to ensure static equilibrium, generalized coordinates are defined. Then, with inverse dynamics, the efforts at the joints are defined. Of course, the work in Figure 3.6 is much more detailed, but it is a sufficient example to explain how inverse dynamics works.

4. DEVELOPMENT OF HIMMETOGLU HEAD AND NECK MODEL

As mentioned in the previous chapters, the model has not been developed from scratch in this thesis. In this thesis, it is aimed that model of Himmetoglu et al. [8] firstly provides static equilibrium and then to find the forces acting on the muscles implemented to the head and neck model with the inverse dynamic method. Firstly, the details of Himmetoglu et al. [8]'s model, which is roughly mentioned in the Literature research section, are mentioned. In other sections, the process of providing static equilibrium of model and finding forces acting on muscles with the inverse dynamics method is explained.

4.1. Details of Himmetoglu et al. [8] Head and Neck Model

Himmetoglu et al. [8] model is a multibody model. This model consists of bodies which represent head, vertebrae, and neck segments from C1 to C7 from top to bottom, T1 vertebra as shown in Figure 4.1. The C1-C7 vertebrae are in the cervical spine and the T1 vertebra is in the thoracic spine. As an example, C1 means first vertebra of cervical spine, C2 means second vertebra of cervical spine and T1 is first vertebra of thoracic spine. C1 is known as atlas and C2 is known as axis in anatomy. The mass of the vertebrae and the surrounding soft tissues and their moments of inertia correspond to the inertial properties of the vertebrae. The movement input of the head and neck model is given from T1. The connection between the vertebrae is formed by revolute joints in model and these joints have rotational springs and dampers inside of them. These revolute joints are also called intervertebral joints. Himmetoglu et al. [8] model is validated with volunteer experiments results of JARI experiments so mechanical properties of dampers and rotational springs in revolute joints are defined from these tests. C1-C7 and T1 have the same stiffness. Plot of rotational stiffness is given in Figure 4.1. In this rotational stiffness plot angle is rotational displacement upper vertebra relative to lower vertebra and when the value of angle is positive this means extension and when the value of angle is negative this means flexion. Extension is the rearward rotation of the upper vertebra relative to the lower vertebra, while flexion is the forward rotation of the upper vertebra relative to the lower vertebra. When motion is given to T1, the joints of the vertebrae and other bodies generate torques against this motion. The head and neck model allows the neck segments, that is,

the bodies in the model, to pass through each other, but this does not affect the dynamic character of the model. The model was developed using MSC VisualNastran 4D.
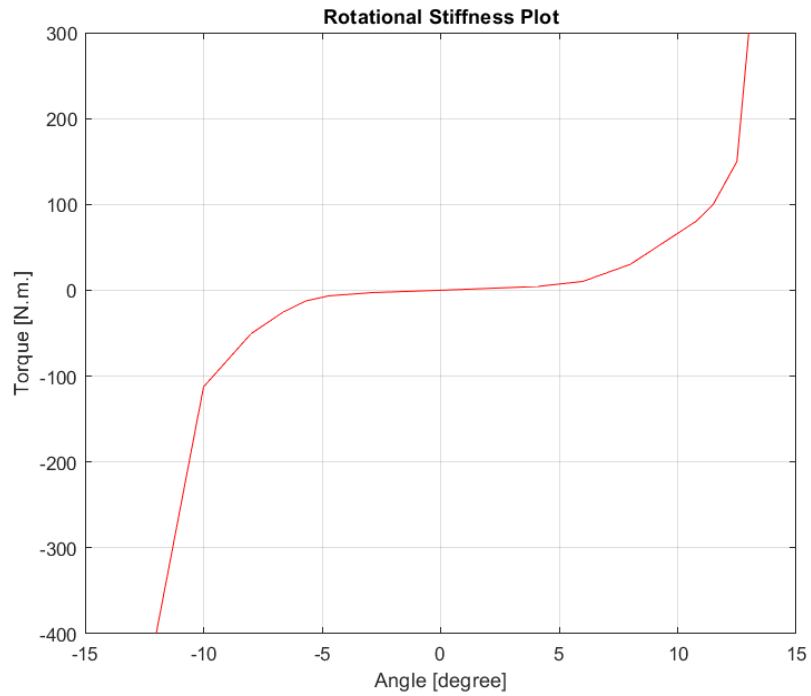
Figure 4.1 Rotational stiffness plot of vertebrae in Himmetoglu et al [8] model.
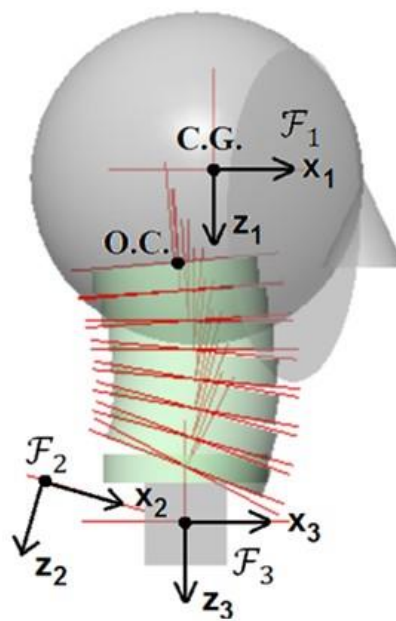
Figure 4.2 Himmetoglu et al head and neck model [8].

The first version was based on the head and neck position of a 50th percentile male when he sits on a seat in a normal driving situation. Accordingly, an arc with a radius of 190 mm and a 37° sector between the Occipital Condyle (O.C.) and the lower plate of the C7 vertebra was drawn as shown in Figure 4.3 [8]. Occipital Condyle is the connection point between Head and C1 vertebra.
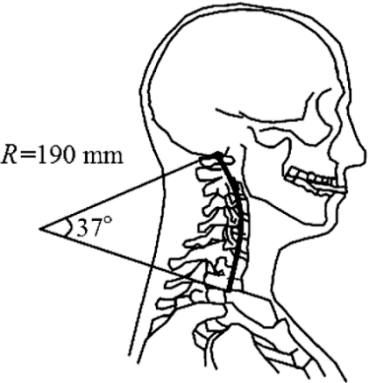
Figure 4.3 Obtained arc for initial configuration of head and neck model [8].

In addition, de Jager's [11] work on the mathematical model gives the mass, moments of inertia, position relative to the body frame origin, position relative to the body's center of gravity and relative orientation of the head, vertebrae C1-C7 and T1. Using all this information, the center position of the vertebrae between C1-C7 and the head was determined as shown in Figure 4.3 [8]. In the model, the vertebrae have their own coordinate systems. These coordinate systems pass through the center of gravity of each vertebra.
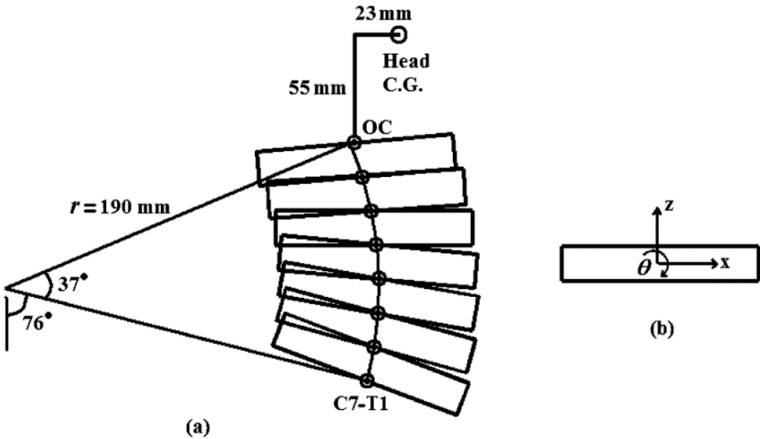
Figure 4.4 a) Neck curvature. b) Neck segment frame axes [8].

4.2. Development of Himmetoglu et al. [8] Head and Neck Model to Provide Static Equilibrium

It has already been mentioned that the method to be used for the static equilibrium of model is Lagragian Mechanics. Basically, since the aim is to achieve static equilibrium, the head and neck model has no kinetic energy and therefore the kinetic energy is not included in the Euler-Lagrange equation. As a force, there is only the gravitational force due to the gravitational acceleration of the head, vertebrae C1-C7 and T1.

The first step is to create a free body diagram of model. The center of gravity of the head, C1-C7 vertebrae and T1 and their connection points with the joint are shown in Figure 4.5.
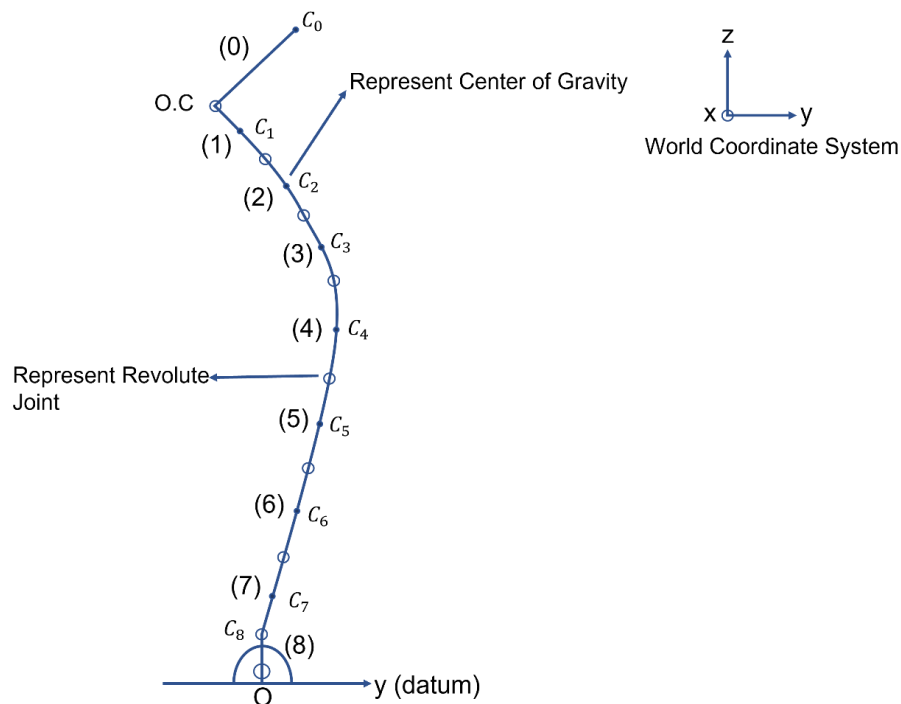
Figure 4.5 Free body diagram of head and neck model.

C_i = Center of Gravity of body i

C_8 = Center of Gravity of T1

r_0 = Length between O.C. and Co

C_0 = Center of Gravity of Head

To calculate the potential energy, it is necessary to find the height of the head, vertebrae C1-C7 and T1 with respect to the ground. At this point, MSC VisualNastran 4D has two coordinate systems. The first one is the coordinate system in which each body, which is defined as body, should be understood as head, C1-C7 vertebrae or T1, is located at its center of gravity. Other one is the world coordinate system shown in Figure 4.5. Potential energy is calculated according to the world coordinate system.

Another critical point to be mentioned in the model is that there is a resistive torque that the head, C1-C7 vertebrae and T1 apply to each other due to the torsional springs in the joints between the head, C1-C7 vertebrae and T1. On the other hand, there is a static torque added by us to provide static equilibrium. Figure 4.6 shows the application of these torques for any two bodies connected to each other by a joint in model.
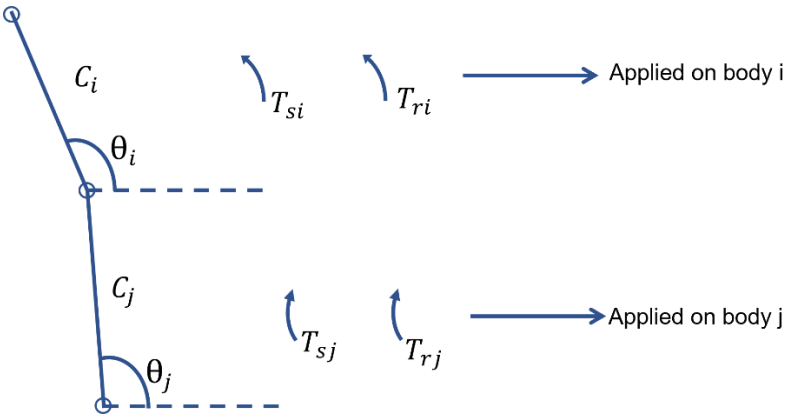
Figure 4.6 Applied static torques and resistive torques for bodies in head and neck model.

Ts_i =   Static torque applied to body i
Tr_i =   Resistive torque applied to body i
Ts_j =   Static torque applied to body j
Tr_j =   Resistive torque applied to body j

At this point, there is a different situation for T1, which is that since T1 is connected to the origin, there is no resistive torque applied to T1 from the origin. This is shown in Figure 4.7.
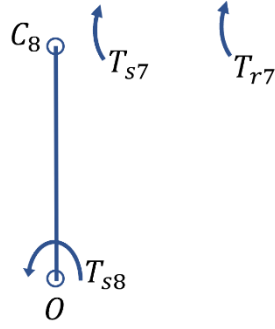
Figure 4.7 Applied static torques and resistive torques.

When the kinetic energy is eliminated in equation (3.8), the resulting equation is given in equation (4.1).

$$\frac{\partial U}{\partial q_i} = Q_i \tag{4.1}$$

Where i = 0, 1, 2, 3, 4, 5, 6, 7, 8

U = Potential energy

q_i = Generalized coordinates

$$U = \sum_{i=0}^{8} U_i \tag{4.2}$$

Generalized coordinates are given below in equation (4.3). Then potential energy equations are given below equation (4.3) through equations (4.12).

$$\bar{q} = [\theta_0, \theta_1, \theta_2, \theta_3, \theta_4, \theta_5, \theta_6, \theta_7, \theta_8]^t \tag{4.3}$$

$$U_8 = m_8 \cdot g \cdot \left(\frac{b_8}{2}\right) \cdot sin\theta_8 \tag{4.4}$$

$$U_7 = m_7 \cdot g \cdot [\left(\frac{b_8}{2}\right) \cdot sin\theta_8 + \left(\frac{b_7}{2}\right) \cdot sin\theta_7)] \tag{4.5}$$

$$U_6 = m_6 \cdot g \cdot [\left(\frac{b_8}{2}\right) \cdot sin\theta_8 + b_7 \cdot sin\theta_7 + \left(\frac{b_6}{2}\right) \cdot sin\theta_6] \tag{4.6}$$

$$U_5 = m_5.g.\left[\left(\frac{b_8}{2}\right).sin\theta_8 + b_7.sin\theta_7 + b_6.sin\theta_6 + \left(\frac{b_5}{2}\right).sin\theta_5\right] \qquad (4.7)$$

$$U_4 = m_4.g.\left[\left(\frac{b_8}{2}\right).sin\theta_8 + b_7.sin\theta_7 + b_6.sin\theta_6 + b_5.sin\theta_5 + \left(\frac{b_4}{2}\right).sin\theta_4\right] \qquad (4.8)$$

$$U_3 = m_3.g.\left[\left(\frac{b_8}{2}\right).sin\theta_8 + b_7.sin\theta_7 + b_6.sin\theta_6 + b_5.sin\theta_5 + b_4.sin\theta_4 + \qquad (4.9)\right.$$
$$\left.\left(\frac{b_3}{2}\right).sin\theta_3\right]$$

$$U_2 = m_2.g.\left[\left(\frac{b_8}{2}\right).sin\theta_8 + b_7.sin\theta_7 + b_6.sin\theta_6 + b_5.sin\theta_5 + b_4.sin\theta_4 + \qquad (4.10)\right.$$
$$\left.b_3.sin\theta_3 + \left(\frac{b_2}{2}\right).sin\theta_2\right]$$

$$U_1 = m_1.g.\left[\left(\frac{b_8}{2}\right).sin\theta_8 + b_7.sin\theta_7 + b_6.sin\theta_6 + b_5.sin\theta_5 + b_4.sin\theta_4 + \qquad (4.11)\right.$$
$$\left.b_3.sin\theta_3 + b_2.sin\theta_2 + \left(\frac{b_1}{2}\right).sin\theta_1\right]$$

$$U_0 = m_0.g.\left[\left(\frac{b_8}{2}\right).sin\theta_8 + b_7.sin\theta_7 + b_6.sin\theta_6 + b_5.sin\theta_5 + b_4.sin\theta_4 + \qquad (4.12)\right.$$
$$\left.b_3.sin\theta_3 + b_2.sin\theta_2 + b_1.sin\theta_1 + r_0.sin\theta_0\right]$$

m_i	=	Mass of body i
g	=	Gravitational acceleration $= 9.81 m/s^2$
b_i	=	Height of neck segment

According to equation (4.1), the equations obtained by taking the first partial derivative according to each generalized coordinates are given below equation (4.13) through equations (4.21) .

$$\frac{\partial U}{\partial \theta_0} = m_0.g.r_0.cos\theta_0 = Ud_0 \qquad (4.13)$$

$$\frac{\partial U}{\partial \theta_1} = m_0.g.b_1.cos\theta_1 + m_1.g\left(\frac{b_1}{2}\right).cos\theta_1 = g.b_1.cos\theta_1.\left(m_0 + \left(\frac{m_1}{2}\right)\right) = \qquad (4.14)$$
$$Ud_1$$

$$\frac{\partial U}{\partial \theta_2} = m_0.g.b_2.cos\theta_2 + m_1.g.b_2.cos\theta_2 + m_2.g\left(\frac{b_2}{2}\right).cos\theta_2 = \tag{4.15}$$

$$g.b_2.cos\theta_2.\left(m_0 + m_1 + \left(\frac{m_1}{2}\right)\right) = Ud_2$$

$$\frac{\partial U}{\partial \theta_3} = m_0.g.b_3.cos\theta_3 + m_1.g.b_3.cos\theta_3 + m_2.g.b_3.cos\theta_3 + \tag{4.16}$$

$$m_3.g\left(\frac{b_3}{2}\right).cos\theta_3 = g.b_3.cos\theta_3.\left(m_0 + m_1 + m_2 + \left(\frac{m_3}{2}\right)\right) = Ud_3$$

$$\frac{\partial U}{\partial \theta_4} = m_0.g.b_4.cos\theta_4 + m_1.g.b_4.cos\theta_4 + m_2.g.b_4.cos\theta_4 + \tag{4.17}$$

$$m_3.g.b_4.cos\theta_3 + m_4.g.\left(\frac{b_4}{2}\right).cos\theta_4 = g.b_4.cos\theta_4.(m_0 + m_1 +$$

$$m_2 + m_3 + \left(\frac{m_4}{2}\right)) = Ud_4$$

$$\frac{\partial U}{\partial \theta_5} = m_0.g.b_5.cos\theta_5 + m_1.g.b_5.cos\theta_5 + m_2.g.b_5.cos\theta_5 + \tag{4.18}$$

$$m_3.g.b_5.cos\theta_5 + m_4.g.b_5.cos\theta_5 + m_5.g.\left(\frac{b_5}{2}\right).cos\theta_5 =$$

$$g.b_5.cos\theta_5.\left(m_0 + m_1 + m_2 + m_3 + m_4 + \left(\frac{m_5}{2}\right)\right) = Ud_5$$

$$\frac{\partial U}{\partial \theta_6} = m_0.g.b_6.cos\theta_6 + m_1.g.b_6.cos\theta_6 + m_2.g.b_6.cos\theta_6 + \tag{4.19}$$

$$m_3.g.b_6.cos\theta_6 + m_4.g.b_6.cos\theta_6 + m_5.g.b_6.cos\theta_6 +$$

$$m_6.g.\left(\frac{b_6}{2}\right).cos\theta_6 = g.b_6.cos\theta_6.(m_0 + m_1 + m_2 + m_3 + m_4 +$$

$$m_5 + \left(\frac{m_6}{2}\right)) = Ud_6$$

$$\frac{\partial U}{\partial \theta_7} = m_0.g.b_7.cos\theta_7 + m_1.g.b_7.cos\theta_7 + m_2.g.b_7.cos\theta_7 + \tag{4.20}$$

$$m_3.g.b_7.cos\theta_7 + m_4.g.b_7.cos\theta_7 + m_5.g.b_7.cos\theta_7 +$$

$$m_6.g.b_7.cos\theta_7 + m_7.g.\left(\frac{b_7}{2}\right).cos\theta_7 = g.b_7.cos\theta_7.(m_0 + m_1 +$$

$$m_2 + m_3 + m_4 + m_5 + m_6 + \left(\frac{m_7}{2}\right)) = Ud_7$$

$$\frac{\partial U}{\partial \theta_8} = m_0.g.b_8.cos\theta_8 + m_1.g.b_8.cos\theta_8 + m_2.g.b_8.cos\theta_8 + \tag{4.21}$$

$$m_3.g.b_8.cos\theta_8 + m_4.g.b_8.cos\theta_8 + m_5.g.b_8.cos\theta_8 +$$

$$m_6. g. b_8. \cos\theta_8 + m_7. g. b_8. \cos\theta_8 + m_8. g. \left(\frac{b_8}{2}\right). \cos\theta_8 =$$

$$g. b_8. \cos\theta_8. (m_0 + m_1 + m_2 + m_3 + m_4 + m_5 + m_6 + m_7 +$$

$$\left(\frac{m_8}{2}\right) = Ud_8$$

The virtual work done by the forces acting on the system in Lagrange mechanics is also calculated here and its equations are given below equation (4.22) through equations (4.32). Here, it is the static torques and resistive torques do the virtual work.

$$\delta W = Ts_8 \delta\theta_8 + (Ts_7 + Tr_7). (\delta\theta_7 - \delta\theta_8) + (Ts_6 + Tr_6). (\delta\theta_6 - \delta\theta_7) + \tag{4.22}$$
$$(Ts_5 + Tr_5). (\delta\theta_5 - \delta\theta_6) + (Ts_4 + Tr_4). (\delta\theta_4 - \delta\theta_5) + (Ts_3 +$$
$$Tr_3). (\delta\theta_3 - \delta\theta_4) + (Ts_2 + Tr_2). (\delta\theta_2 - \delta\theta_3) + (Ts_1 + Tr_1). (\delta\theta_1 -$$
$$\delta\theta_2) + (Ts_0 + Tr_0). (\delta\theta_0 - \delta\theta_1)$$

$$\delta W = \sum_{i=0}^{8} Q_i. \delta\theta_i \tag{4.23}$$

$$Q_0 = Ts_0 + Tr_0 = Ud_0 \tag{4.24}$$

$$Q_1 = -(Ts_0 + Tr_0) + (Ts_1 + Tr_1) = Ud_1 \tag{4.25}$$

$$Q_2 = -(Ts_1 + Tr_1) + (Ts_2 + Tr_2) = Ud_2 \tag{4.26}$$

$$Q_3 = -(Ts_2 + Tr_2) + (Ts_3 + Tr_3) = Ud_3 \tag{4.27}$$

$$Q_4 = -(Ts_3 + Tr_3) + (Ts_4 + Tr_4) = Ud_4 \tag{4.28}$$

$$Q_5 = -(Ts_4 + Tr_4) + (Ts_5 + Tr_5) = Ud_5 \tag{4.29}$$

$$Q_6 = -(Ts_5 + Tr_5) + (Ts_6 + Tr_6) = Ud_6 \tag{4.30}$$

$$Q_7 = -(Ts_6 + Tr_6) + (Ts_7 + Tr_7) = Ud_7 \tag{4.31}$$

$$Q_8 = -(Ts_7 + Tr_7) + Ts_8 = Ud_8 \tag{4.32}$$

Static torque terms are moved to the left side in the equation (4.22) through equation (4.32) and rearranged equations given below equation (4.33) through equation (4.41) and the following equations are obtained.

$$Ts_0 = Ud_0 - Tr_0 \tag{4.33}$$

$$Ts_1 = Ud_1 + (Ts_0 + Tr_0) - Tr_1 \tag{4.34}$$

$$Ts_2 = Ud_2 + (Ts_1 + Tr_1) - Tr_2 \tag{4.35}$$

$$Ts_3 = Ud_3 + (Ts_2 + Tr_2) - Tr_3 \tag{4.36}$$

$$Ts_4 = Ud_4 + (Ts_3 + Tr_3) - Tr_4 \tag{4.37}$$

$$Ts_5 = Ud_5 + (Ts_4 + Tr_4) - Tr_5 \tag{4.38}$$

$$Ts_6 = Ud_6 + (Ts_5 + Tr_5) - Tr_6 \tag{4.39}$$

$$Ts_7 = Ud_7 + (Ts_6 + Tr_6) - Tr_7 \tag{4.40}$$

$$Ts_8 = Ud_8 + (Ts_7 + Tr_7) \tag{4.41}$$

The weights of the head, C1-C7 vertebrae and T1 and their lengths are given in Table 4.1 and Table 4.2.

Table 4.1 Weights of head, C1-C7 vertebrae and T1.

m_0	m_1	m_2	m_3
4.6 kg	0.22 kg	0.25 kg	0.24 kg
m_4	m_5	m_6	m_7
0.23 kg	0.23 kg	0.24 kg	0.22 kg
m_8			
1.0235 kg			

Table 4.2 Lengths of head, C1-C7 vertebrae and T1.

r_0	b_1	b_2	b_3
59.61 mm	17.4 mm	18.23 mm	0.24 kg
b_4, b_5, b_6, b_7			
17.4 mm			
b_8			
16.6 mm			

The equations needed for the static equilibrium of the head and neck model are defined and the values of weight and length in the equations are given. The length values given are the lengths of each body in model and these lengths are measured with respect to the body's own coordinate system. To achieve static equilibrium, the lengths must be defined with respect to the world coordinate system because potential energy can be found from height of the body with respect to the world coordinate system. The theta angles mentioned in the equations above are not sufficient alone to define the height of head or vertebrae in model with respect to the world coordinate.
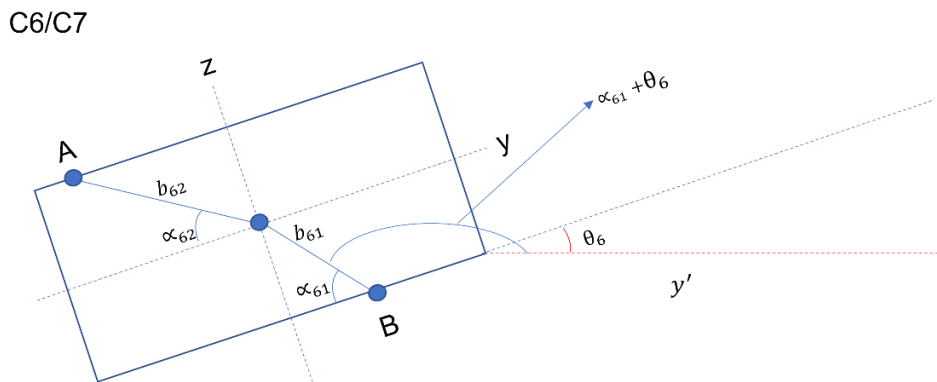
Figure 4.8 Example analysis of C6 vertebra.

Figure 4.8 shows the analysis of the C6 vertebra. In this figure, points A and B show the joint location of the C6 vertebra with C7 on the B side and with C5 on the A side, and these locations are taken from the head and neck model in MSC VisualNastran 4D. The axes denoted by y and z are the axes of the coordinate system passing through the center of mass of the C6 vertebra and y' is y axis of world coordinate system. To find the height of center of gravity point of vertebra C6 with respect to the world coordinate system, it is necessary to define the angle of link b_{61} with respect to the world coordinate system. The

height of vertebra C6 is defined. Since the coordinates of points A and B are also defined, the lengths b_{61}, b_{62} and angles α_{61} and α_{62} can be calculated with the help of the geometric solution. The height of vertebra C6 with respect to the world coordinate can be found by the angle of b_{61} with respect to the world coordinate and the heights of C7 and T1 with respect to world coordinate. The angle of b_{61} with respect the world coordinate is equal to the sum of α_{61} and θ_8 defined in the static equilibrium equations. In this way, the analysis in Figure 4.8 was done individually for the head, vertebrae C1-C7 and T1 and the static equilibrium equations were organized according to this notation. A similar study on coordinate systems was done by Himmetoglu [23]. In this study, the visualization of coordinate systems is Figure 4.8. Model used in Figure 4.8 is the same as the head neck model used in this study. Occipital condyle (O.C.) is connection point between head and C1 vertebra in model.

Figure 4.9 Explaining coordinate systems on head and neck model [23].

C7/C8

Figure 4.10 Analysis of C7/C8 vertebrae.

C6/C7

Figure 4.11 Analysis of C6/C7 vertebrae.
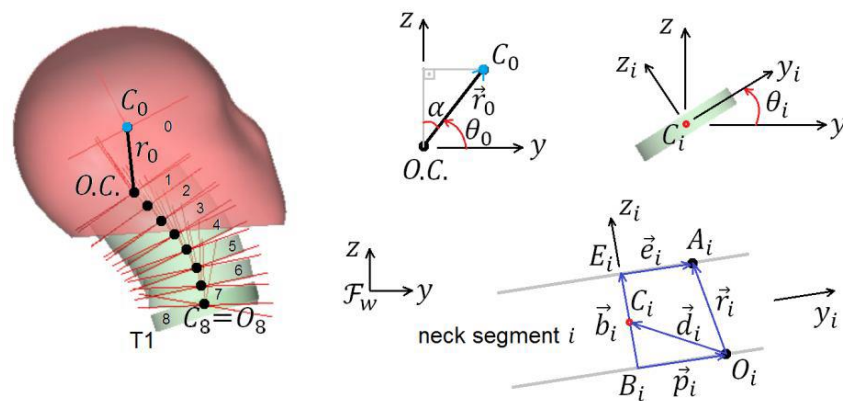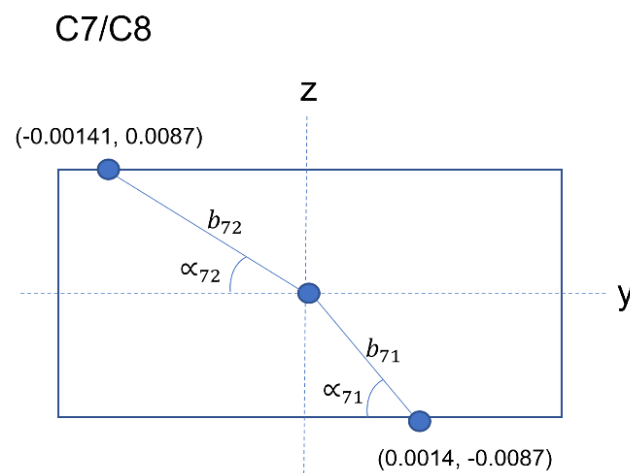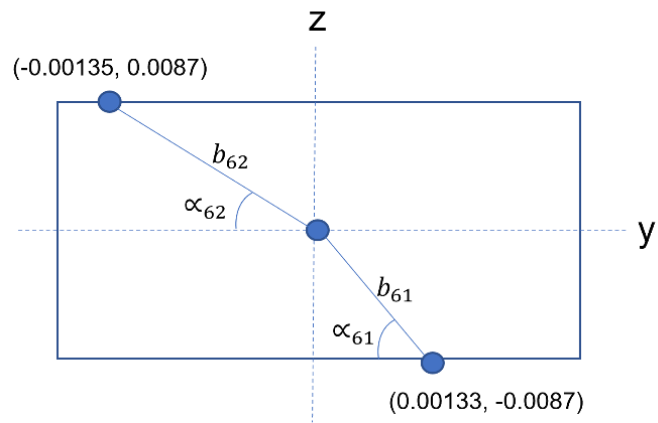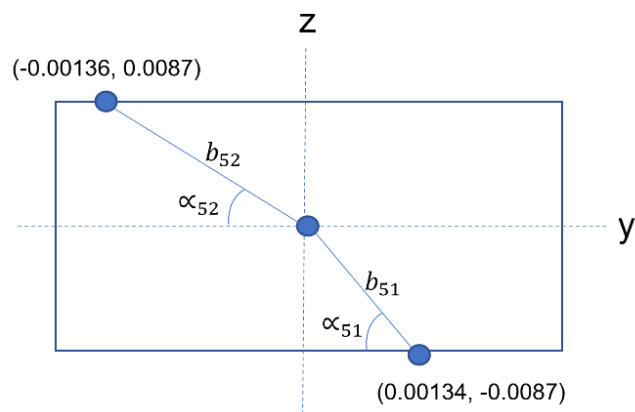
C5/C6

Figure 4.12 Analysis of C5/C6 vertebrae.
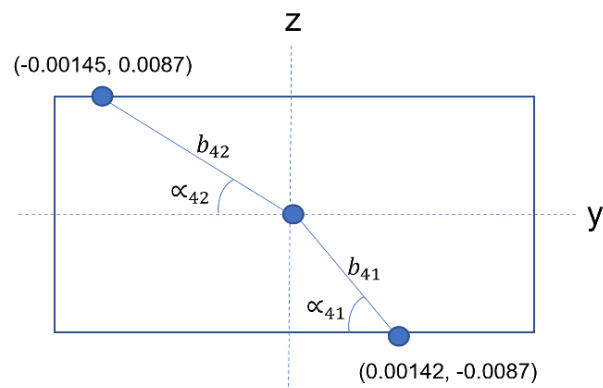
C4/C5

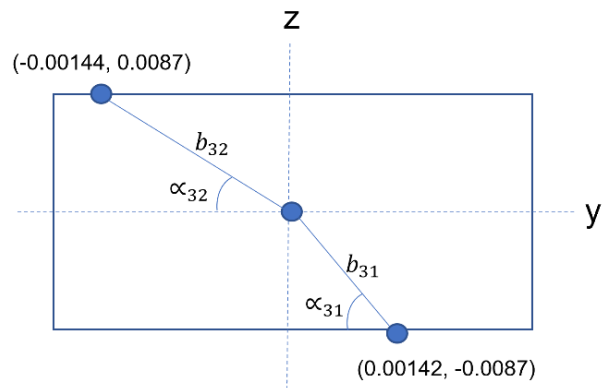Figure 4.13 Analysis of C4/C5 vertebrae.

C3/C4

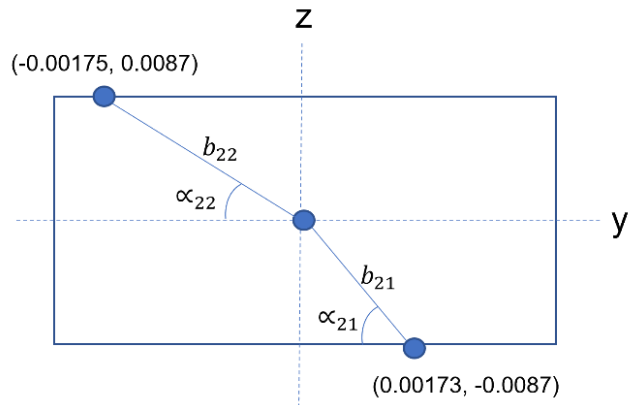Figure 4.14 Analysis of C3/C4 vertebrae.

C2/C3
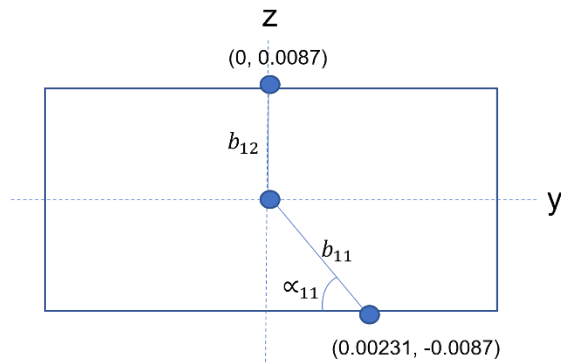

Figure 4.15 Analysis of C2/C3 vertebrae.

C1/C2

Figure 4.16 Analysis of C1/C2 vertebrae.

Arranged potantial energy equations of head and neck model for static equilibrium is given below equations (4.42) through (4.50).

$$U_8 = m_8 . g . \left(\frac{b_8}{2}\right) . sin\theta_8 \tag{4.42}$$

$$U_7 = m_7 . g . \left[\left(\frac{b_8}{2}\right) . sin\theta_8 + b_{71} . \sin(\theta_7 + \alpha_{71})\right] \tag{4.43}$$

$$U_6 = m_6 . g . \left[\left(\frac{b_8}{2}\right) . sin\theta_8 + b_{71} . \sin(\theta_7 + \alpha_{71}) + b_{72} . \sin(\theta_7 + \alpha_{72}) + \right. \tag{4.44}$$
$$\left. b_{61} . \sin(\theta_6 + \alpha_{61})\right]$$

$$U_5 = m_5 . g . \left[\left(\frac{b_8}{2}\right) . sin\theta_8 + b_{71} . \sin(\theta_7 + \alpha_{71}) + b_{72} . \sin(\theta_7 + \alpha_{72}) + \right. \tag{4.45}$$
$$\left. b_{61} . \sin(\theta_6 + \alpha_{61}) + b_{62} . \sin(\theta_6 + \alpha_{62}) + b_{51} . \sin(\theta_5 + \alpha_{51})\right]$$

$$U_4 = m_4 . g . \left[\left(\frac{b_8}{2}\right) . sin\theta_8 + b_{71} . \sin(\theta_7 + \alpha_{71}) + b_{72} . \sin(\theta_7 + \alpha_{72}) + \right. \tag{4.46}$$
$$b_{61} . \sin(\theta_6 + \alpha_{61}) + b_{62} . \sin(\theta_6 + \alpha_{62}) + b_{51} . \sin(\theta_5 + \alpha_{51}) +$$
$$\left. b_{52} . \sin(\theta_5 + \alpha_{52}) + b_{41} . \sin(\theta_4 + \alpha_{41})\right]$$

$$U_3 = m_3 . g . \left[\left(\frac{b_8}{2}\right) . sin\theta_8 + b_{71} . \sin(\theta_7 + \alpha_{71}) + b_{72} . \sin(\theta_7 + \alpha_{72}) + \right. \tag{4.47}$$
$$b_{61} . \sin(\theta_6 + \alpha_{61}) + b_{62} . \sin(\theta_6 + \alpha_{62}) + b_{51} . \sin(\theta_5 + \alpha_{51}) +$$
$$b_{52} . \sin(\theta_5 + \alpha_{52}) + b_{41} . \sin(\theta_4 + \alpha_{41}) + b_{41} . \sin(\theta_4 + \alpha_{42}) +$$
$$\left. b_{31} . \sin(\theta_3 + \alpha_{31})\right]$$

$$U_2 = m_2 . g . \left[\left(\frac{b_8}{2}\right) . sin\theta_8 + b_{71} . \sin(\theta_7 + \alpha_{71}) + b_{72} . \sin(\theta_7 + \alpha_{72}) + \right. \tag{4.48}$$
$$b_{61} . \sin(\theta_6 + \alpha_{61}) + b_{62} . \sin(\theta_6 + \alpha_{62}) + b_{51} . \sin(\theta_5 + \alpha_{51}) +$$
$$b_{52} . \sin(\theta_5 + \alpha_{52}) + b_{41} . \sin(\theta_4 + \alpha_{41}) + b_{42} . \sin(\theta_4 + \alpha_{42}) +$$
$$\left. b_{31} . \sin(\theta_3 + \alpha_{31}) + b_{32} . \sin(\theta_3 + \alpha_{32}) + b_{21} . \sin(\theta_2 + \alpha_{21})\right]$$

$$U_1 = m_1 . g . \left[\left(\frac{b_8}{2}\right) . sin\theta_8 + b_{71} . \sin(\theta_7 + \alpha_{71}) + b_{72} . \sin(\theta_7 + \alpha_{72}) + \right. \tag{4.49}$$
$$b_{61} . \sin(\theta_6 + \alpha_{61}) + b_{62} . \sin(\theta_6 + \alpha_{62}) + b_{51} . \sin(\theta_5 + \alpha_{51}) +$$
$$b_{52} . \sin(\theta_5 + \alpha_{52}) + b_{41} . \sin(\theta_4 + \alpha_{41}) + b_{42} . \sin(\theta_4 + \alpha_{42}) +$$

$$b_{31}.\sin(\theta_3 + \propto_{31}) + b_{32}.\sin(\theta_3 + \propto_{32}) + b_{21}.\sin(\theta_2 + \propto_{21}) +$$
$$b_{22}.\sin(\theta_2 + \propto_{22}) + b_{11}.\sin(\theta_1 + \propto_{11})]$$

$$U_0 = m_0.g.\left[\left(\frac{b_8}{2}\right).sin\theta_8 + b_{71}.\sin(\theta_7 + \propto_{71}) + b_{72}.\sin(\theta_7 + \propto_{72}) + \tag{4.50}$$
$$b_{61}.\sin(\theta_6 + \propto_{61}) + b_{62}.\sin(\theta_6 + \propto_{62}) + b_{51}.\sin(\theta_5 + \propto_{51}) +$$
$$b_{52}.\sin(\theta_5 + \propto_{52}) + b_{41}.\sin(\theta_4 + \propto_{41}) + b_{42}.\sin(\theta_4 + \propto_{42}) +$$
$$b_{31}.\sin(\theta_3 + \propto_{31}) + b_{32}.\sin(\theta_3 + \propto_{32}) + b_{21}.\sin(\theta_2 + \propto_{21}) +$$
$$b_{22}.\sin(\theta_2 + \propto_{22}) + b_{11}.\sin(\theta_1 + \propto_{11}) + b_{12}.\sin(\theta_1) + r_0.sin\theta_0]$$

Arranged partial derivatives of potantial energy equations of head and neck model for static equilibrium is given below equations (4.51) through (4.59).

$$\frac{\partial U}{\partial \theta_0} = m_0.g.r_0.cos\theta_0 = Ud_0 \tag{4.51}$$

$$\frac{\partial U}{\partial \theta_1} = (m_0 + m_1).g.b_{11}.\cos(\theta_1 + \propto_{11}) + m_0.b_{12}.\cos(\theta_1 + \propto_{12}) = Ud_1 \tag{4.52}$$

$$\frac{\partial U}{\partial \theta_2} = m_2.g.b_{21}.\cos(\theta_2 + \propto_{21}) + (m_0 + m_1).g.(b_{21}.\cos(\theta_2 + \propto_{21}) + \tag{4.53}$$
$$b_{22}.\cos(\theta_2 + \propto_{22}) = Ud_2$$

$$\frac{\partial U}{\partial \theta_3} = m_3.g.b_{31}.\cos(\theta_3 + \propto_{31}) + (m_0 + m_1 + m_2).g.(b_{31}.\cos(\theta_3 + \tag{4.54}$$
$$\propto_{31}) + b_{32}.\cos(\theta_3 + \propto_{32}) = Ud_3$$

$$\frac{\partial U}{\partial \theta_4} = m_4.g.b_{41}.\cos(\theta_4 + \propto_{41}) + (m_0 + m_1 + m_2 + m_3).g.(b_{41}.\cos(\theta_4 + \tag{4.55}$$
$$\propto_{41}) + b_{42}.\cos(\theta_4 + \propto_{42}) = Ud_4$$

$$\frac{\partial U}{\partial \theta_5} = m_5.g.b_{51}.\cos(\theta_5 + \propto_{51}) + (m_0 + m_1 + m_2 + m_3 + \tag{4.56}$$
$$m_4).g.(b_{51}.\cos(\theta_5 + \propto_{51}) + b_{52}.\cos(\theta_5 + \propto_{52}) = Ud_5$$

$$\frac{\partial U}{\partial \theta_6} = m_6 . g . b_{61} . \cos(\theta_6 + \propto_{61}) + (m_0 + m_1 + m_2 + m_3 + m_4 + \tag{4.57}$$

$$m_5). g. (b_{61}. \cos(\theta_6 + \propto_{61}) + b_{62}. \cos(\theta_6 + \propto_{62}) = Ud_6$$

$$\frac{\partial U}{\partial \theta_7} = m_7 . g . b_{71} . \cos(\theta_7 + \propto_{71}) + (m_0 + m_1 + m_2 + m_3 + m_4 + m_5 + \tag{4.58}$$

$$m_6). g. (b_{71}. \cos(\theta_7 + \propto_{71}) + b_{72}. \cos(\theta_7 + \propto_{72}) = Ud_7$$

$$\frac{\partial U}{\partial \theta_8} = m_8 . g . \left(\frac{b_8}{2}\right) . \cos(\theta_8) + (m_0 + m_1 + m_2 + m_3 + m_4 + m_5 + m_6 + \tag{4.59}$$

$$m_7). b_8. \cos(\theta_8)$$

All these defined equations were implemented into the head and neck model created in MSC VisualNastran 4D and some changes were made to the settings of the model. The lengths of all the links defined in the equations and the angles with specific values were calculated manually and implemented to the model. After these operations, when the head and neck model was run for the first time, it was observed that the model did not remain in static equilibrium. The state of the model is shown in Figure 4.17.
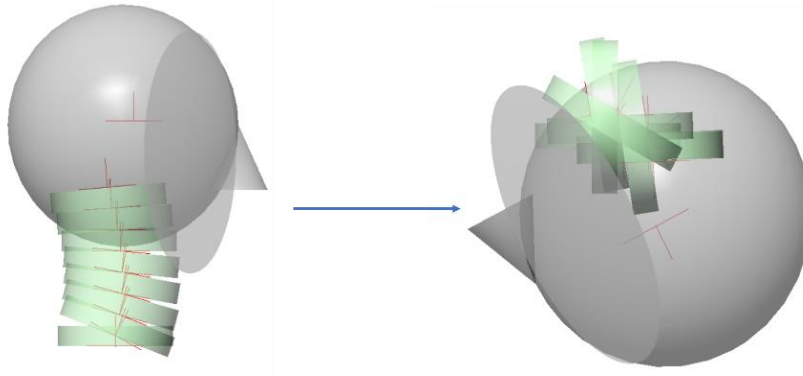
Figure 4.17 Head and neck model that does not achieve static equilibrium due to incorrect implementation of the equations.

When the cause of this error was investigated, it was found that the head and neck model was too sensitive. During the implementation of the equations into the head and neck model, the head and neck model could not achieve static equilibrium because the link lengths were defined as value into equation and the body representing the head in the head and neck model was not in the appropriate shape and the model was sensitive about

these situations. After link lengths to calculated trigonometrically ,like sine and cosine of angles of bodies with their own coordinate system, by the MSC VisualNastran and replacing the body representing the head in the head and neck model with an appropriate one, the head and neck model achieved static equilibrium as shown in Figure 4.18. In addition, it is shown in Figure 4.19 and Figure 4.20 that it achieved static equilibrium at -30° and +30° degrees.

Time = 0 ms   Time = 300 ms

Figure 4.18 Static equilibrium of head and neck model at 0 °.

Time = 0 ms   Time = 300 ms

Figure 4.19 Static equilibrium of head and neck model at -30°.
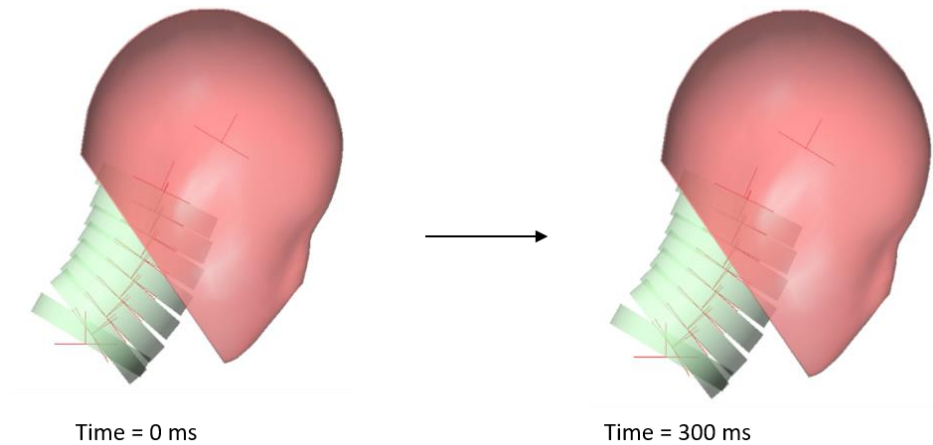
Figure 4.20 Static equilibrium of head and neck model at +30°.

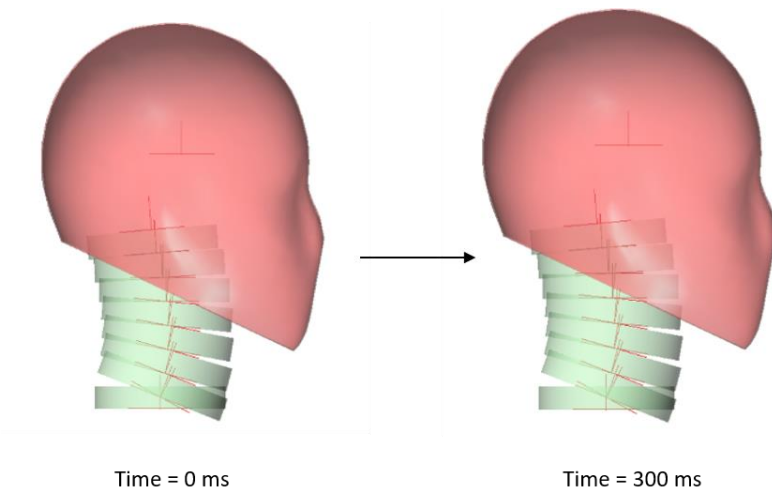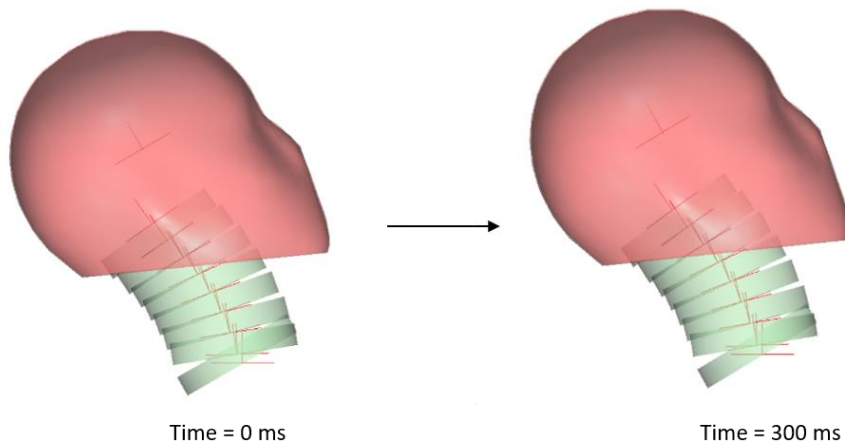The static equilibrium of model was completed in this way and the next step was to implement of muscles and find the forces of these muscles with the inverse dynamics method.

4.3. Development of Himmetoglu et al. [8] Head and Neck Model with Inverse Dynamics Method

Digitizing and interpolating of plots found in the reference [7] that can be input to the head and neck model was the necessary step to solve the inverse dynamics equation and to give the accelerations of O.C. and T1 with respect to the ground as input to the head and neck model and to extract the muscle forces that provide them. In this section, the work of setting up the inverse dynamics equation and implementing inputs into the system was done.

4.4. Digitizing of Input and Interpolation Process of Inputs

The plots of the input motions, which are used as input in the inverse dynamics equation to be discussed in the next section and which will contribute to the solution of this equation, are digitized and interpolated in this section.

First, the studies from which these graphs are taken from the reference [7] are mentioned.

Figure 4.21 Occipital condyle with respect to T1-x displacement vs. time [7].

Figure 4.22 Occipital condyle with respect to T1-z displacement vs. time [7].
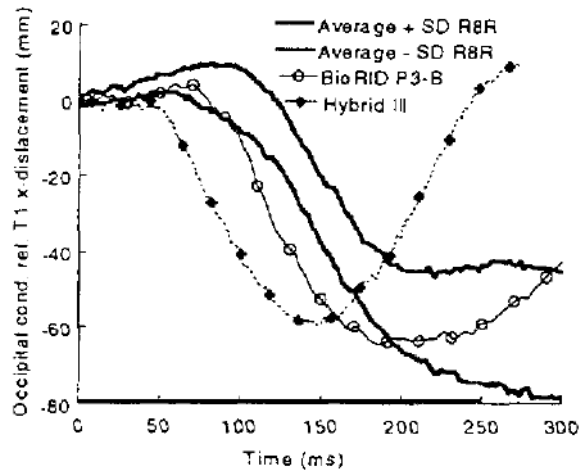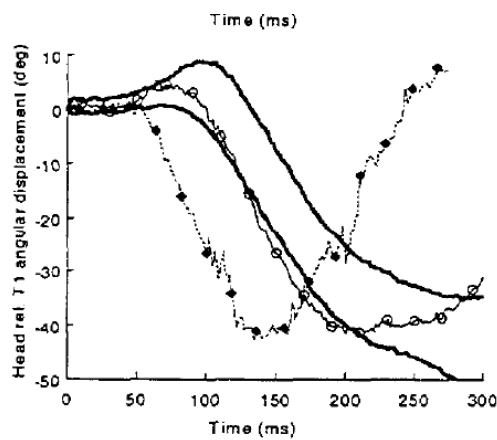

Figure 4.23 Head with respect to T1 angular displacement vs.. time [7].

41
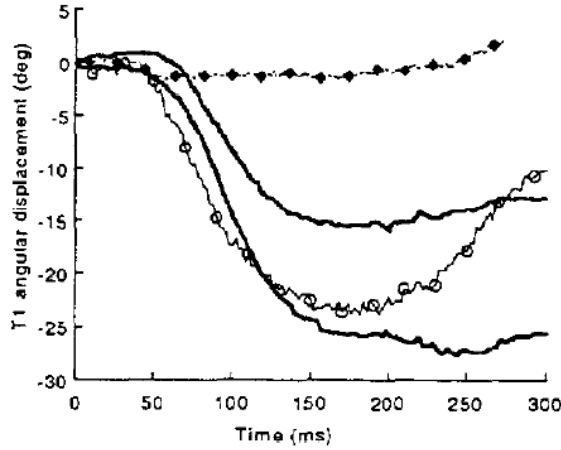
Figure 4.24 T1 angular displacement vs.. time [7].
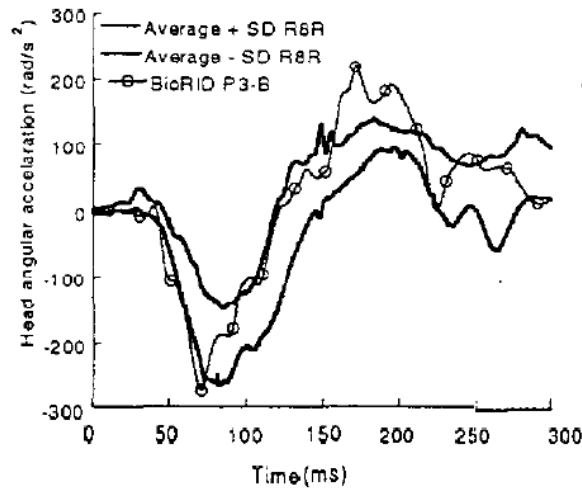
Figure 4.25 Head angular acceleration vs.. time [7].

When examine the figures from Figure 4.21 to Figure 4.25, it is not possible to give them as input to model because they are taken from the reference [7] and can only be used for visual purposes. For this reason, a graph digitization program was used to create points on the curves that vary according to the mean value and standard deviation in the graphs and these points were created as a table. After the table was created, as can be seen in the graphs, the minimum point on the time axis was 0 and the maximum point was 300 seconds. When the graphs were digitized, the points selected on the curves, no matter how precisely they were selected, were not selected so that the first time value was 0 and the last time value was 300. For this reason, the first time value of the time axis in the

42

tables created was set to 0 and the last time value to 300. The main reason for this is to ensure that when these data are interpolated, they are all in the same time interval.

The interpolation process was done by writing code on MATLAB. There are also curves created by averaging the standard deviation as the third curve on the graphs, which will be used in the next stage. The graphs created as a result of interpolation are given below Figure 4.26 through Figure 4.29
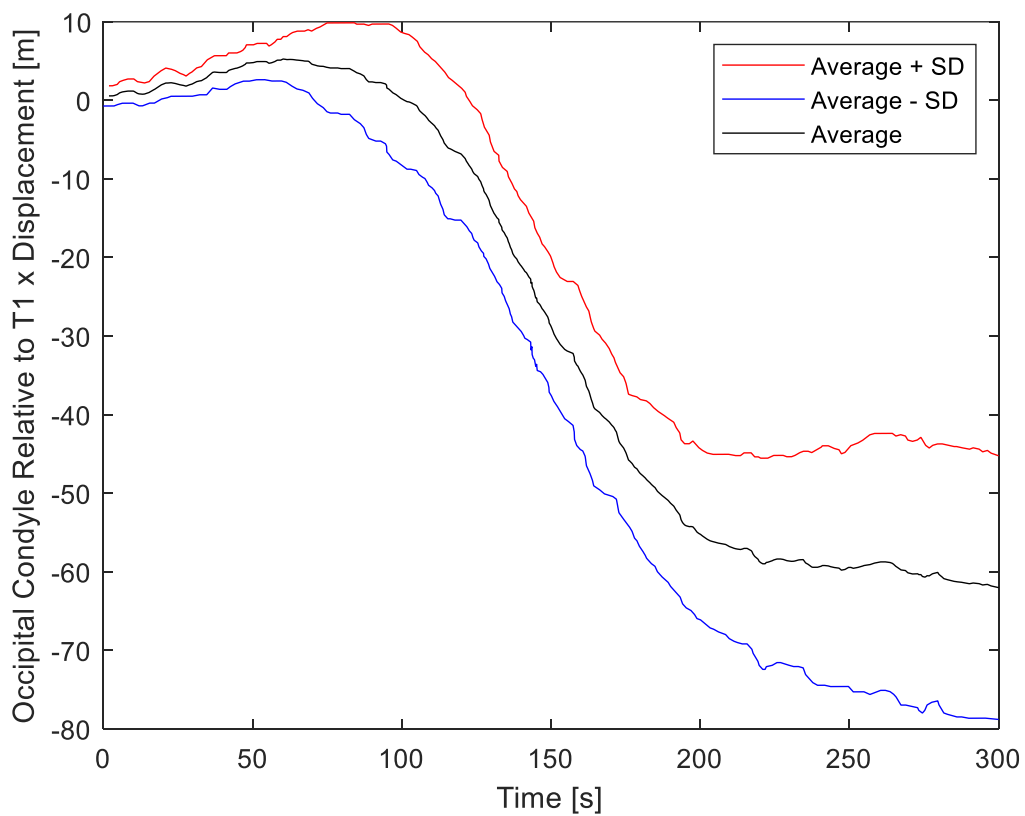
Figure 4.26 Occipital condyle with respect to T1-x displacement vs. time (interpolated).
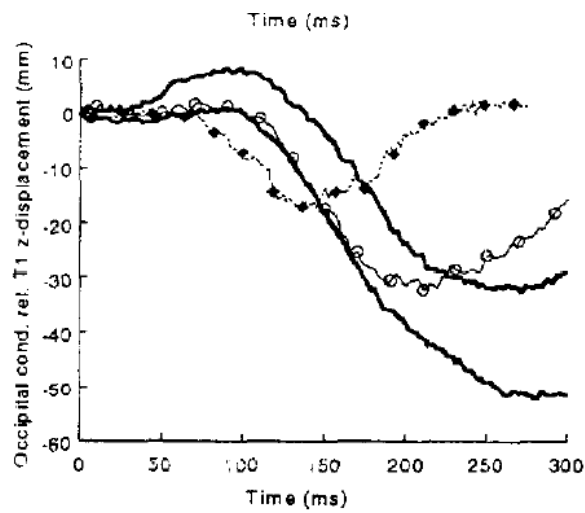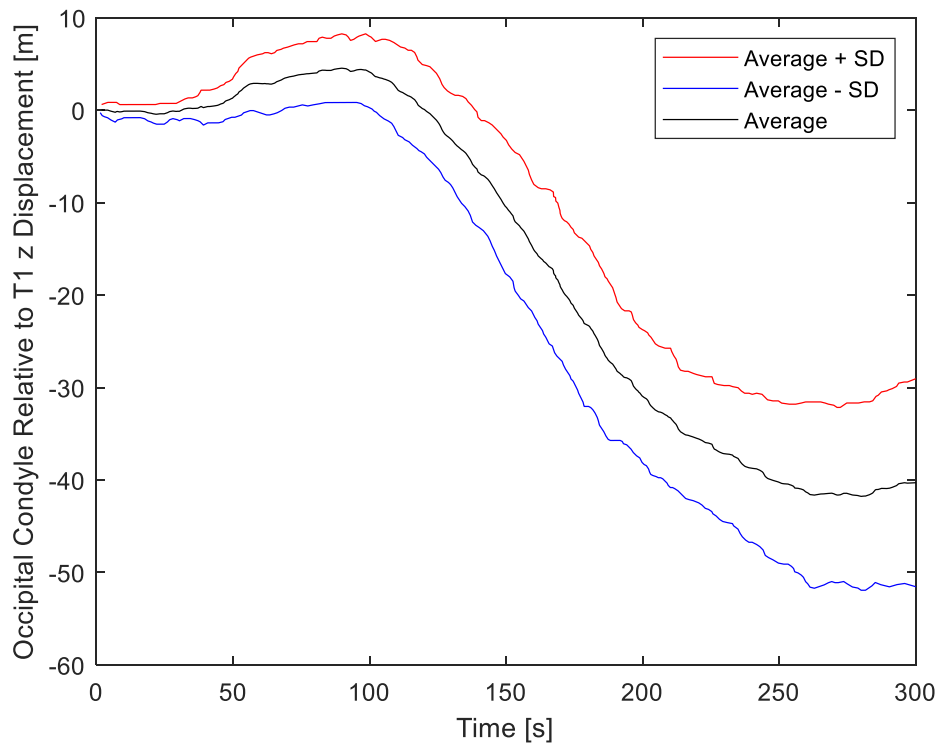
Figure 4.27 Occipital condyle with respect to T1-z displacement vs. time (interpolated).
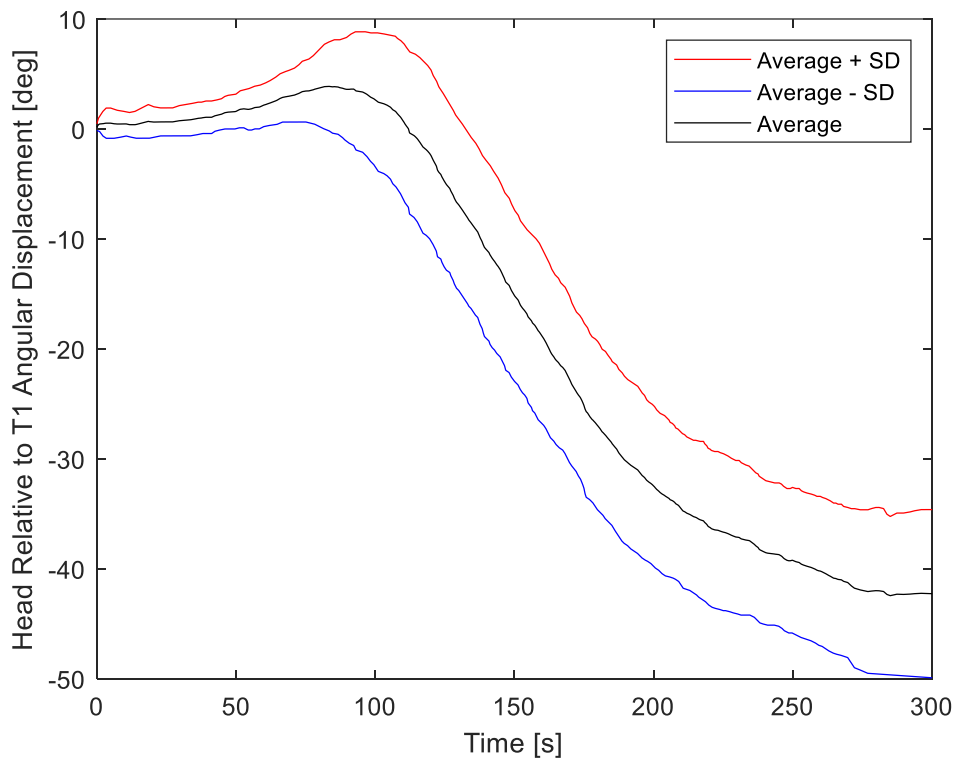
Figure 4.28 Head with respect to T1 angular displacement vs. time (interpolated).
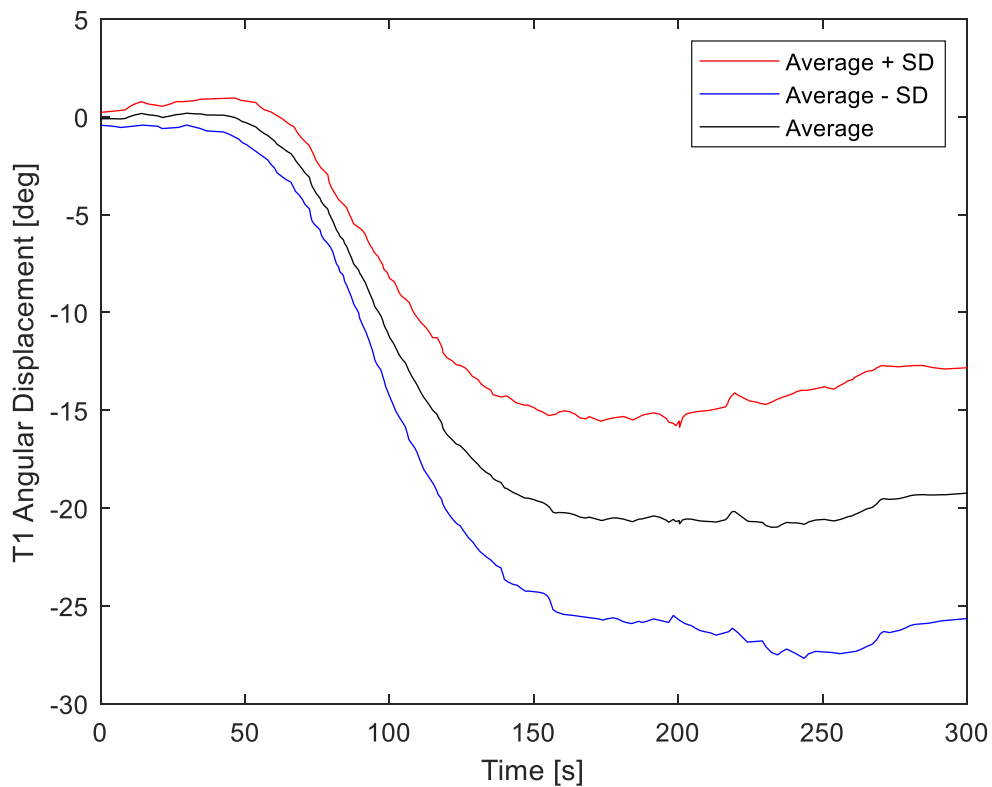
Figure 4.29 T1 angular displacement vs.. time (interpolated).

These digitized and interpolated graphs coincide with the graphs obtained from the reference [7], which means that the digitization and interpolation processes were successful. At this point, since the data to be used in the next stage are the average values of the graphs, these average values were exported and stored to be used in the next stage.

4.5. Development of Inverse Dynamics Equations

In the analysis of the head, C1-C7 vertebrae and T1 vertebrae to find the potential energy in model was stated that each body has its own coordinate system and in addition to this, there is a world coordinate system. Similar to this situation, in this section there are two coordinate systems used to create the equation.
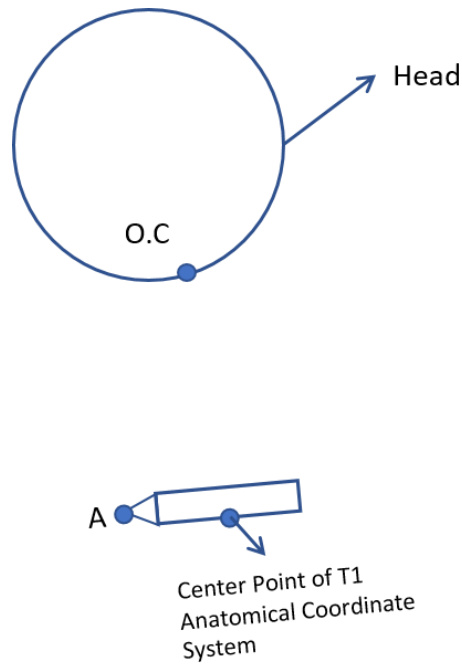
Figure 4.30 Position of head and T1 in inertial coordinate frame.

Point A in Figure 4.30 is the T1 spinous process point, which is the dorsal extension of the T1 vertebra in the volunteer experiments, and this point can be seen as "T1 skin film target and accelerometer" in Figure 2.9. At the T1 spinous process point, accelerometers are placed on its x and z axes in the volunteer experiments and these accelerometers measure the total acceleration of T1 with respect to the ground in its own coordinate system. These measurements are shown in Figure 4.31.
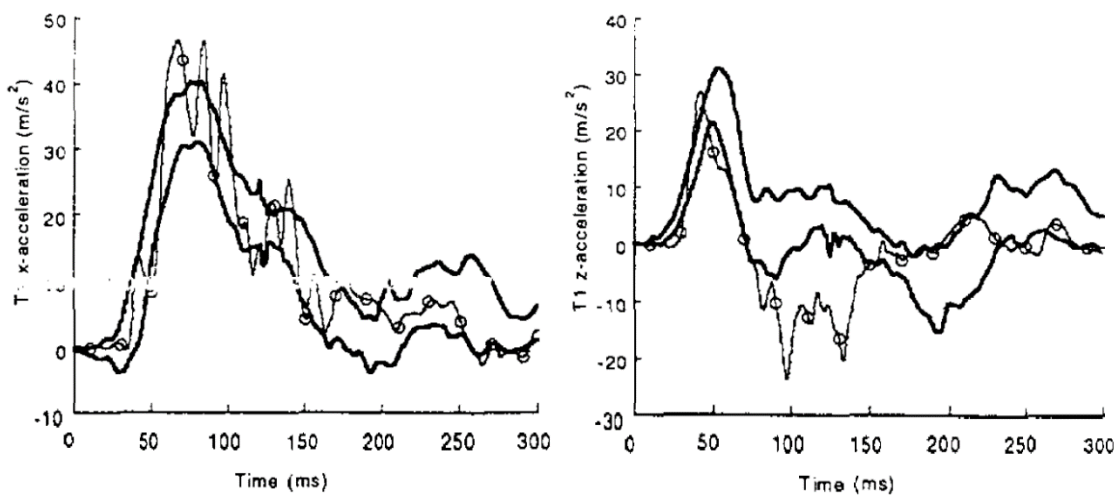
Figure 4.31 Measured T1-x and T1-z accelerations vs.. time [7].

Using accelerometer and some video analysis, the displacement of the O.C. with respect to T1 was measured and these are graphically represented in the reference [7] as shown in Figure 4.21 and Figure 4.22. In addition, these graphs were digitized and interpolated as shown in Figure 4.26 and Figure 4.27.

The process to be done at this stage will be to calculate the muscle forces that will provide these movements given the total acceleration of O.C. with respect to the ground and the total acceleration of T1 with respect to the ground.

The inertial coordinate frame shown in Figure 4.30 is actually the coordinate system on the ground, which rotates with the earth but is considered fixed. The axes of the inertial coordinate frame are shown in Figure 4.30, but MSC VisualNastran 4D's x and z axes are different from the inertial coordinate frame. For this reason, we first worked on the axis where the experiment was performed and then transferred it to model in MSC VisualNastran 4D in accordance with its own coordinate system.
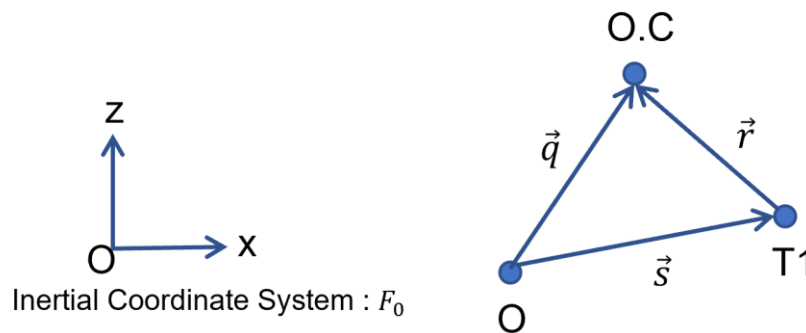

Figure 4.32 Inertial coordinate frame and vector triangle.

The inertial coordinate frame is called F_o, which stands for zero frame. A vector triangle is formed between point O, the center of the inertial coordinate frame, point O.C. and T1. Within this vector triangle, the equation q = r + s can be established. When it is desired to express this equation in the inertial coordinate frame, the equation is given by (4.60) below.

$$\bar{q}^{(0)} = \bar{s}^{(0)} + \bar{r}^{(0)} \tag{4.60}$$

When time is zero, the anatomical coordinate system of T1 and the inertial coordinate frame are on the same axis, but in Figure 4.33 the components of point A are at an angle with the anatomical coordinate system of T1 and the inertial coordinate frame. There is an angle value of 17 degrees between the T1 anatomical coordinate system and the component of point A on the x-axis and this value is constant. This is shown in Figure 4.33.
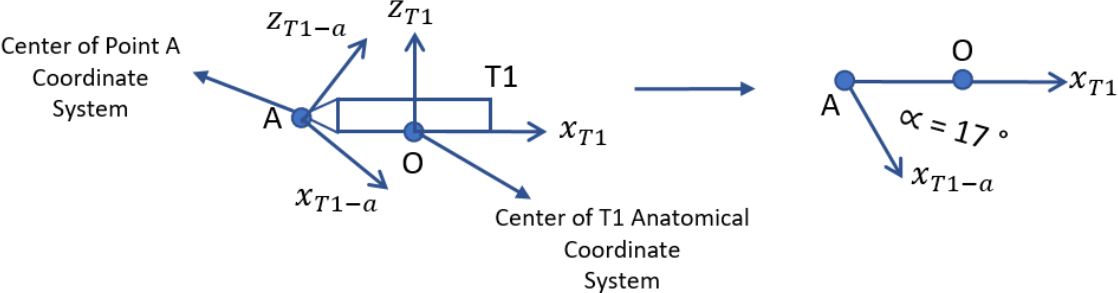
Figure 4.33 Angle between x axis of point A and x axis of T1 anatomical coordinate system.

The components of the T1 anatomical coordinate system and the inertial coordinate frame are shown in Figure 4.34. In Figure 4.34, the axis denoted by 1 is the x-axis and the axis denoted by 3 is the z-axis.
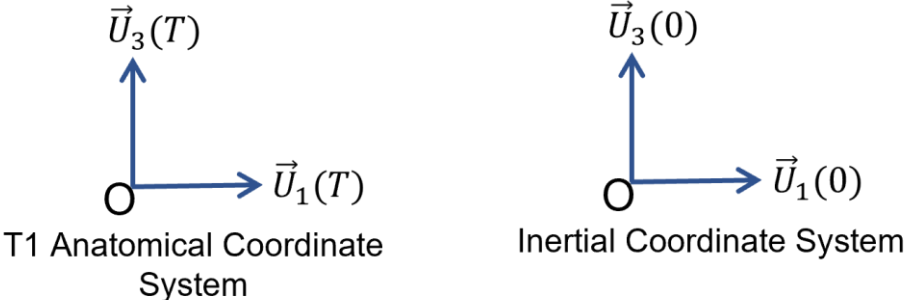
Figure 4.34 Components of T1 Anatomical Coordinate Frame and Inertial Coordinate System.

When we decompose equation (4.60) into its components, the resulting equation is given by equation (4.61). Equation (4.61) expresses the components of the q, s and r vectors in the inertial coordinate frame.

$$\vec{q} = q_1.\vec{U}_1^{(0)} + q_3.\vec{U}_3^{(0)} \tag{4.61}$$

$$\vec{s} = s_1.\vec{U}_1^{(0)} + s_3.\vec{U}_3^{(0)}$$

$$\vec{r} = r_1.\vec{U}_1^{(0)} + r_3.\vec{U}_3^{(0)}$$

At time zero, O.C. is in a specific position relative to T1 and their position relative to each other is numerically known because the position of O.C. and T1 relative to each other at time zero can be obtained from the head and neck model in MSC VisualNastran 4D. The position of O.C. relative to T1 at time zero is represented by the vector r, which is written in the anatomical coordinate system T1. The components of this vector r in the T1 anatomical coordinate system are given in equation (4.62). This situation is shown in Figure 4.37 for representation.

Figure 4.35 The representation of position of O.C. relative to T1 at time is equal to zero.

$$\vec{r}^{(T)} = r_{10}.\vec{U}_1 + r_{30}.\vec{U}_3 \tag{4.62}$$

Where,

$$r_{10} = -6.7184 \ mm$$
$$r_{30} = 130.74 \ mm$$

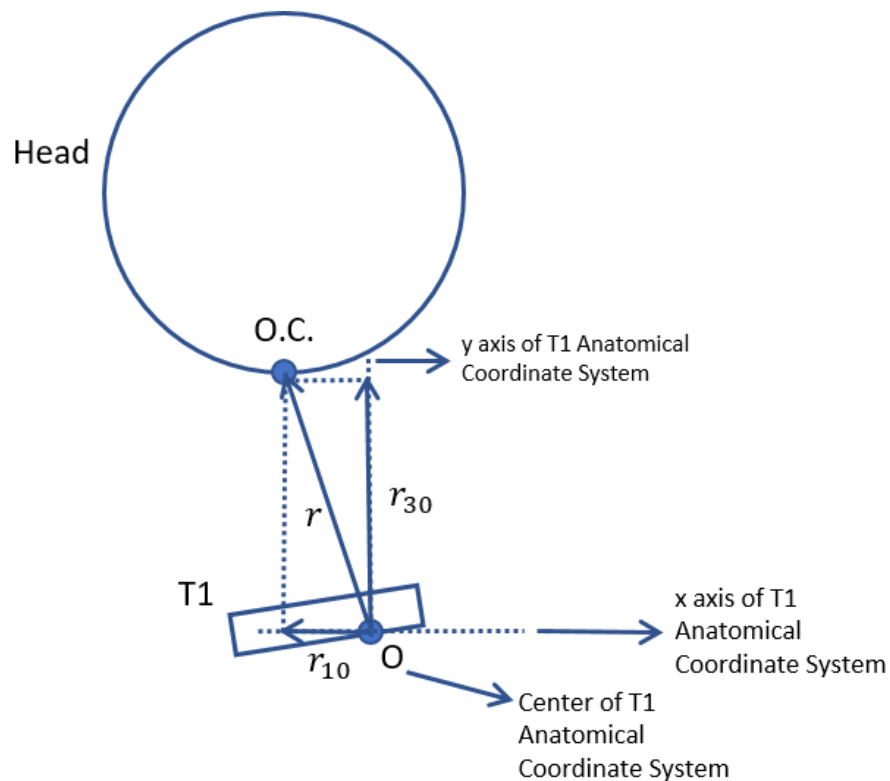The coordinate system of the digitized plots of reference [7] is the T1 anatomical coordinate system. It was mentioned that O.C. is in a certain position relative to T1 when time is zero, but in these plots, the position of O.C. in x and z directions relative to T1 is taken as zero, that is, the graph is subtracted from its initial value and plotted as such. Therefore, when defining the r vector in the T1 anatomical coordinate system, it is necessary to add the x and z components of the position of O.C. at time zero. The resulting equation is given in equation (4.63).

$$\bar{r}^{(T)} = (r_{1n} + r_{10}).\vec{U}_1 + (r_{3n} + r_{30}).\vec{U}_3 \tag{4.63}$$

In equation (4.63) r_{1n} and r_{3n} vectors are Occipital condyle relative to T1-x displacement and Occipital condyle relative to T1-z displacement and these are points of average curves in Figure 4.26 and Figure 4.27.

Since the aim of this section is to describe the motion of O.C. according to the inertial coordinate frame, it is necessary to multiply the vector r by the transformation matrix and convert it from the T1 anatomical coordinate frame to the inertial coordinate frame. The transformation matrix describes the rotation that occurs when transforming the inertial coordinate frame into the T1 anatomical coordinate frame. The amount of this rotation is defined by the θ angle and is shown visually in Figure 4.36.
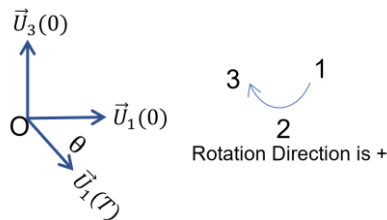

Figure 4.36 Transformation of T1 anatomical coordinate frame to inertial coordinate frame.

50

The value of the θ angle is also a given value and is equal to the T1 angular displacement in Figure 4.29. The equations obtained from the translation of the vector r defined in the anatomical coordinate system T1 into the inertial coordinate frame are given below.

$$\bar{r}^{(0)} = \hat{C}^{(0,T)}.\bar{r}^{(T)} \tag{4.64}$$

$$\hat{C}^{(0,T)} = e^{\widetilde{u_2}\theta} \tag{4.65}$$

The components of the vector r defined in the inertial coordinate frame are given in the following equations.

$$\bar{r}^{(0)} = e^{\widetilde{u_2}\theta}.[\,(r_{1n} + r_{10}).\vec{U}_1 + (r_{3n} + r_{30}).\vec{U}_3] \tag{4.66}$$

$$\bar{r}^{(0)} = (r_{1n} + r_{10}).(\vec{U}_1 cos\theta - \vec{U}_3 sin\theta) + (r_{3n} + r_{30}).(\vec{U}_3 cos\theta + \vec{U}_1 sin\theta) \tag{4.67}$$

$$\bar{r}^{(0)} = \vec{U}_1[(r_{1n} + r_{10}).cos\theta + [(r_{3n} + r_{30})).sin\theta] + \vec{U}_3[-(r_{1n} + r_{10}).sin\theta + [(r_{3n} + r_{30})).cos\theta] \tag{4.68}$$

As an expression.

$$(r_{1n} + r_{10}) = R_1 \tag{4.69}$$

$$(r_{3n} + r_{30}) = R_3$$

When the first derivative of equation (4.68) is taken, the velocity vector defined in the inertial coordinate frame is obtained and the second derivative of equation (4.68) is given acceleration vector. Obtained equations are given below.

$$\bar{V}^{(0)} = \vec{U}_1.\left[\dot{r}_{1n}.cos\theta - R_1.\dot{\theta}.sin\theta + \dot{r}_{3n}.sin\theta - R_3.\dot{\theta}.cos\theta\right] + \vec{U}_3.\left[-\dot{r}_{1n}.sin\theta - R_1.\dot{\theta}.cos\theta + \dot{r}_{3n}.cos\theta - R_3.\dot{\theta}.sin\theta\right] \tag{4.70}$$

$$\bar{a}^{(0)} = \vec{U}_1. [\; \ddot{r}_{1n}. cos\theta - \dot{r}_{1n}. \dot{\theta}. sin\theta + \cdots \qquad (4.71)$$

Here,

$$\dot{R}_1 \quad = \quad \dot{r}_{1n}$$

$$\ddot{R}_1 \quad = \quad \ddot{r}_{1n}$$

$$\dot{R}_3 \quad = \quad \dot{r}_{3n}$$

$$\ddot{R}_3 \quad = \quad \ddot{r}_{3n}$$

$$\bar{r}^{(0)} \quad = \quad \bar{V}_0^{\;(0)}$$

$$\ddot{\bar{r}}^{(0)} \quad = \quad \bar{a}^{(0)}$$

As seen in equation (4.71), when the second order derivative of the vector r defined in the inertial coordinate frame is taken, the resulting equation is too long to be solved. Therefore, this equation is solved numerically.

$$\ddot{q}_1 = \ddot{s}_1 + \ddot{r}_1 \qquad (4.72)$$

$$\ddot{q}_3 = \ddot{s}_3 + \ddot{r}_3$$

Equation (4.72) is defined in the inertial coordinate frame. According to this equation, $\ddot{s}_1$, $\ddot{s}_3$, $\ddot{r}_1$ and $\ddot{r}_3$ are required to obtain $\ddot{q}_1$ and $\ddot{q}_3$, r_1 and r_3 are Occipital condyle with respect to T1-x displacement and Occipital condyle with respect to T1-z displacement and these are points of average curves in Figure 4.26 and Figure 4.27. To find $\ddot{q}_1$ and $\ddot{q}_3$, it is necessary to numerically take second order derivatives of r_1 and r_3. $\ddot{s}_1$ and $\ddot{s}_3$ are included as graphics in the head and neck model in MSC VisualNastran 4D. Digitization and interpolation were also performed for this graph.
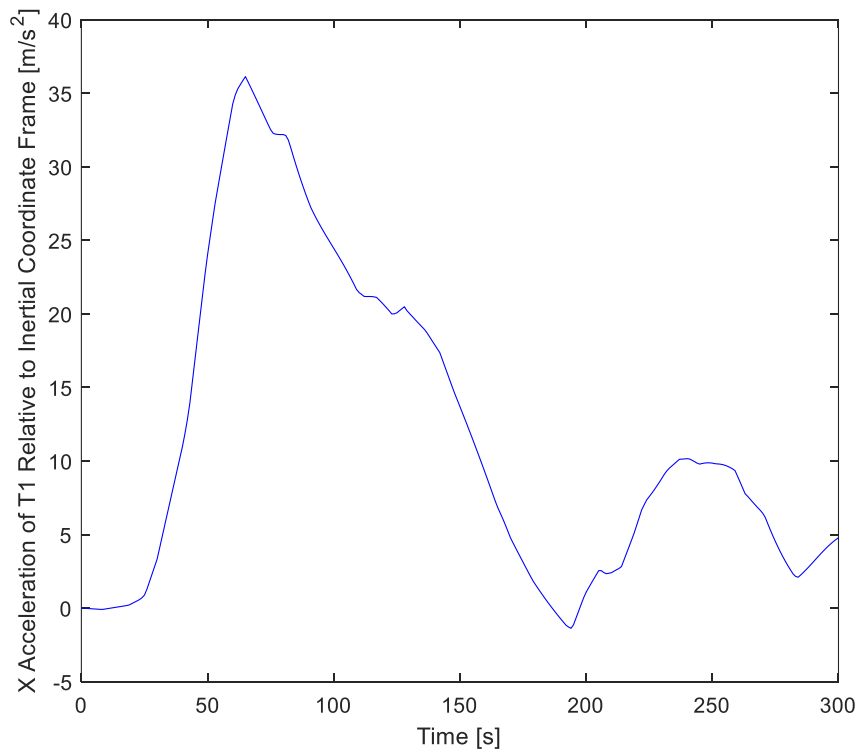
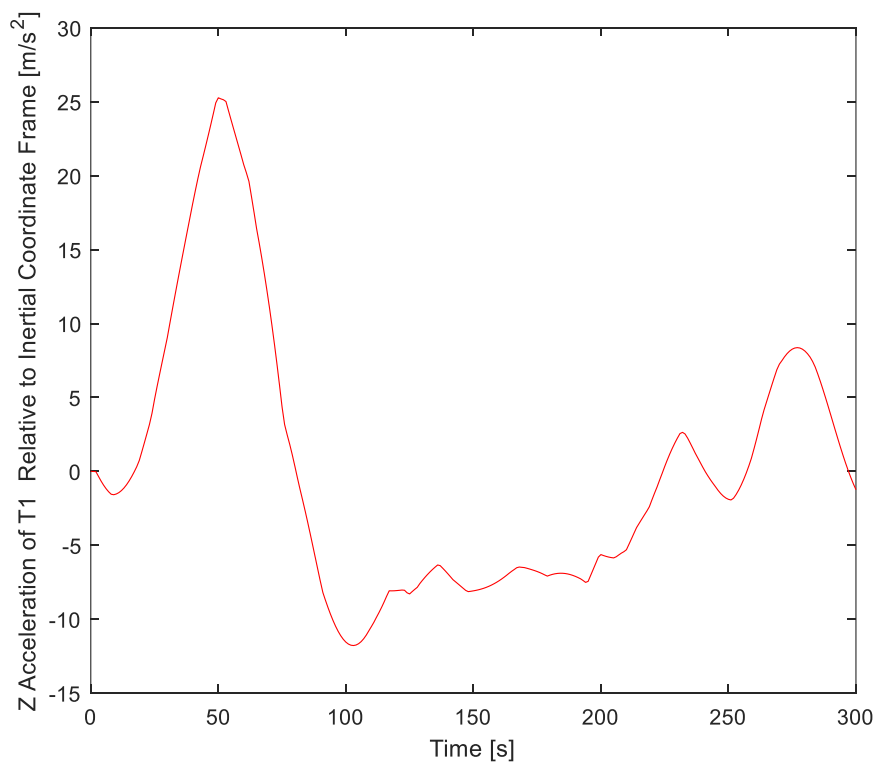Figure 4.37 X acceleration of T1 with respect to inertial coordinate frame vs. time ($\ddot{s}_1$).

Figure 4.38 Z acceleration of T1 with respect to inertial coordinate frame vs. time ($\ddot{s}_3$).

53

One of the important points here is that the q vector describes the motion of the head in the translational axis, but in addition to this, there is also a rotational motion of the head, and this also needs to be calculated. The equation used in this calculation is given below as equation (4.73).

$$\theta_{hT} = \theta_h - \theta_T \qquad (4.73)$$

$$\theta_h = \theta_{hT} + \theta_T$$

Here,

θ_{hT} $=$ *Head rotation with respect to T*1

θ_T $=$ *T*1 *rotation with respect to inertial coordinate frame*

θ_h $=$ *Head angle with respect to inertial coordinate frame*

In here, θ_{hT} is Figure 4.28 and which is head with respect to T1 angular displacement plot. θ_T is equal to Figure 4.29 which is T1 angular displacement. θ_{hT} is therefore easily found. Then the second order derivative was taken numerically.

Equation (4.69) and (4.72) were solved numerically with the code written in MATLAB. In the MATLAB code, firstly the r_{1n}, r_{3n} and θ values written in equation (4.68) were plotted. It was mentioned before that r_{1n} is O.C. with respect to T1 average x Displacement (average curve in Figure 4.26), r_{3n} is O.C. with respect to T1 average z Displacement (average curve in Figure 4.27) and θ is T1 angular displacement (average curve in Figure 4.28).
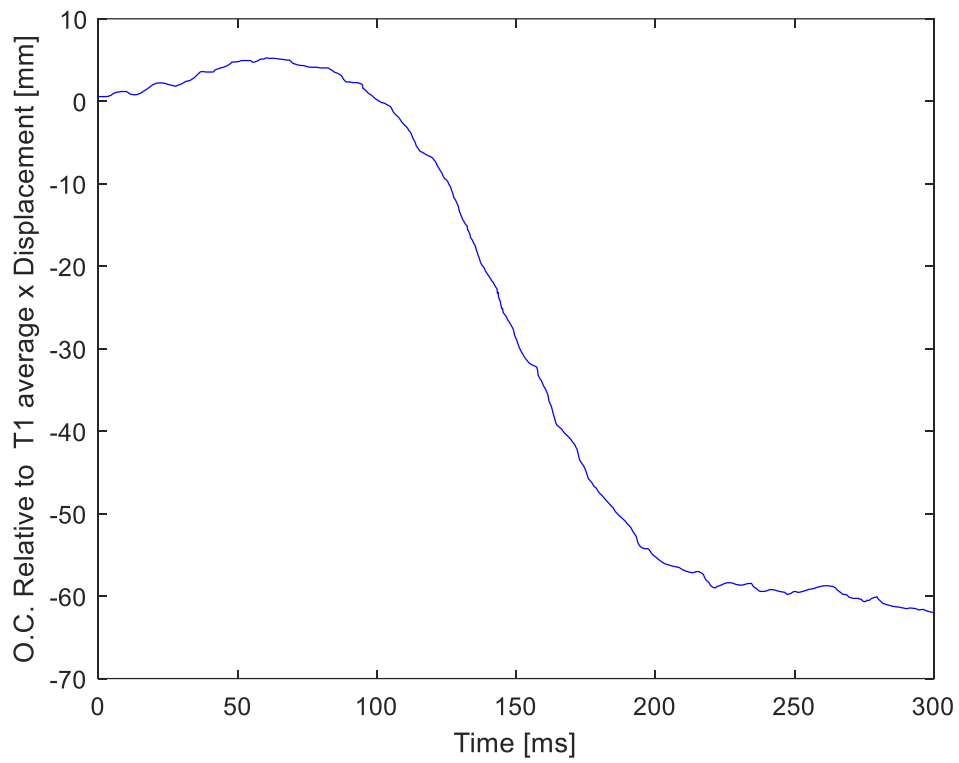
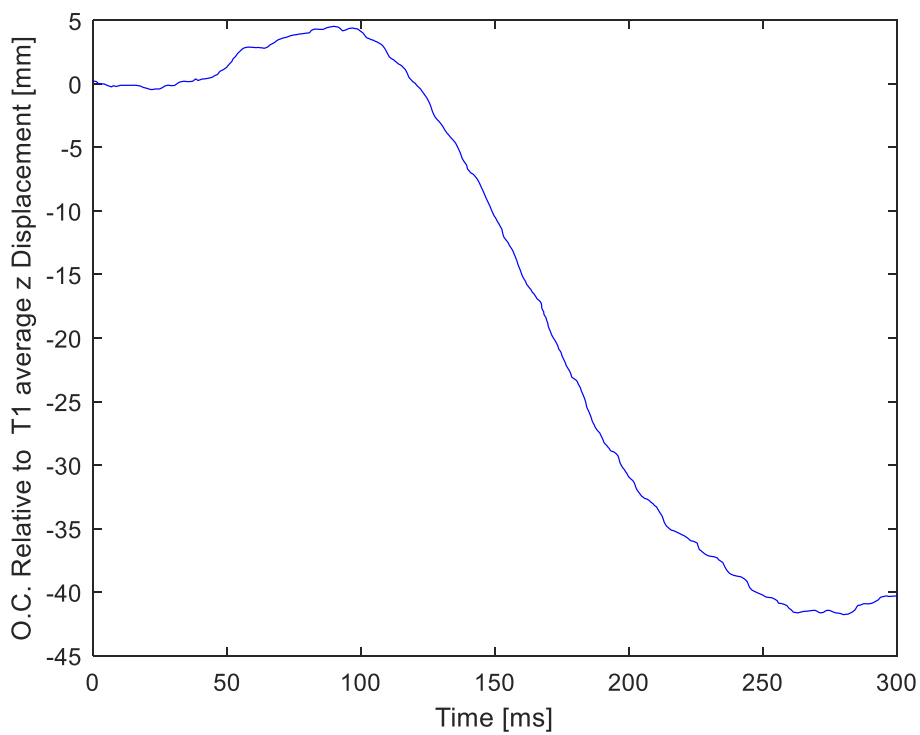Figure 4.39 O.C. with respect to T1 average x Displacement (r_{1n}).

Figure 4.40 O.C. with respect to T1 average z Displacement (r_{3n}).

Figure 4.41 T1 rotation (θ).

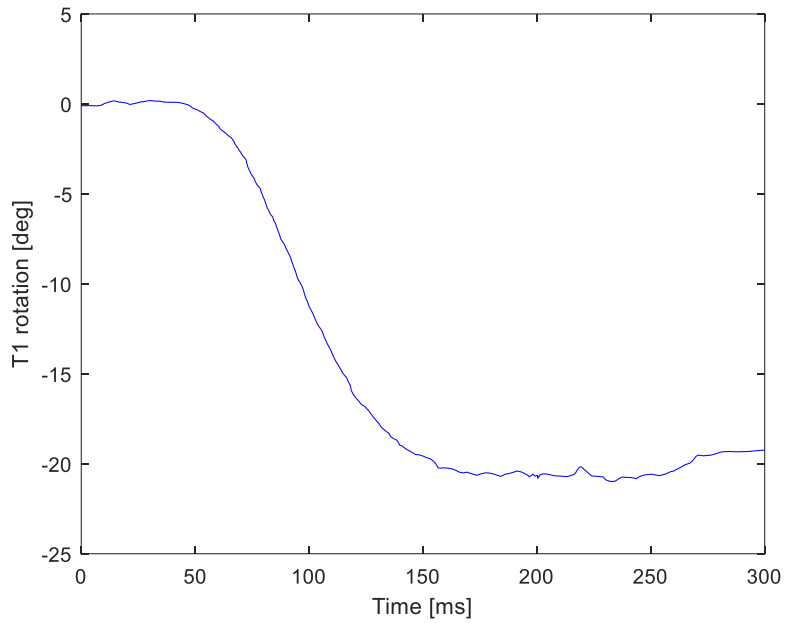The two components of the vector r in the inertial coordinate frame, R_1 and R_3, were calculated and plotted separately in MATLAB since they define all the data required to calculate Equation (4.68). Here the θ angle is converted to radians and displacements are written in meters.

Figure 4.42 O.C. with respect to T1 vector x Position in Inertial Coordinate Frame vs. time (R_1).

Figure 4.43 O.C. with respect to T1 vector z Position in Inertial Coordinate Frame vs. time (R_3).

Then not a knot cubic spline fitting was performed to take the second order derivative of R_1 and R_3.

Figure 4.44 Fitted cubic spline of O.C. with respect to T1 vector x position in Inertial Coordinate Frame vs. time data.
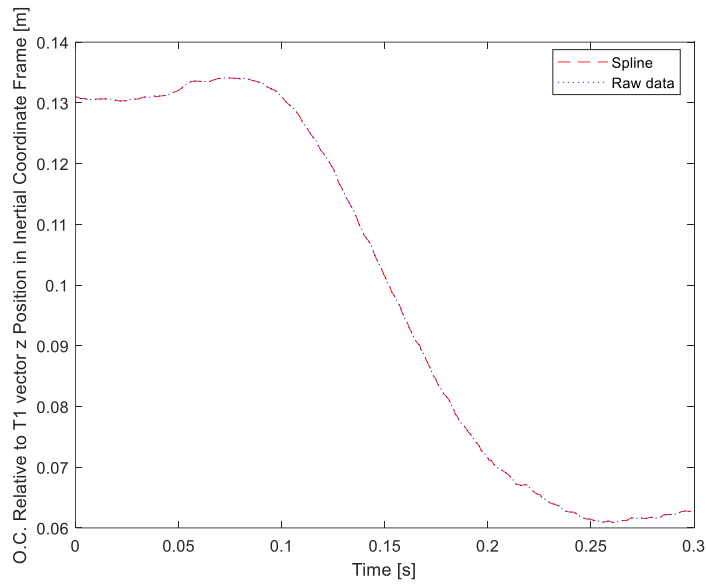
Figure 4.45 Fitted cubic spline to O.C. with respect to T1 vector z position in Inertial
Coordinate Frame vs. time data.

As can be seen in Figure 4.45 and Figure 4.46, the fitted cubic spline and the raw data match exactly. In the next process, the second order derivative of this fitted cubic spline was taken and the acceleration of the O.C. in x and z directions in the inertial coordinate frame with respect to the T1 vector was calculated. After the calculation, the result was filtered to remove misleading data.
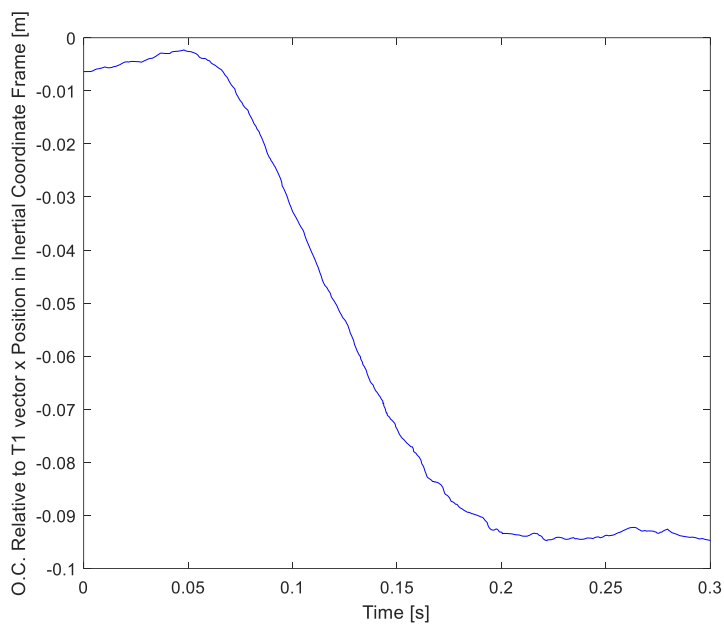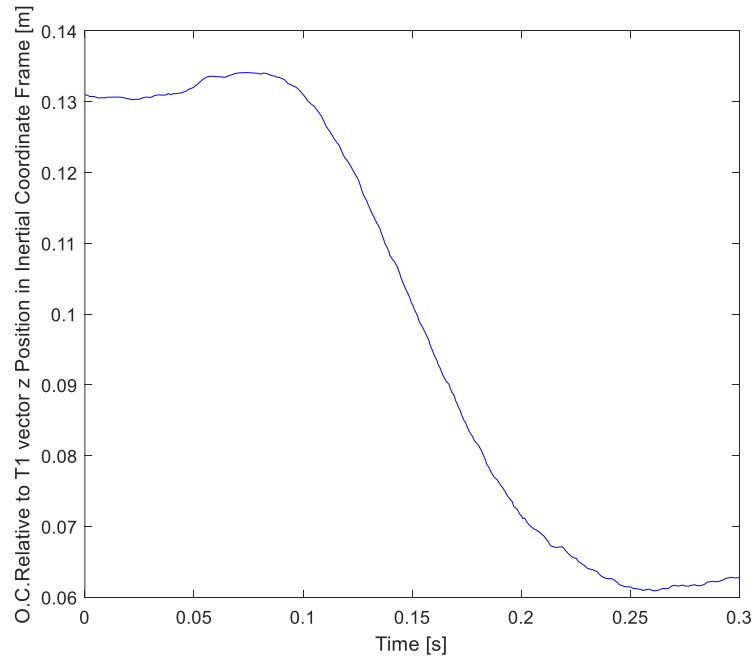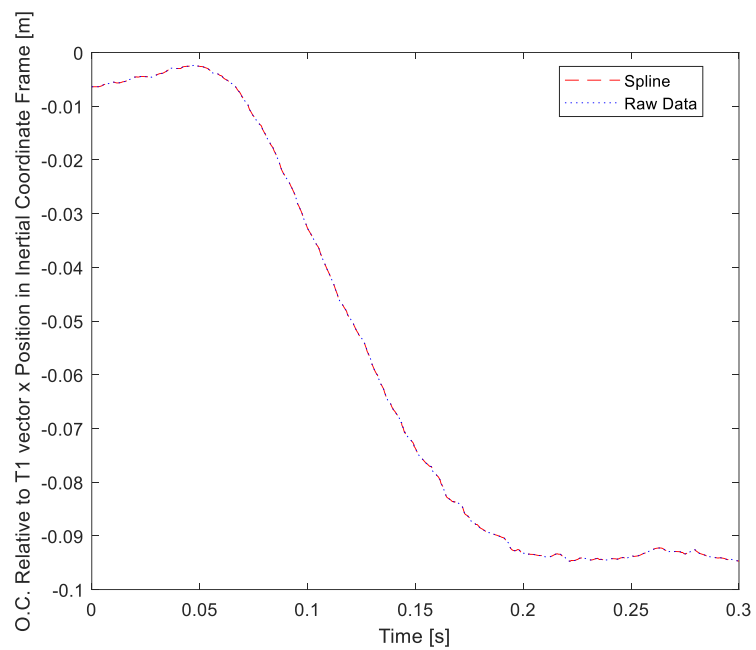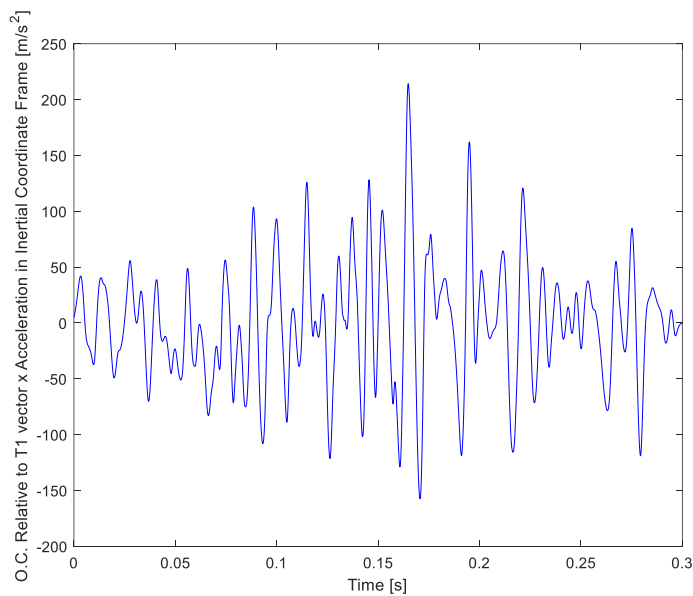

Figure 4.46 O.C. with respect to T1 vector x acceleration in inertial coordinate
frame ($\ddot{R}_1$).
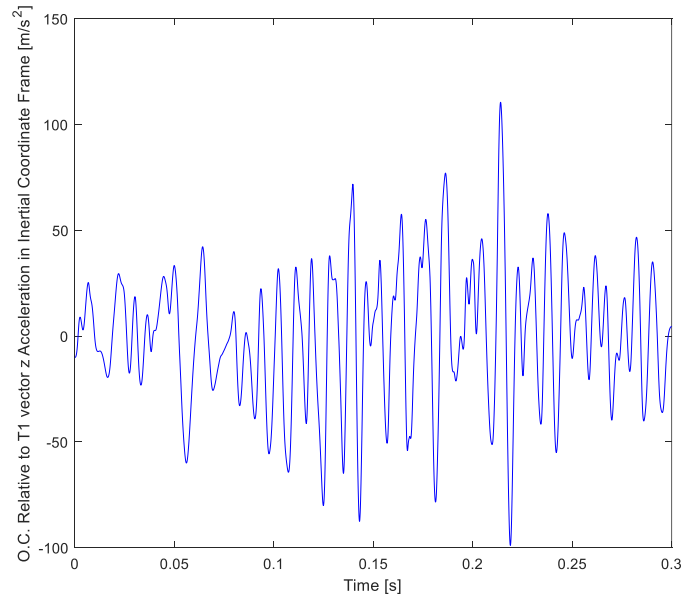
Figure 4.47 O.C. with respect to T1 vector z acceleration in inertial coordinate frame ($\ddot{R}_3$).

To find the angular acceleration of T1, it is necessary to find the second derivative of T1 rotation (θ). For this, first a not a knot cubic spline is fitted to T1 rotation and then the angular acceleration of T1 is calculated in inertial coordinate frame by taking its second order derivative.
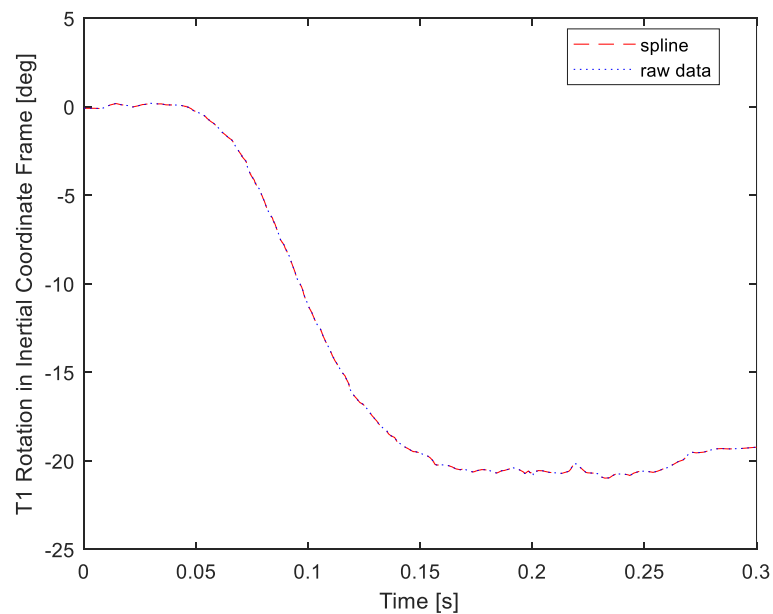
Figure 4.48 Fitted cubic spline to T1 Rotation in Inertial Coordinate Frame vs. time data.

59
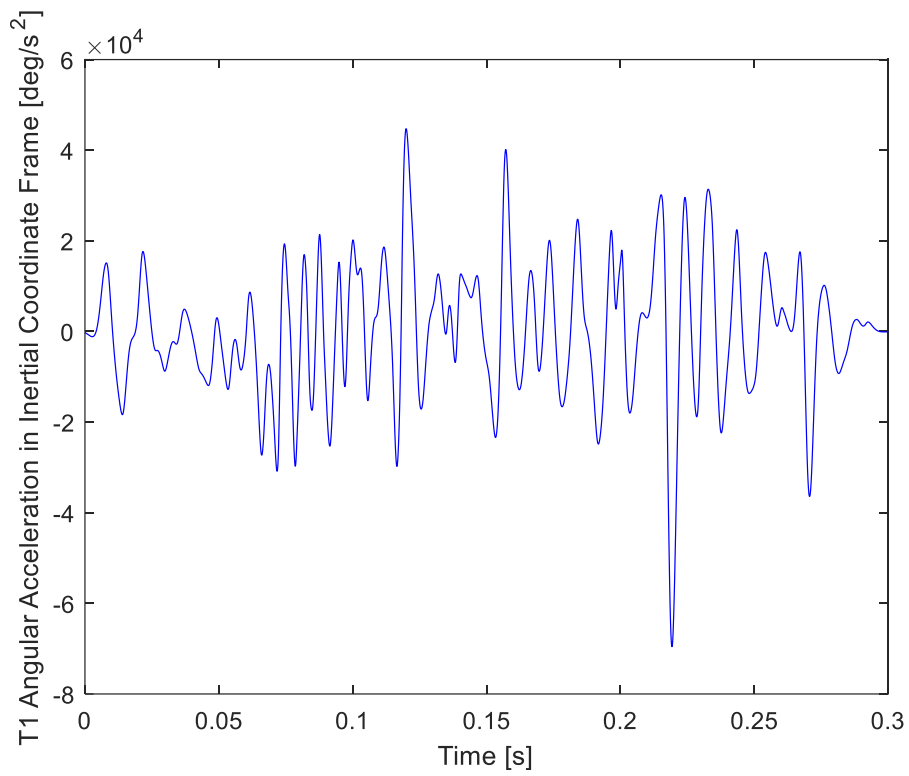
Figure 4.49 T1 angular acceleration in inertial coordinate frame in deg/s^2 ($\ddot{\theta}$).
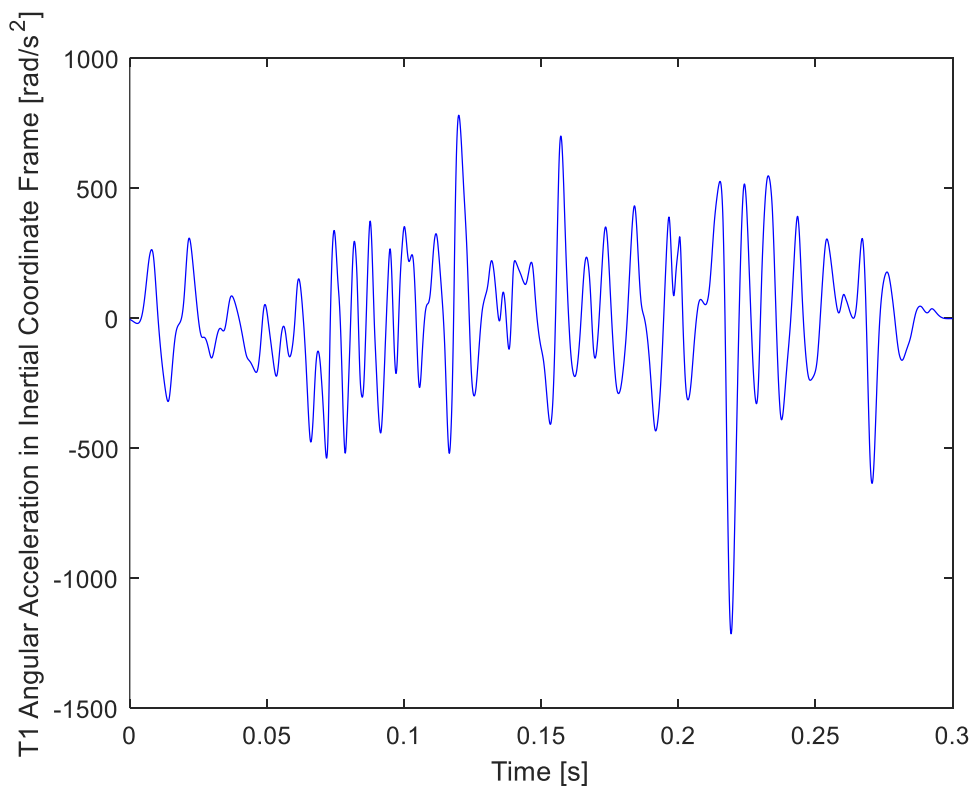
Figure 4.50 T1 angular acceleration in inertial coordinate frame in rad/s^2 ($\ddot{\theta}$).

The data required to find the $\ddot{q}_1$ and $\ddot{q}_3$ vectors in equation (4.69), are prepared. To calculate these vectors, vector summation was done in MATLAB and the result was found.
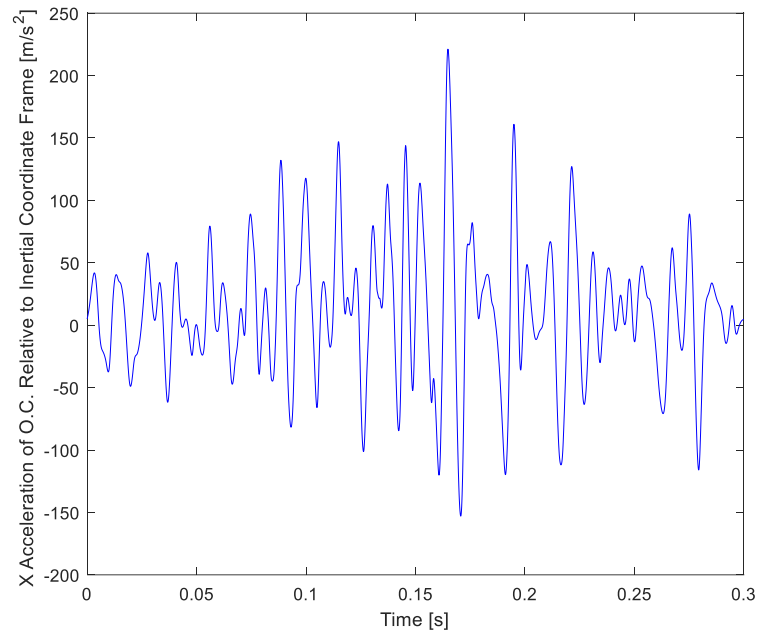
Figure 4.51 Acceleration of O.C. with respect to inertial coordinate frame$(\ddot{q}_1)$ in x axis.
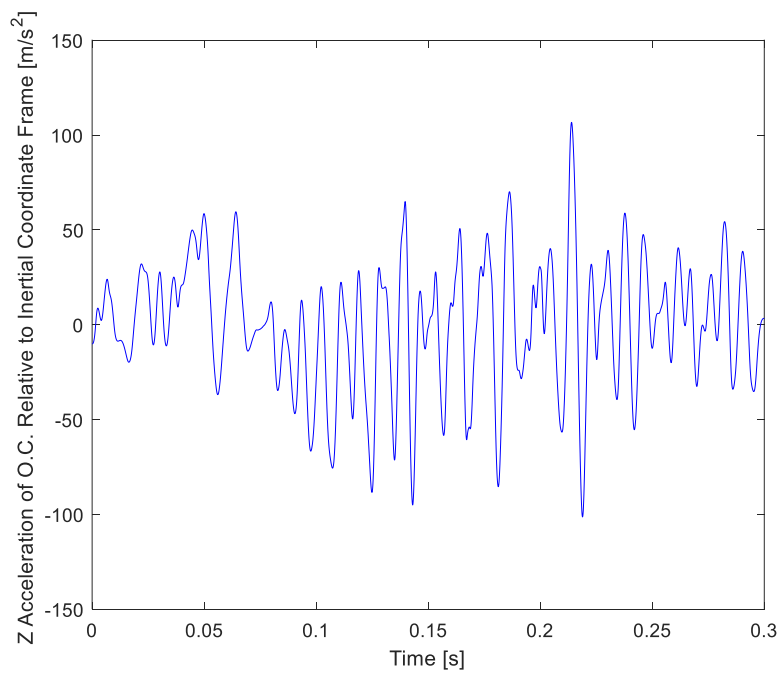
Figure 4.52 Acceleration of O.C. with respect to inertial coordinate frame$(\ddot{q}_3)$ in z axis.

4.6. Implementation of Muscles to Model

As stated in the aim of the thesis, muscles belonging to specific muscle groups need to be implemented for the thesis study to be a source for new rear impact test dummies to be produced in the future. At this point, the muscles implemented in the model are the sternocleidomastoid muscle on both sides of the head, the flexor muscle in the front and the extensor muscle in the back.

The disadvantage of implementing muscles to model is that it is not possible to determine exactly where the muscles are attached. In the literature search about this subject, an article was found that could supply information about the positions of the muscles to be implemented to the head and neck model.

In the study by Borst et al [17]; they obtained information such as length, weight, origin and insertion positions of the muscles with help of placed sensors on muscles on the cadaver.

The muscles to be implemented in this thesis study were selected from the study of van der Horst [15]. According to van der Horst [15], the muscles to be implemented are lumped hyoid, splenius capitis and sternocleidomastoid muscles. In the study of Borst et al [17], these muscles are included as muscle groups. For this reason, the most visually similar muscles and the muscles with the highest weight and length were selected among these muscle groups.

As a result, splenius [24], sternohyoid [25] and sternocleidomastoid [26] muscles are the muscles that most closely represent the muscles to be inserted in this thesis.
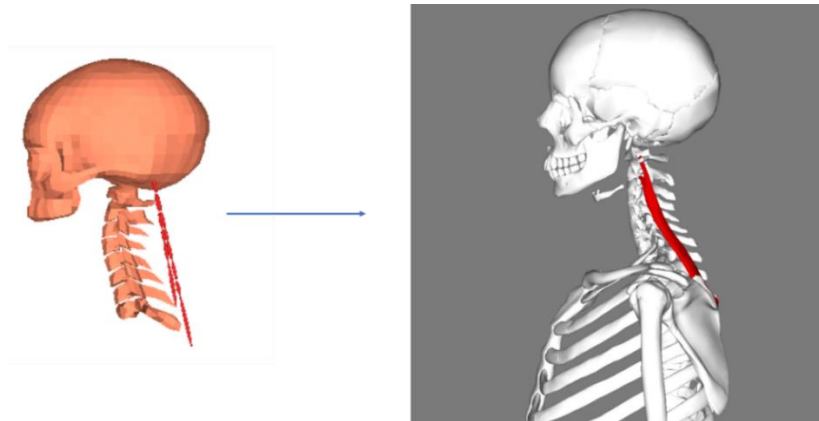
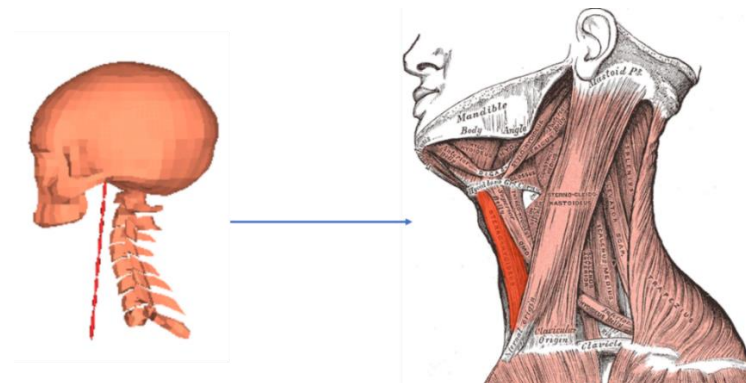Figure 4.53 Splenius muscle implemented to the head and neck model and its anatomical appearance [24].

Figure 4.54 Sternohyoid muscle implemented to the head and neck model and its anatomical appearance [25].
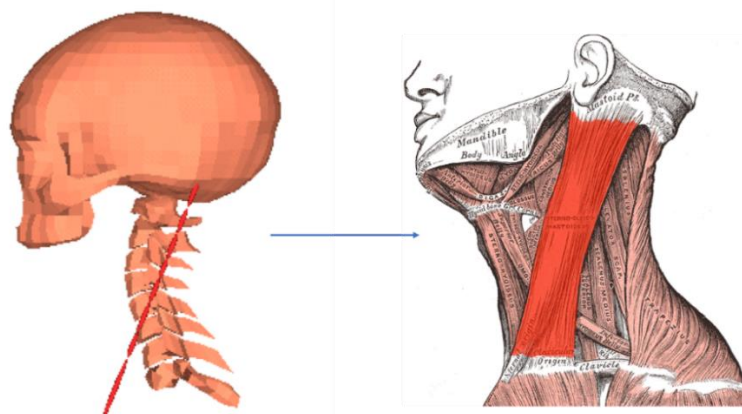

Figure 4.55 Sternocleidomastoid muscle implemented to the head and neck model and its anatomical appearance [26].

These muscles are also included in the study by Borst et al [17]. The data in this study has the necessary information for the implementation of the muscles in the model. However, since these muscles are included in the table as muscle groups, all muscles were implemented to the model to find the muscle connected to the muscle group that best represents the muscles to be implemented. In the study, the positions of the muscles in x, y and z coordinates at the start and end points were given and the coordinate system of the head and neck model did not overlap with the coordinate system in article. The x-axis in the article corresponds to the y-axis in MSC VisualNastran 4D, the y-axis in the article corresponds to the z-axis in MSC VisualNastran 4D and the z-axis in the article corresponds to the x-axis in MSC VisualNastran 4D. In addition, the unit in the article is given as millimeters and the unit in MSC VisualNastran 4D is given as meters, which has also been converted. The last difference between the article and MSC VisualNastran 4D is that the origin of the head in model is not at origin of the world coordinate, so when axes in the article were transferred to MSC VisualNastran 4D, -1.9503 meters were added to the y-axis and -0.031356 meters were added to the z-axis after unit and orientation conversion.

Taking this into account, after the muscles were implemented in the model, residual muscles were removed from the head and neck model, except for the muscles that visually resemble the muscles to be implemented in the thesis study.

The muscles implemented in the thesis only had positions for those on one side of the head only. Therefore, the insertion and origin coordinates of the sternohyoid, splenius and sternocleidomastoid muscles on one side of the head were symmetrized with respect to the 0 point of the coordinate system and these muscles were provided on both sides of the head. To produce these muscles with steel cables as in the BioRID-III dummy, the insertion and origin coordinates of the sternohyoid and splenius muscles, except the sternocleidomastoid muscle, were averaged and reduced to one in the model.

When implementing the muscles to the model, each muscle is designed as a system of two pistons that can move within each other, and in MSC VisualNastran 4D, they are modeled as linear actuators and are shown in Figure 4.56.
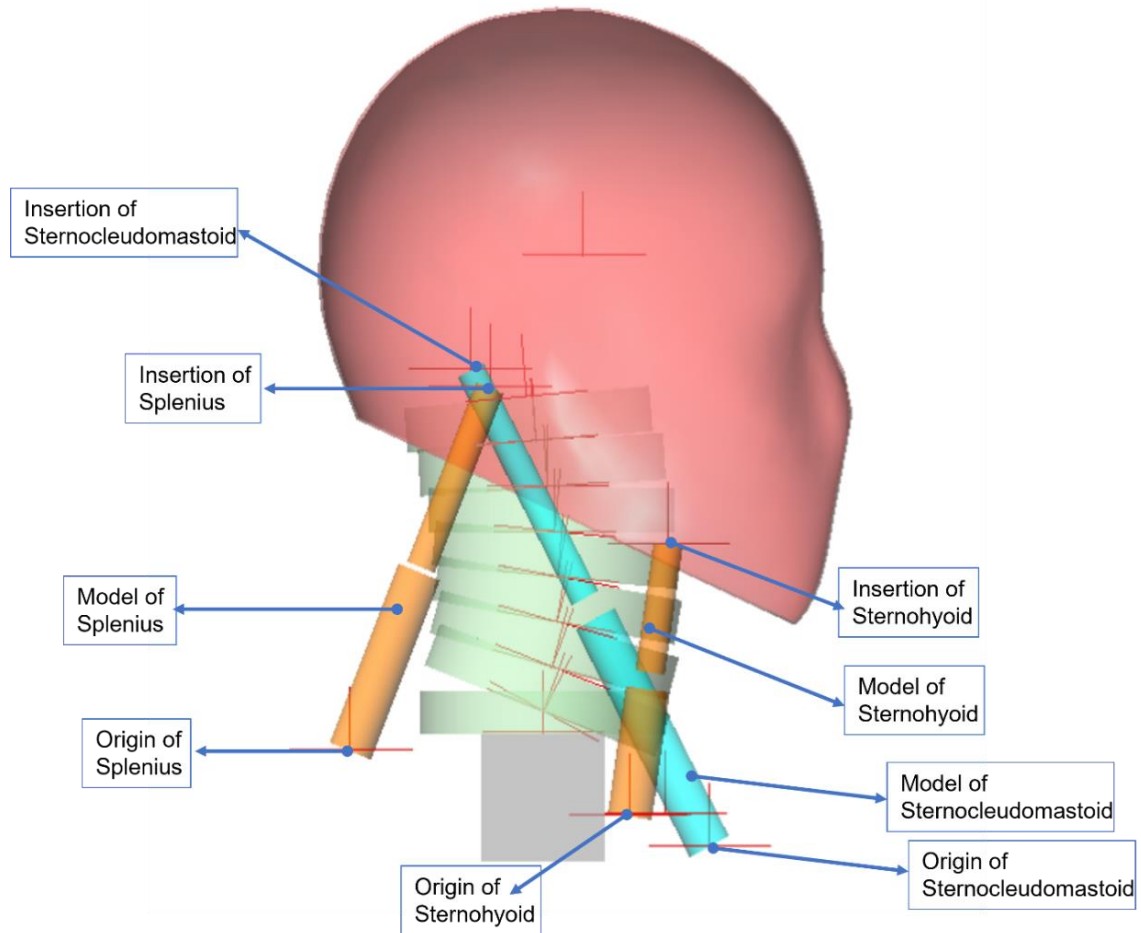
Figure 4.56 The model in Himmetoglu et al. [8] with the implementation of the sternocleidomastoid, splenius and sternohyoid muscles.

4.7. Running of Head and Neck Model Simulation

The motion of O.C. with respect to the inertial coordinate frame and the motion of T1 obtained in the previous section were given as input to the head and neck model in MSC VisualNastran 4D and the simulation was run. As a result of this application, the model did not show behavior in accordance with the voluntary movements of the model and gave an error. The reason for this problem is that these digitized and interpolated volunteer experiment data are averaged and used. Averaging volunteer experiment data may not correspond to a volunteer movement. It is not known whether the average volunteer movement corresponds to any volunteer movement. For this reason, the movement of O.C. in the head and neck model was taken from Himmetoglu et al. [8]'s previously used model, which shows behavior close to volunteer movements. In addition,

the motion of T1 was input to the model as the average motion calculated in this thesis and did not cause any problems in the model.
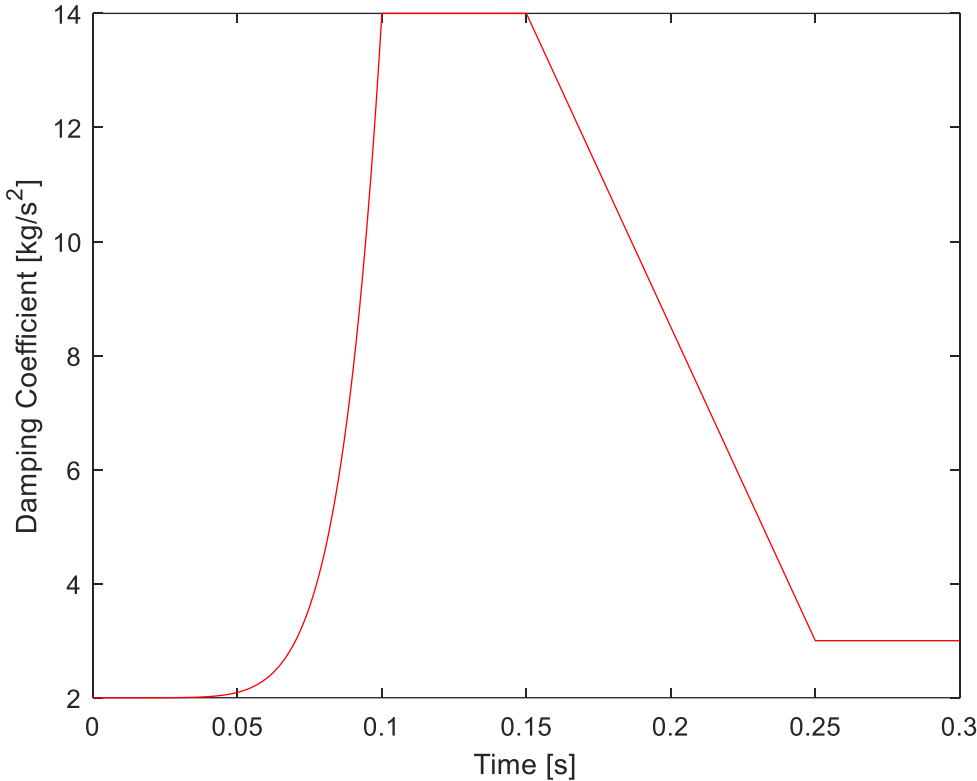

Figure 4.57 Damping coefficient and time graph of Himmetoglu et al. [8] head and neck model.

Figure 4.57 shows that the damping coefficient varies with time. Considering the physical production of the model, a damper should be placed for each of the intervertebral joints so that the damping coefficient can change with time, but this is an inconvenient situation in terms of physical production. For this reason, pistons have been created here as a representation of muscles. When the model is to be physically produced, steel cables will be passed through the pistons that represent the muscles and the end of these steel cables will be connected to a damper in the chest that can apply a time-dependent damping coefficient. In this way, it will be possible for the model to physically provide this movement. This situation allows to control the muscles or to change the effects of the muscles from passive to active and changeable since the dummies are passive elements.

Sternocleidomastoid was implemented as two muscles to the head and neck model. For MSC VisualNastran 4D, having two separate linear actuators as the sternocleidomastoid muscle was a problem when input motions were given to O.C. and T1 and the model did not work properly. The reason for that is that the head and neck model is a planar model with three degrees of freedom and therefore only requires three input elements. Therefore, the sternocleidomastoid muscle was implemented as a single muscle element by averaging the origin and insertion points to create a new origin and insertion coordinate. But in this way, the sternocleidomastoid passes through the vertebrae and this will not be suitable when the model is physically produced. For this reason, when the sternocleidomastoid muscle model is to be produced, it can be produced by creating two copies of the single reduced version in parallel directions. In this way, half of the force on the sternocleidomastoid muscle reduced to one will correspond to the force on the two sternocleidomastoid muscles formed in parallel, and the answer to the question of how it can be produced can be given in this way. Flexor and extensor muscles will also be physically reproduced in the head and neck model, which will be physically reproduced, by making cavities in the vertebrae.
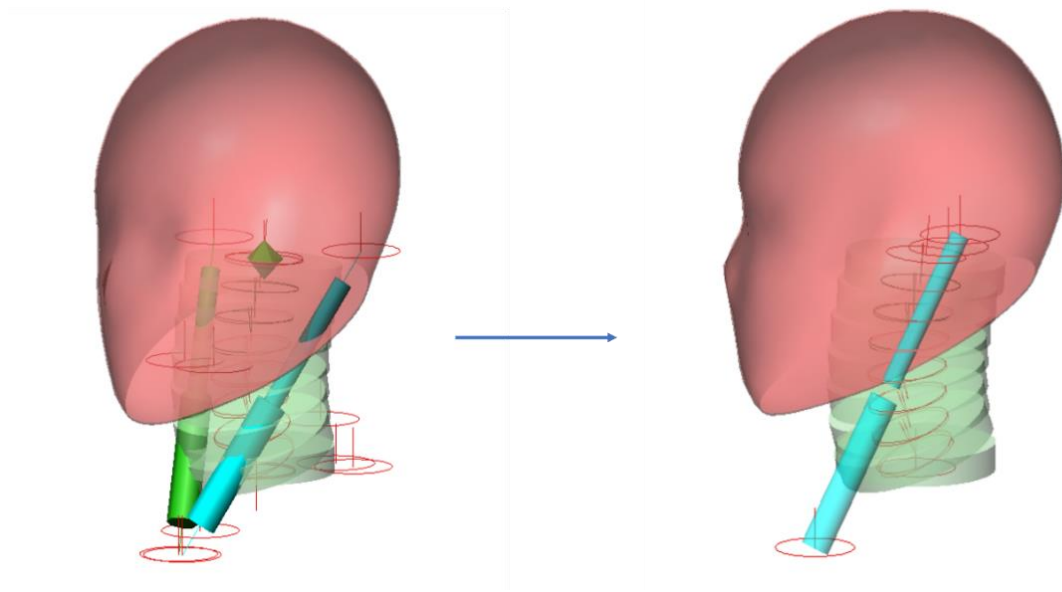

Figure 4.58 Reduction of the sternocleidomastoid muscle to one in a head and neck model.
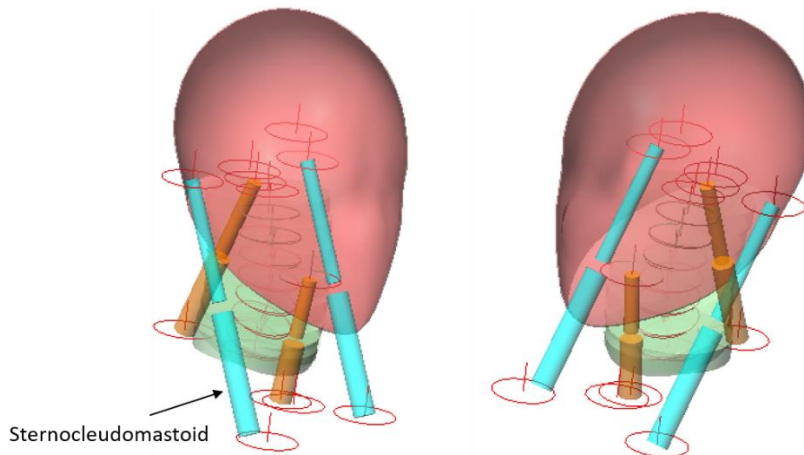
Figure 4.59 Position of the sternocleidomastoid muscles for physical production of the head and neck model.

Then, since the muscle elements are represented as a system consisting of two intertwined pistons, there are two coordinates at the top of the lower piston and two coordinates at the bottom of the upper piston that provide the connection between each other. By adding a meter in MSC VisualNastran 4D, the movement of these two coordinates relative to each other was calculated and the accelerations of the muscles were measured these are given below figure from Figure 4.60 to Figure 4.65.
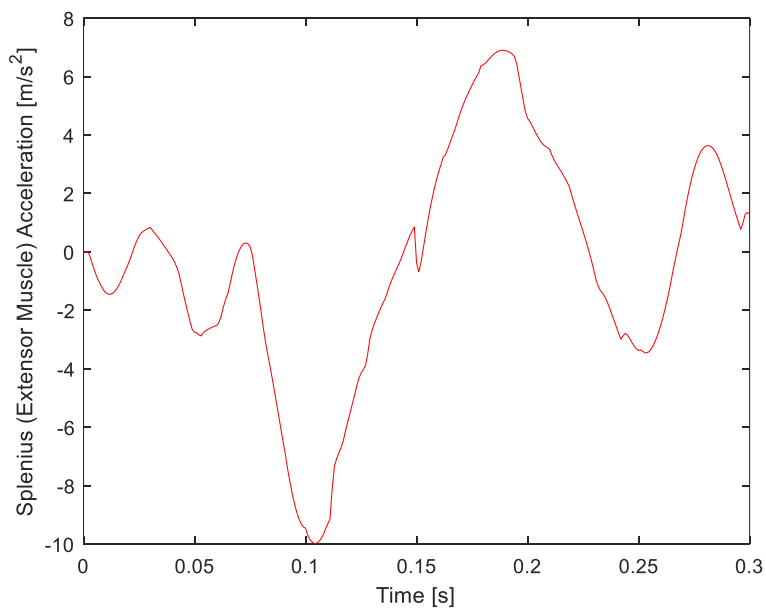

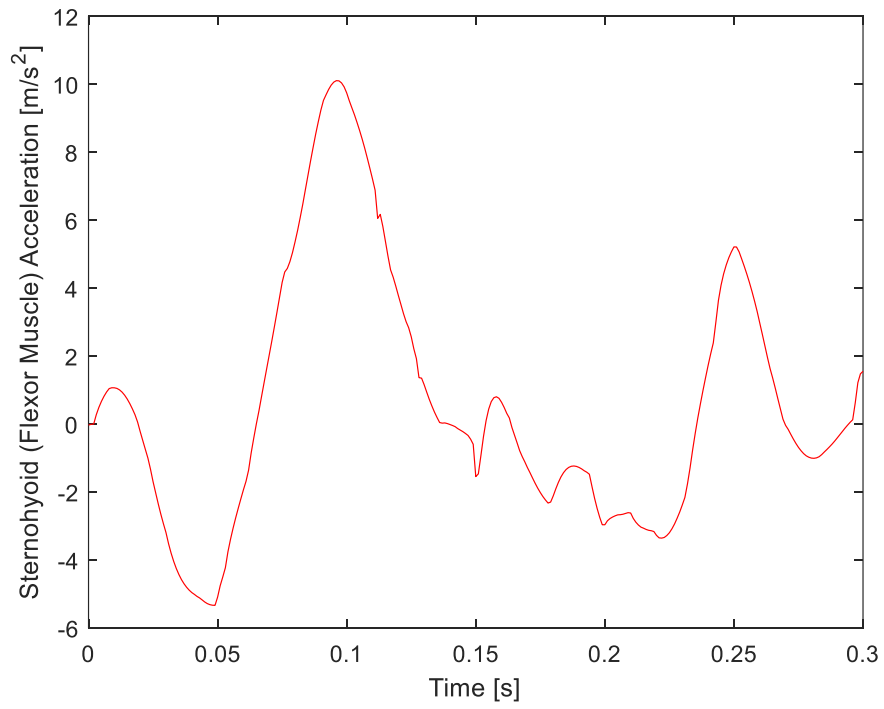Figure 4.60 Splenius (extensor muscle) acceleration graph.

Figure 4.61 Sternohyoid (flexor muscle) acceleration graph.
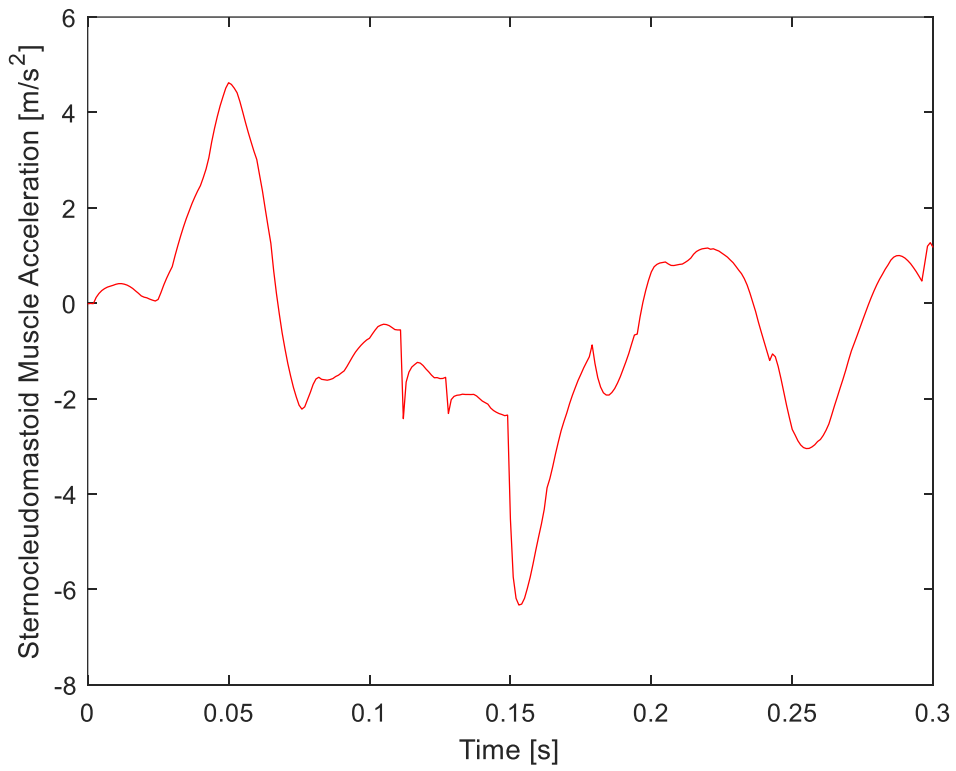

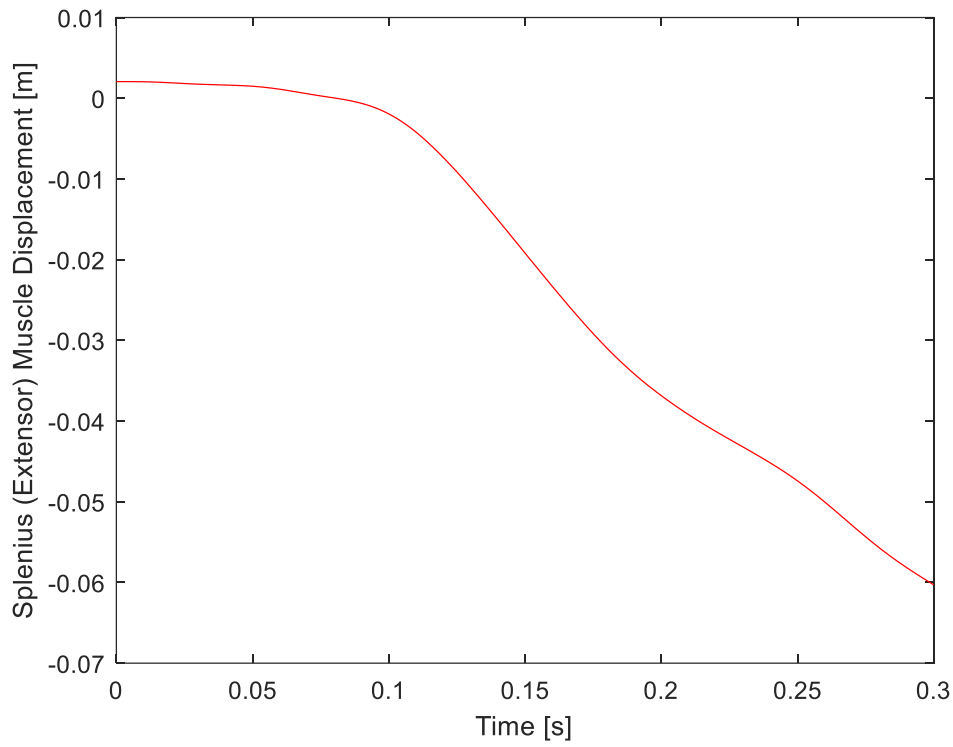Figure 4.62 Sternocleidomastoid acceleration graph.

Figure 4.63 Splenius (extensor muscle) muscle displacement graph.
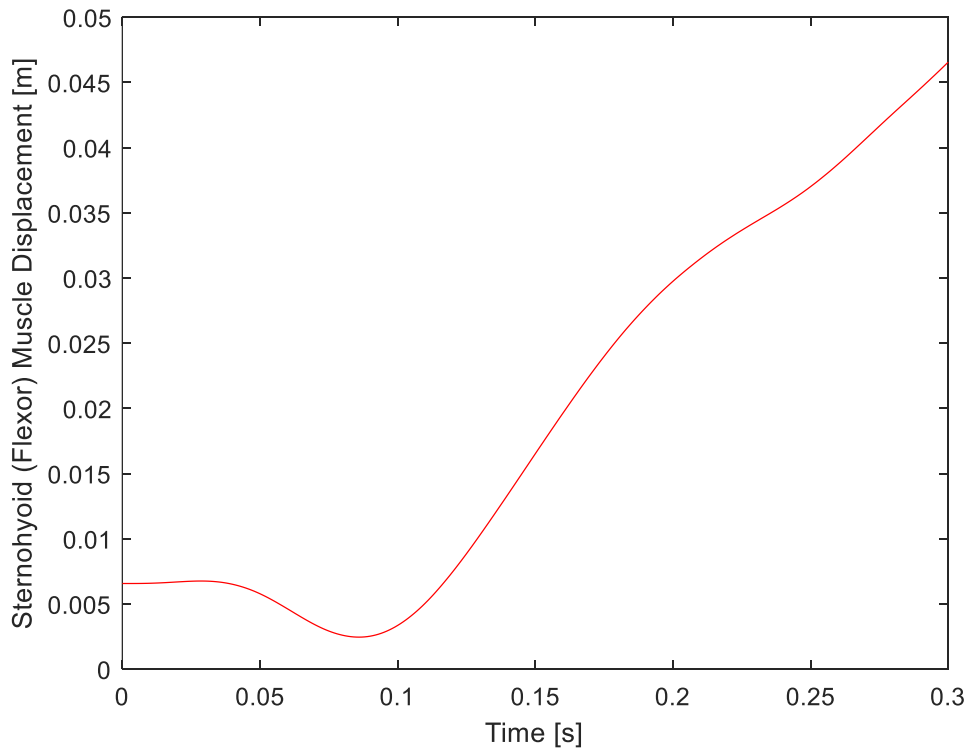

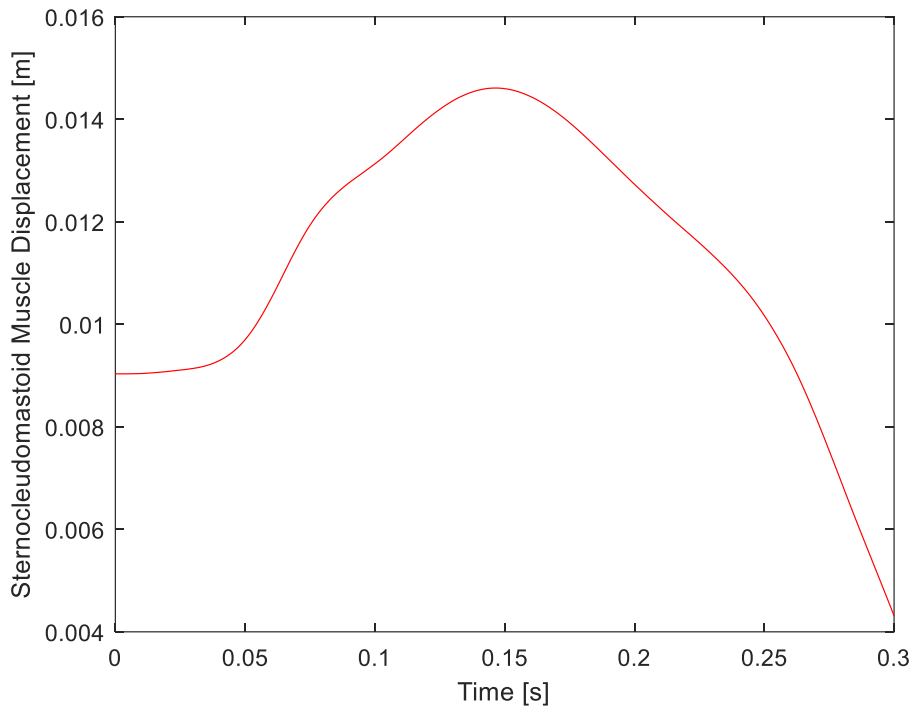Figure 4.64 Sternohyoid (flexor muscle) muscle displacement graph.

Figure 4.65 Sternocleidomastoid (flexor muscle) muscle displacement graph.

As a next step, the motion of the O.C. given as input was removed from the system because the input is given only from T1, and the calculated accelerations were applied as input into the linear actuators representing the muscles. When the simulation of the cranial neck model was run in MSC VisualNastran 4D, the head and neck model showed worse behavior compared to the earlier case and this was thought to be due to MSC VisualNastran 4D.

When this method did not work, the second method was tried. In the second method, since the muscle elements are represented as a system consisting of two interlocking pistons, the displacement of the two coordinates that provide the connection between the upper part of the lower piston and the lower part of the upper piston were measured relative to each other. Then the forces of the nested pistons representing the muscles were measured. In addition, the velocities of the coordinates connecting the pistons relative to each other were measured. Forces and velocity graph of muscles are given below as a figure from Figure 4.66 to Figure 4.71 .

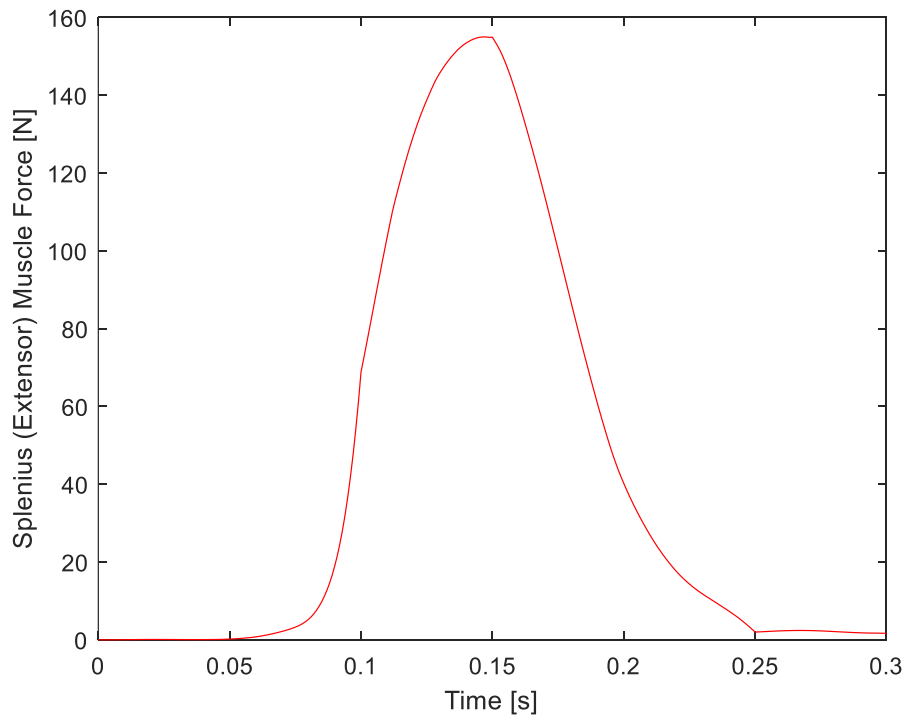71

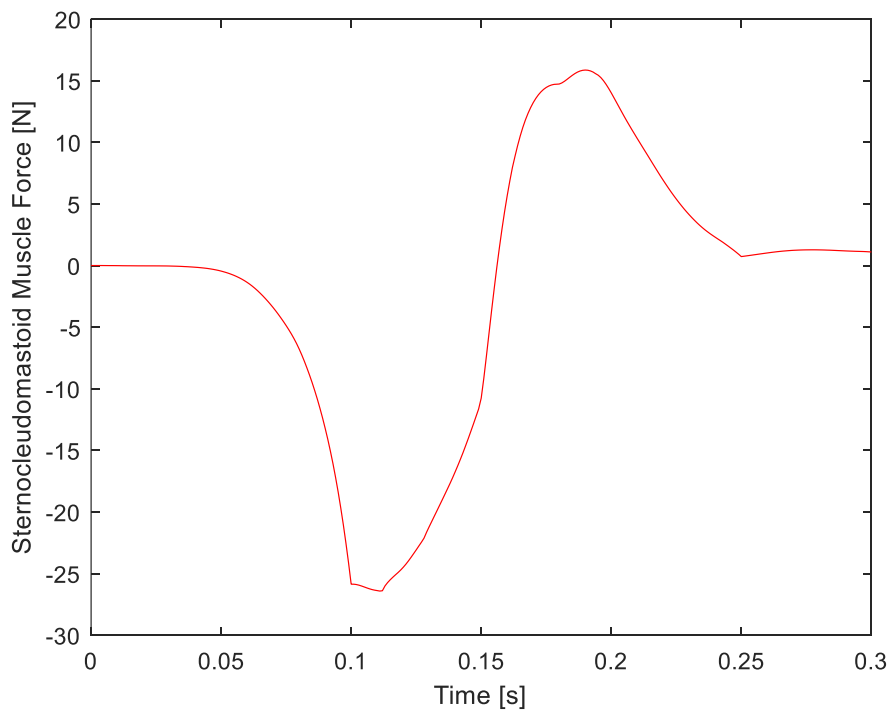Figure 4.66 Splenius (extensor muscle) muscle force graph.

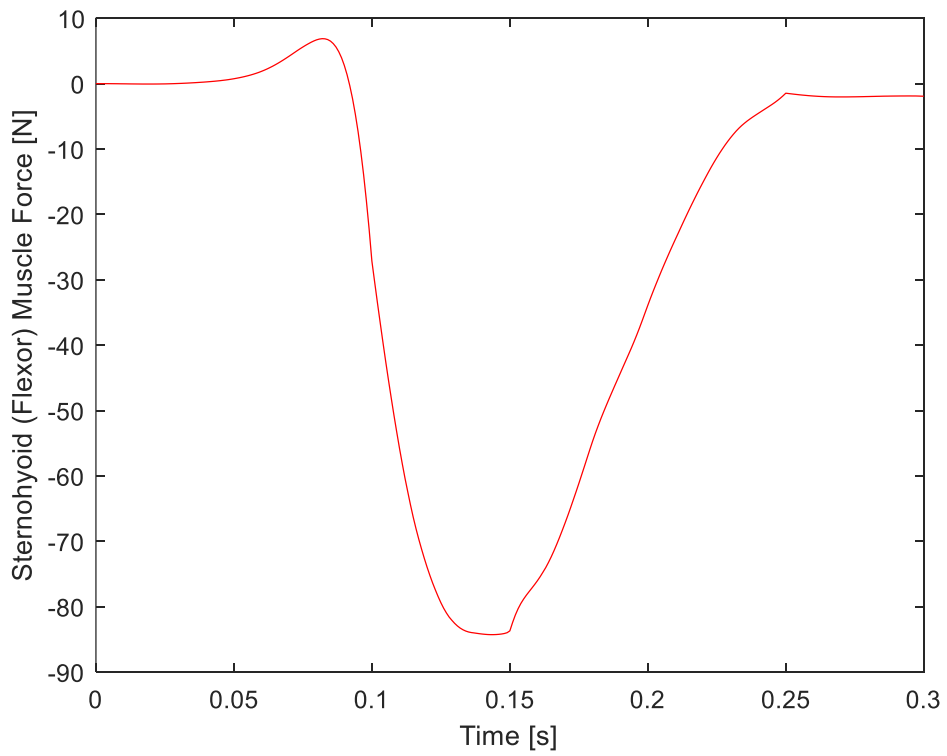Figure 4.67 Sternohyoid (flexor muscle) muscle force graph.

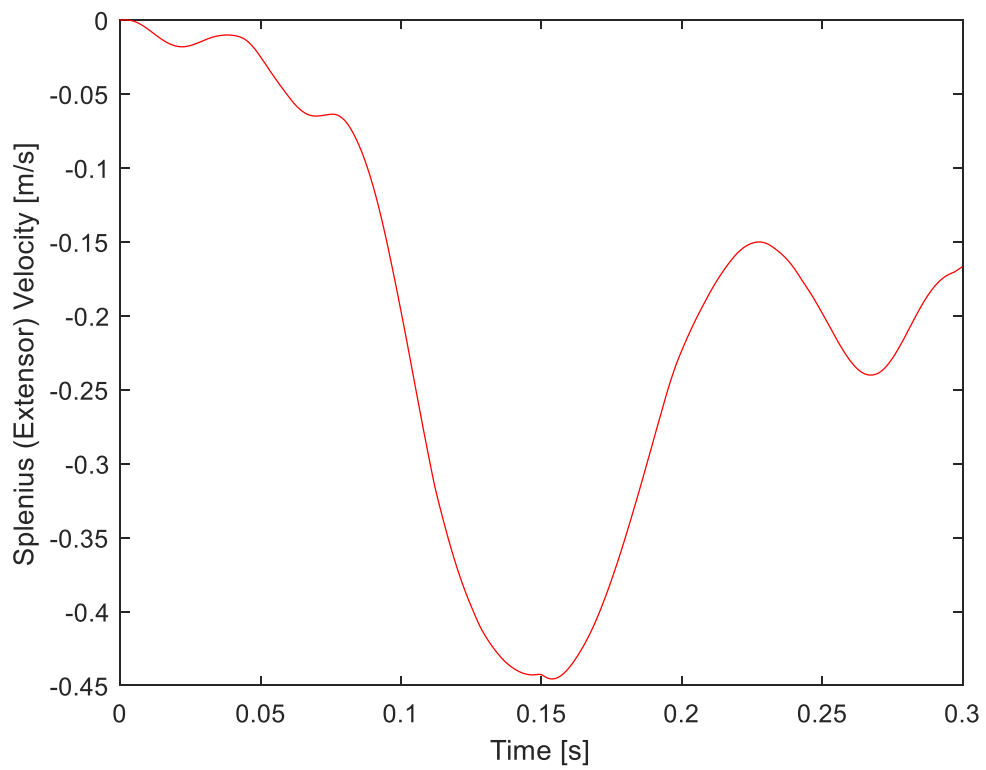Figure 4.68 Sternocleidomastoid (flexor muscle) muscle force graph.

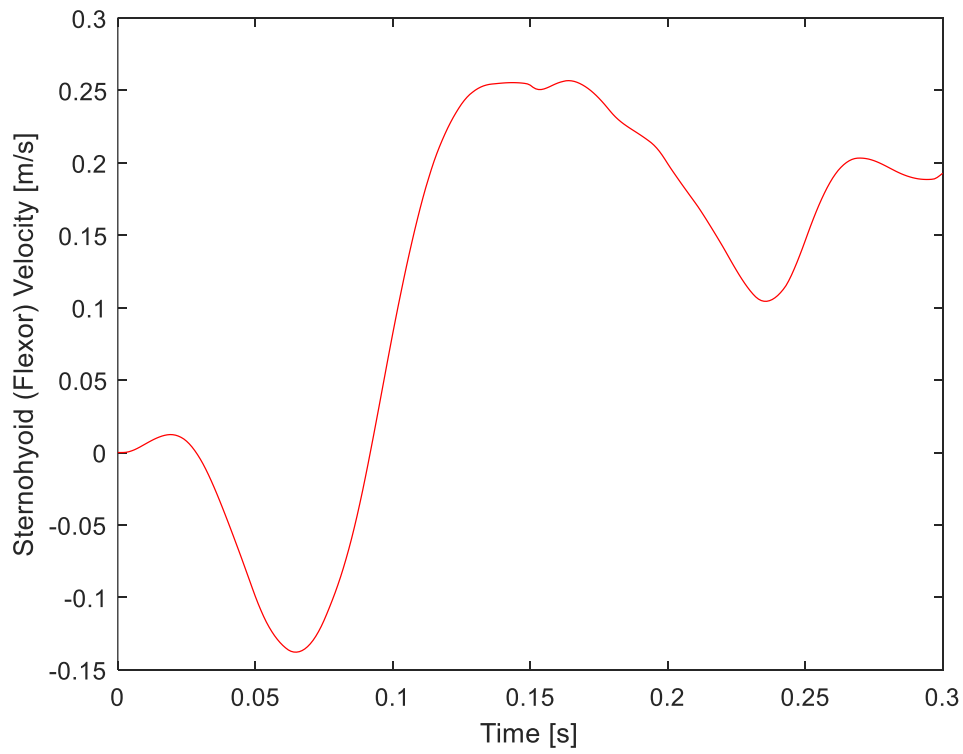Figure 4.69 Splenius (extensor muscle) muscle velocity graph.

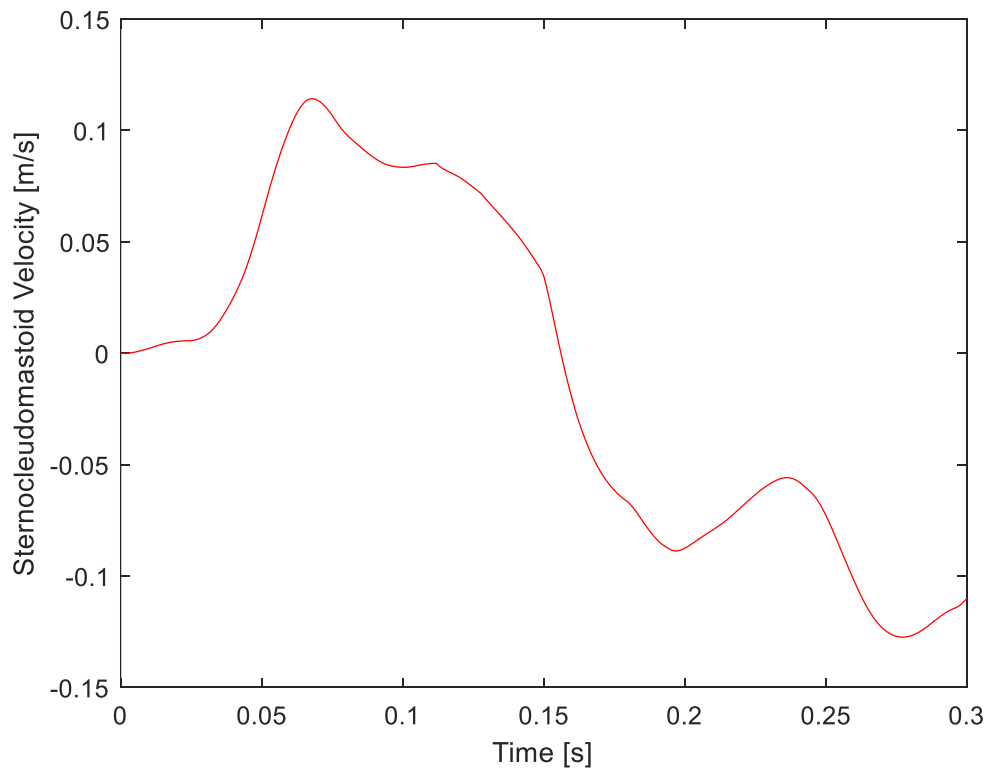Figure 4.70 Sternohyoid (flexor muscle) muscle velocity graph.

Figure 4.71 Sternocleidomastoid (flexor muscle) muscle velocity graph.

When the force and velocity graph is analyzed, for example for splenius, the maximum force is 140 N, and the maximum velocity is 0.4 m/s. From the formula F=c.V, the damping coefficient (c) 140 N /0.4 (m/s) corresponds to a damping coefficient of 350 kg/s. Splenius muscle force graph shows that the force first increases and then decreases, which is actually the same as the electromyography signals of the muscles and muscle activation in volunteer experiments. In addition, the variation of the damping coefficient with respect to time simulates the active contraction of muscles and the dynamic hardening of tissues with viscoelastic properties. Head and neck in Himmetoglu et al. [8], there were no muscle elements, and a time-varying damping coefficient was applied between the joints connecting the vertebrae. In the head and neck model in this thesis, instead of the joints between the vertebrae, a time-varying damping coefficient was applied to the pistons, which we define as muscle elements. The next step is to apply first acceleration and then displacement as input to the pistons forming the muscles, and this time force is given as input. The calculation of the input force was done by multiplying the time-varying damping coefficient graph defined by the formulation in MSC VisualNastran 4D and the measured velocity graph. As a result, when the head and neck model simulation was run, it showed a behavior remarkably close to the volunteer movements.
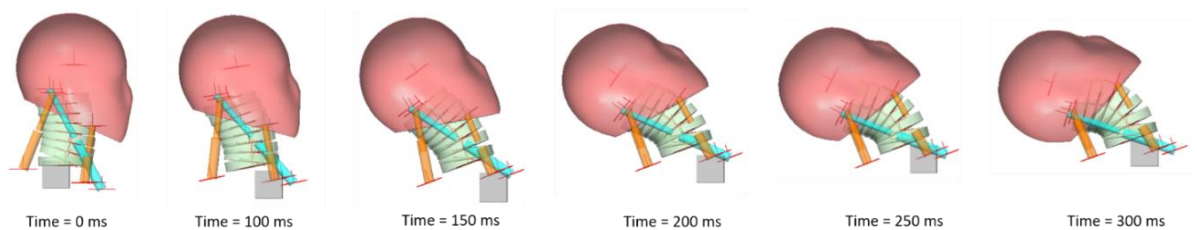

Figure 4.72 Movement of Himmetoglu et al. [8] head and neck model in simulation after solving the problem in model.
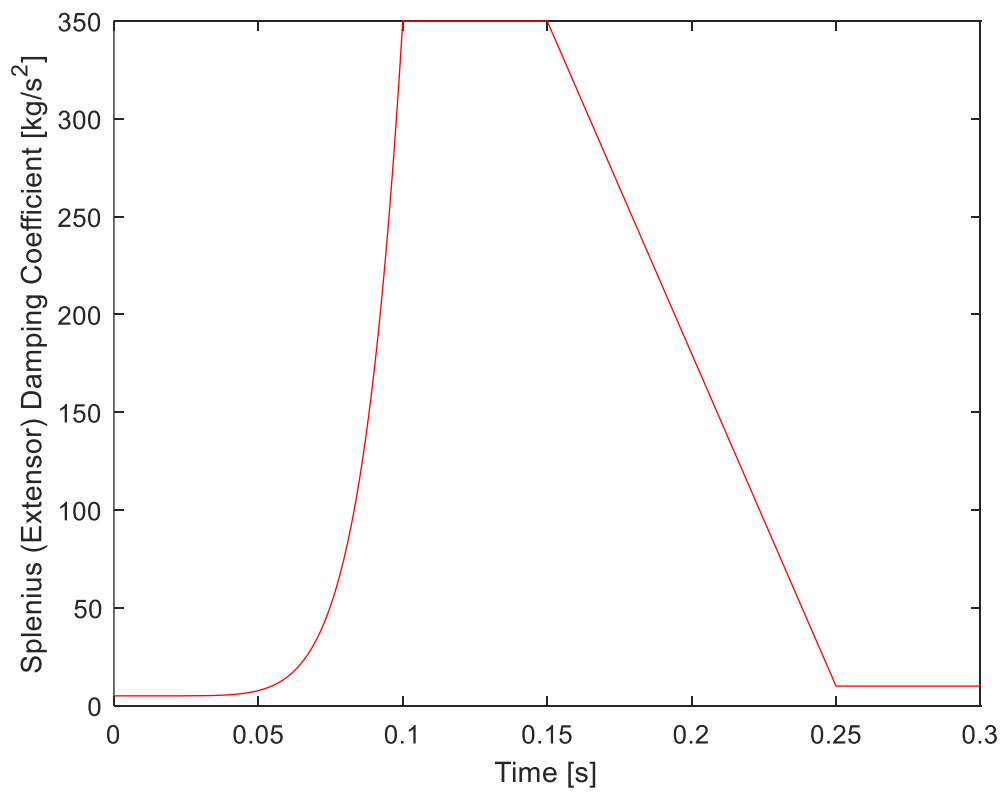
Figure 4.73 Splenius (extensor muscle) muscle damping coefficient graph.
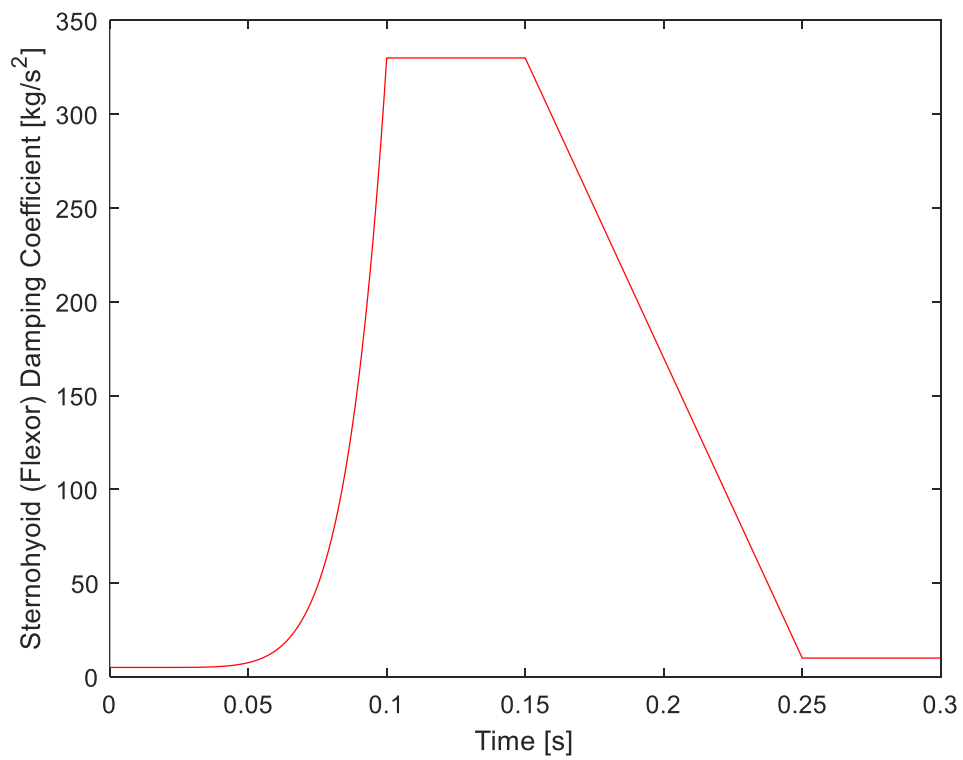
Figure 4.74 Sternohyoid (flexor muscle) muscle damping coefficient graph.
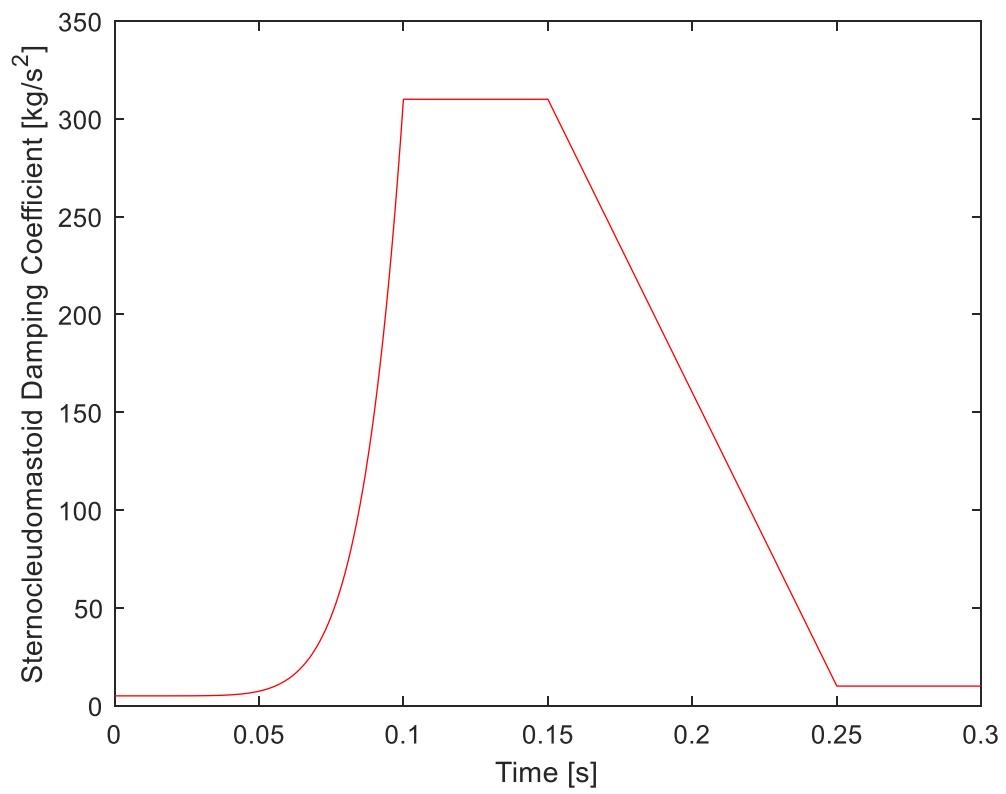
Figure 4.75 Sternocleidomastoid (flexor muscle) muscle damping coefficient graph.

5. SIMULATION MATRIX FOR DAMPING COEFFICIENT OF MUSCLES

In the previous section, it was stated that the simulation of the head and neck model was run and showed movements similar to the movements of the volunteer experiments. In this section, changes were made to the start, end and peak values in the damping coefficient graph of the muscles in Figure 4.73, Figure 4.74, Figure 4.75, and the results were compared with the volunteer experiments data in the study by Himmetoglu [23]. As an example, start, end and peak values in the damping coefficient graph given Figure 4. 83. Obtained scenarios are given below from Table 5.1 to Table 5.4.

Figure 5.1 Start, end and maximum value of damping coefficient graph.

Table 5.1 Applied modifications and created scenarios for the variation of the maximum value of the damping coefficient graph for muscles (1).

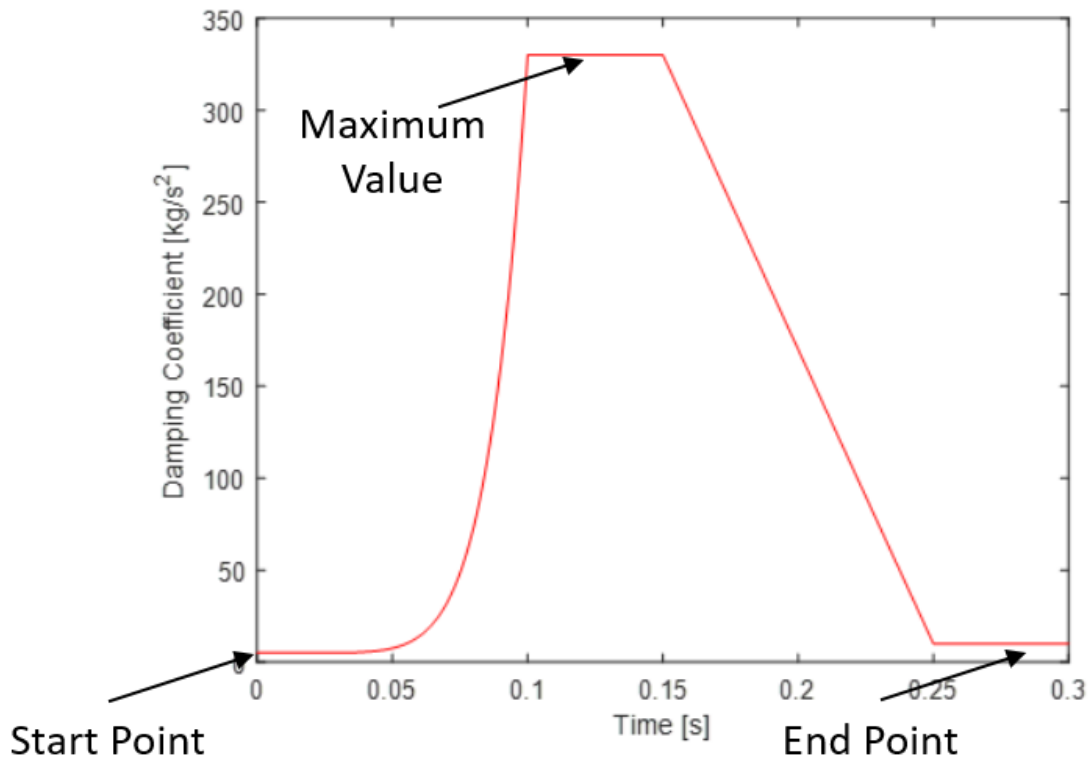| SCENARIO	1	2	3	4
Extensor (Splenius)	Increase Maximum Damping Coefficient %25	Decrease Maximum Damping Coefficient %25	Increase Maximum Damping Coefficient %25	Increase Maximum Damping Coefficient %25
Flexor (Sternohyoid)	Increase Maximum Damping Coefficient %25	Decrease Maximum Damping Coefficient %25	Decrease Maximum Damping Coefficient %25	Increase Maximum Damping Coefficient %25
Sternocleidomastoid	Increase Maximum Damping Coefficient %25	Decrease Maximum Damping Coefficient %25	Decrease Maximum Damping Coefficient %25	Decrease Maximum Damping Coefficient %25

Table 5.2 Applied modifications and created scenarios for the variation of the maximum value of the damping coefficient graph for muscles (2).

SCENARIO	5	6	7	8
Extensor (Splenius)	Increase Maximum Damping Coefficient %25	Decrease Maximum Damping Coefficient %25	Decrease Maximum Damping Coefficient %25	Decrease Maximum Damping Coefficient %25
Flexor (Sternohyoid)	Decrease Maximum Damping Coefficient %25	Increase Maximum Damping Coefficient %25	Decrease Maximum Damping Coefficient %25	Increase Maximum Damping Coefficient %25
Sternocleidomastoid	Increase Maximum Damping Coefficient %25	Decrease Maximum Damping Coefficient %25	Increase Maximum Damping Coefficient %25	Increase Maximum Damping Coefficient %25

Table 5.3 Applied modifications and created scenarios for the variation of the start and end values of the damping coefficient graph for muscles (1).

SCENARIO	9	10	11	12	13	14	15	16
Start Point of Damping Coefficient Graph	Increase %30	Decrease %30	Increase %30	Decrease %30	Increase %30	-	Decrease %30	-
End Point of Damping Coefficient Graph	Decrease %30	Increase %30	Increase %30	Decrease %30	-	Increase %30	-	Decrease %30

Table 5.4 Applied modifications and created scenarios for the variation of the maximum value of the damping coefficient graph for muscles (2).

SCNERIO	17	18	19	20
Start Point of Damping Coefficient Graph	5 Times of the Start Value	2 Times of the Start Value	0.5 Times of the Start Value	0.2 Times of the Start Value
End Point of Damping Coefficient Graph	5 Times of the Start Value	2 Times of the Start Value	0.5 Times of the Start Value	0.2 Times of the Start Value

The data in the scenario tables were applied to model and the results were obtained and these results were superimposed and compared with the volunteer movement graphs in Himmetoglu [23]. There was no change in the results when Scenario 9 through Scenario 16 were applied to model. The reason for this is that increasing and decreasing the start and end points together does not change the motion of model.
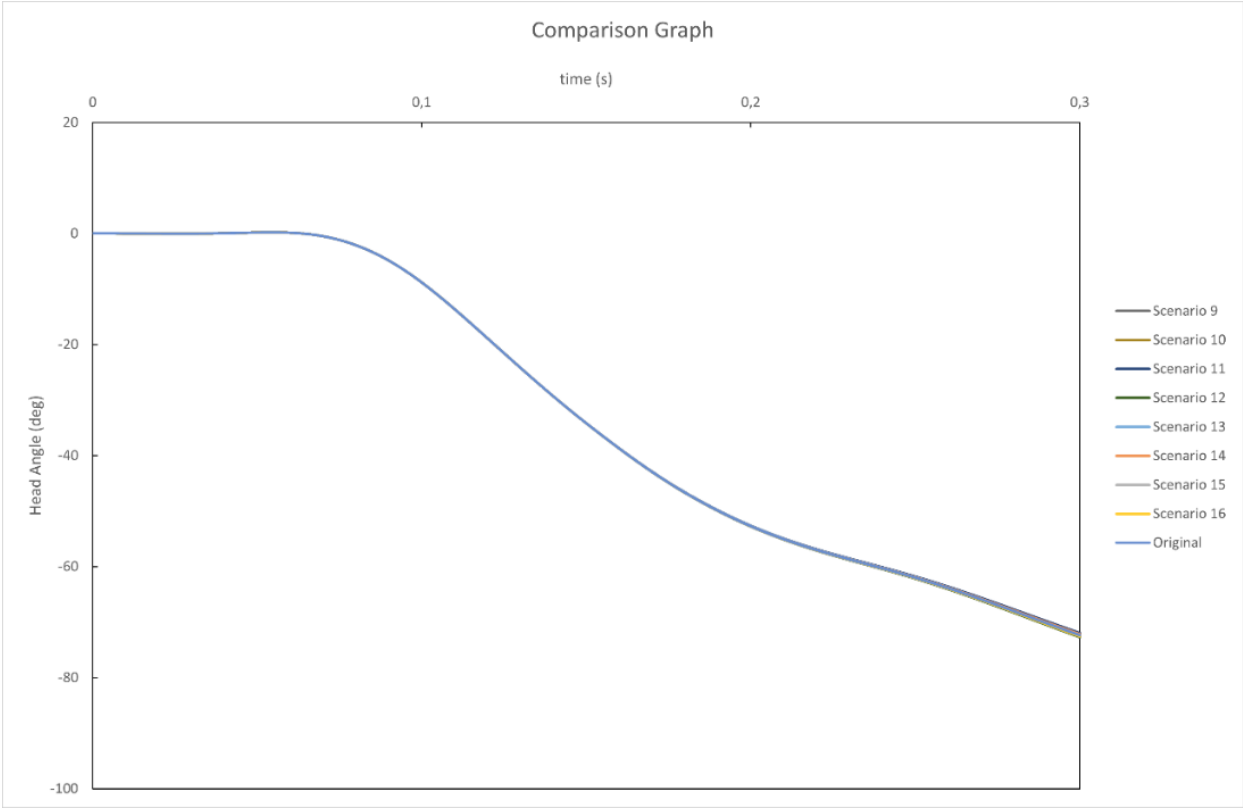

Figure 5.2 Comparison head angle values of head and neck model between scenarios 9 through 16 and original.
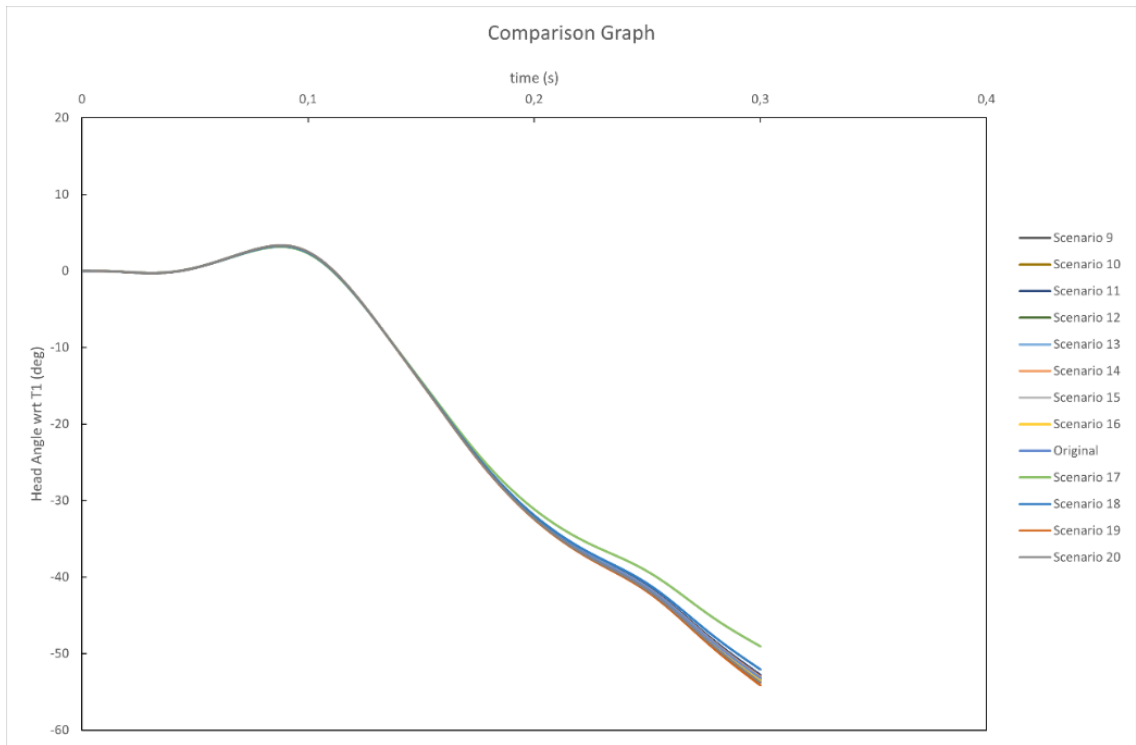
Figure 5.3 Comparison head angle with respect to T1 values of head and neck model between scenarios 9 through 16 and original.
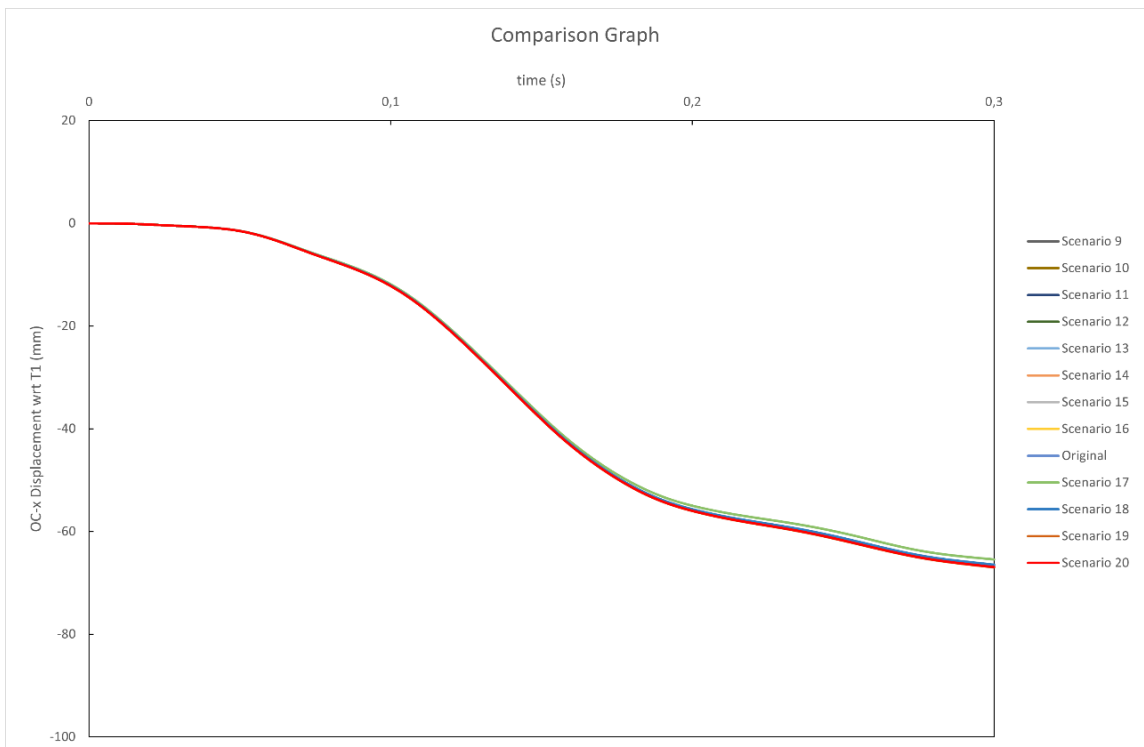

Figure 5.4 Comparison O.C. x displacement with respect to T1 values of head and neck model between scenarios 9 through 16 and original.
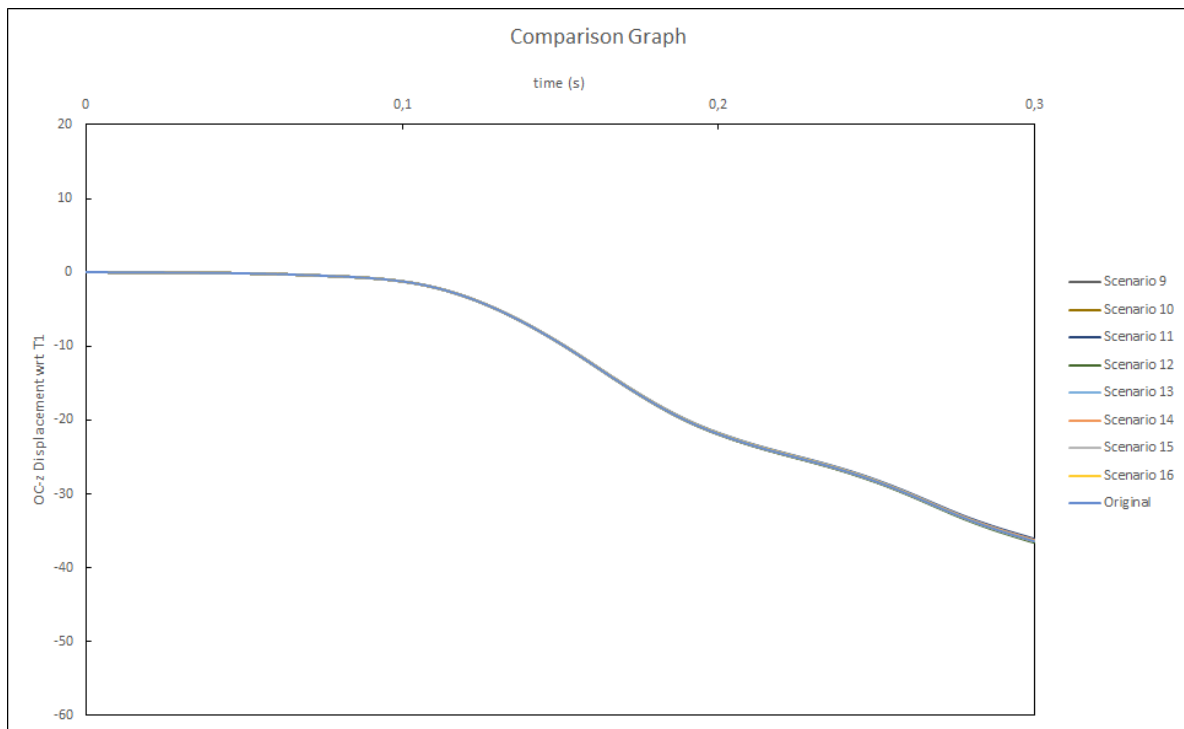
Figure 5.5 Comparison O.C. z displacement with respect to T1 of head and neck model between scenarios 9 through 16 and original.
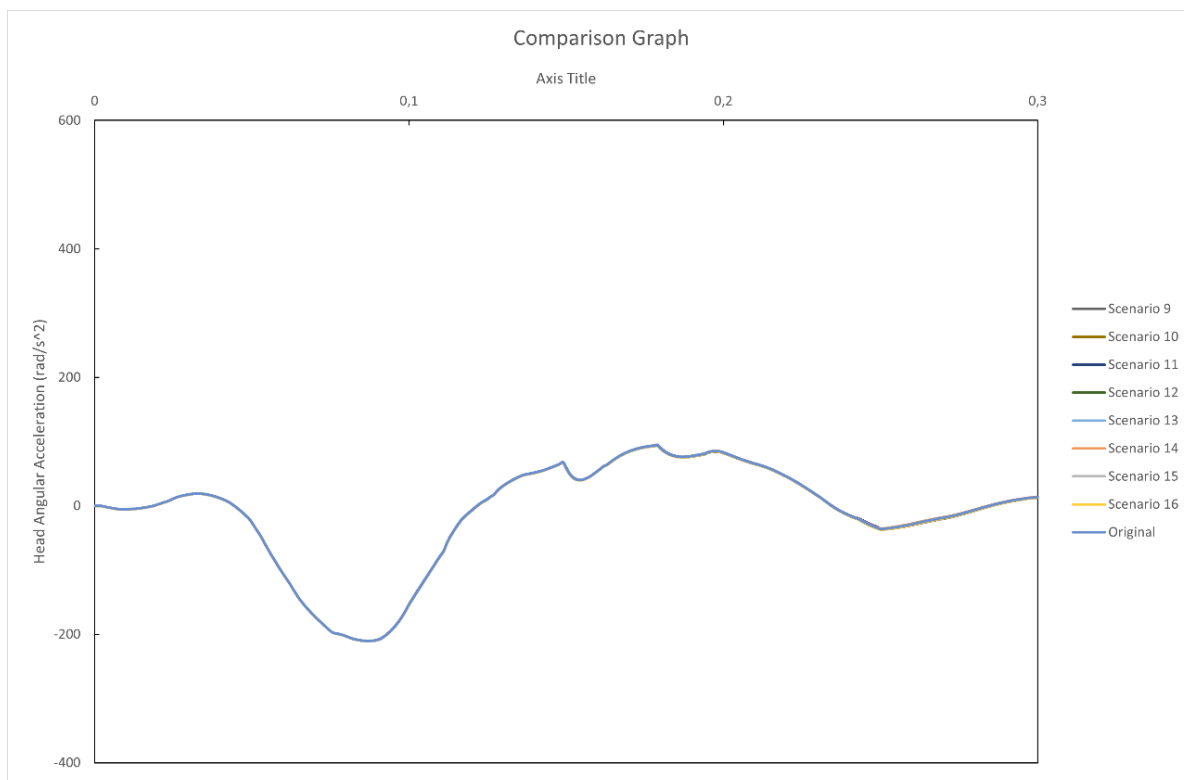

Figure 5.6 Comparison head angular acceleration values of head and neck model between scenarios 9 through 16 and original.
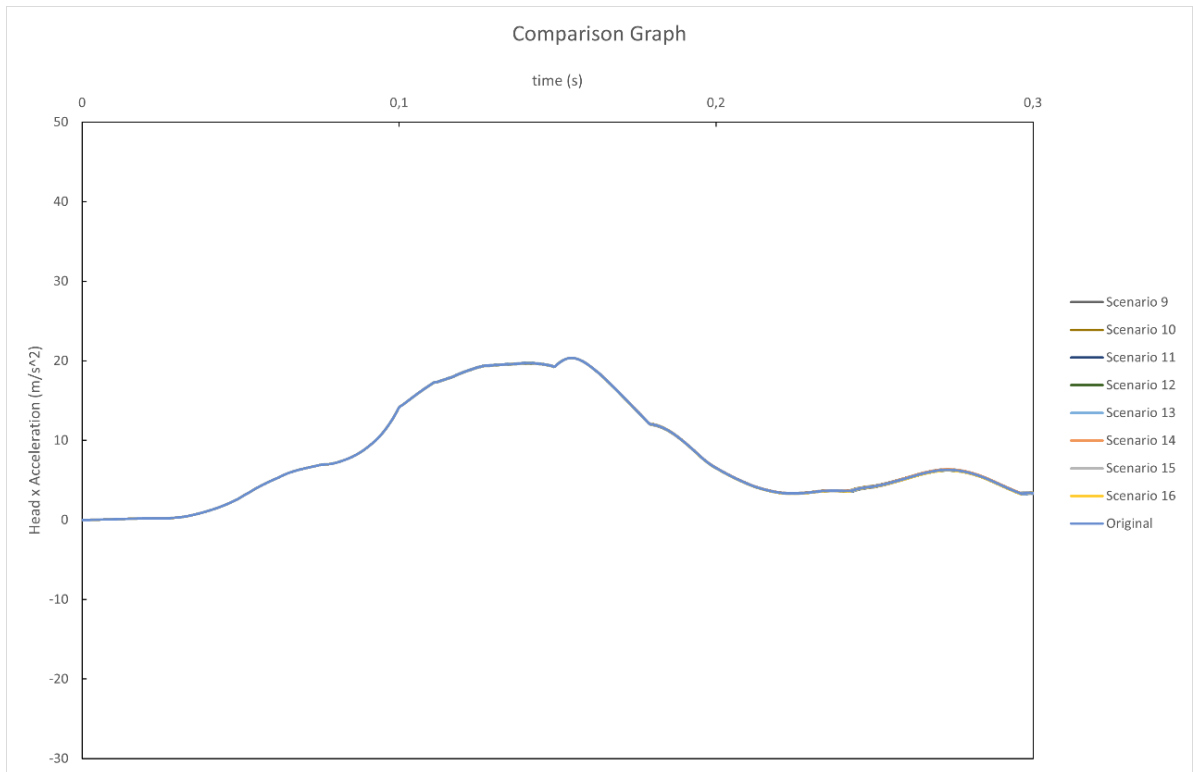
Figure 5.7 Comparison head acceleration values of head and neck model between scenarios 9 through 16 and original.

The important point in the graphs between Figure 5.3 and Figure 5.7 is that the original curve and the curves of the between scenarios 9 and 16 are the same. Here, the original is the head and neck model that shows a behavior close to the movements of the volunteer experiment obtained in this thesis before the changes in the scenarios were applied.

When Scenarios 1 through 8 and Scenarios 17 through 19 were applied to the head and neck model, the results changed. The results were compared with the results before the changes in the scenarios were applied to the head and neck model. Comparison plots are given between Figure 5.8 and Figure 5.13.
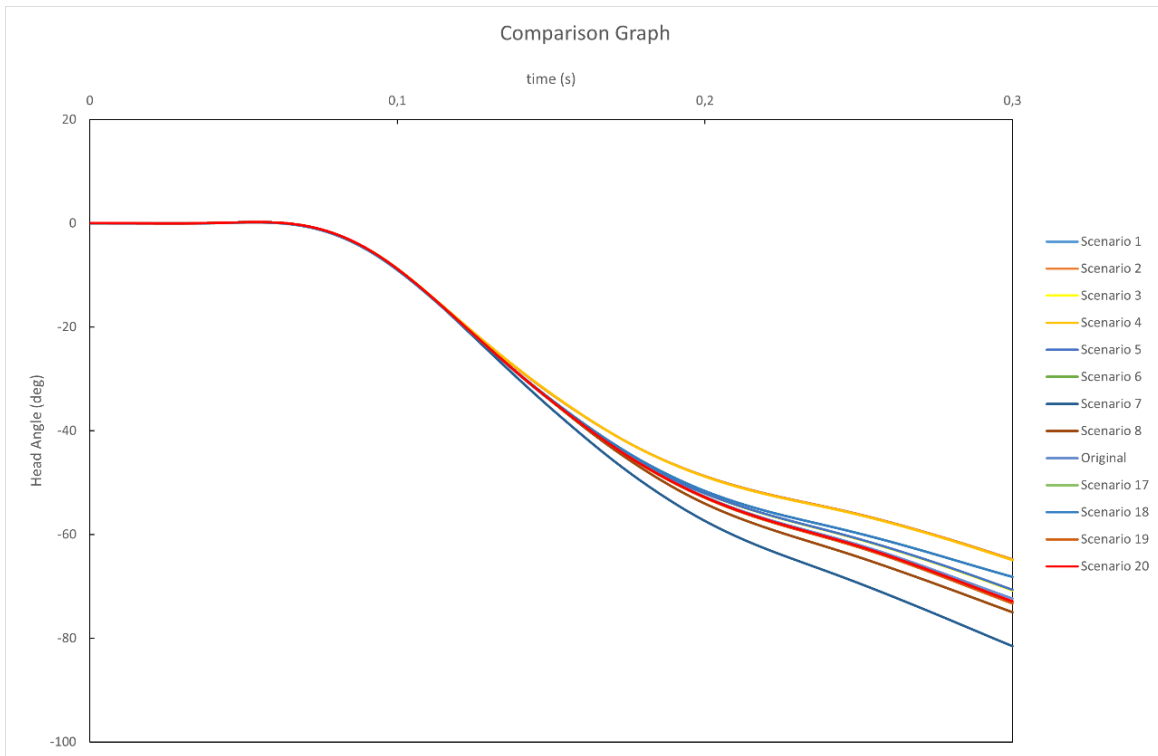
Figure 5.8 Comparison head angle values of head and neck model between scenarios 1 through 8, scenarios 17 through 20 and original.

Figure 5.9 Comparison head angle with respect to T1 values of head and neck model between scenarios 1 through 8, scenarios 17 through 20 and original.

Figure 5.10 Comparison O.C. x displacement with respect to T1 values of head and neck model between scenarios 1 through 8, scenarios 17 through 20 and original.

Figure 5.11 Comparison O.C. z displacement with respect to T1 of head and neck model between scenarios 1 through 8, scenarios 17 through 20 and original.

Figure 5.12 Comparison head angular acceleration values of head and neck model between scenarios 1 through 8, scenarios 17 through 20 and original.
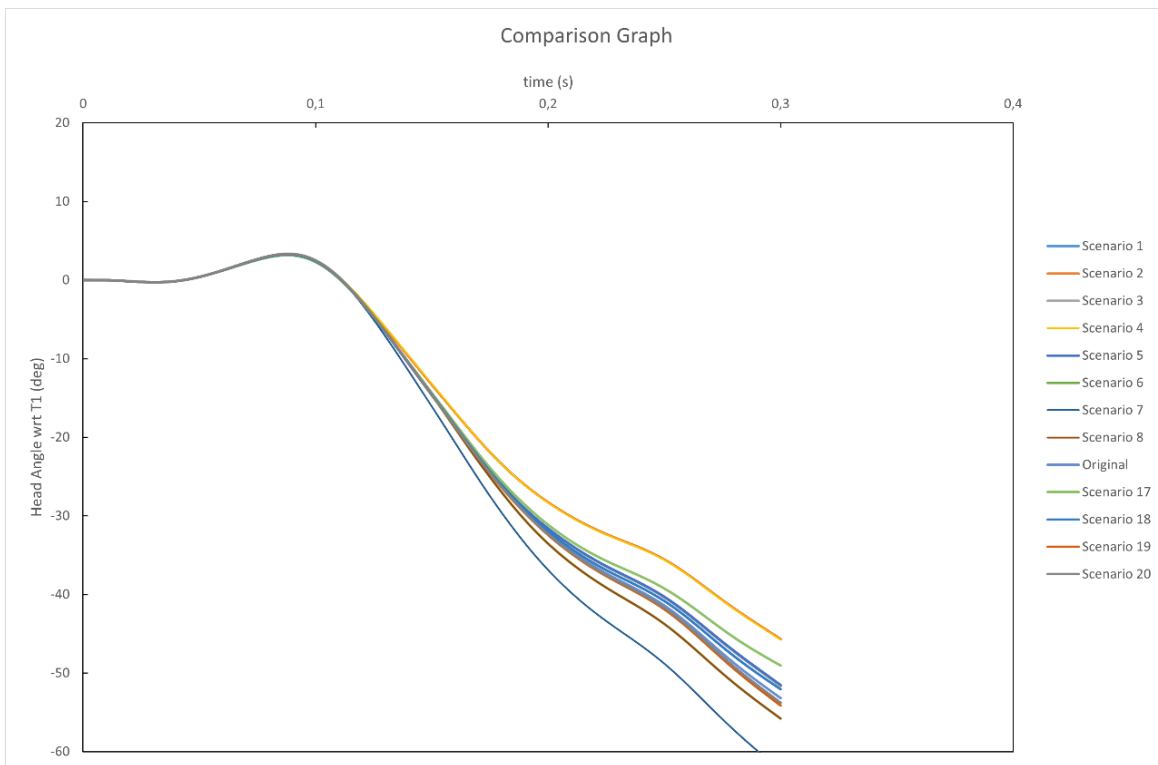

Figure 5.13 Comparison head acceleration values of head and neck model between scenarios 1 through 8, scenarios 17 through 20 and original.

The results obtained when Scenarios 1 to 8 and Scenarios 17 to 19 were applied to the head and neck model and the results obtained before the changes in the scenarios were applied to the head and neck model were compared with the volunteer experiment graphs in Himmetoglu [23]. The gray curves in the graphs represent the responses of the volunteers in the JARI experiments given in reference [23] and the red curve represents the Himmetoglu head and neck model in reference [8] in which the model did not involve separate muscle elements and muscle tone.

Figure 5.14 Comparison head angle values of head and neck model between scenarios 1 through 8, scenarios 17 through 20, original and volunteer experiment data in Himmetoglu [23].
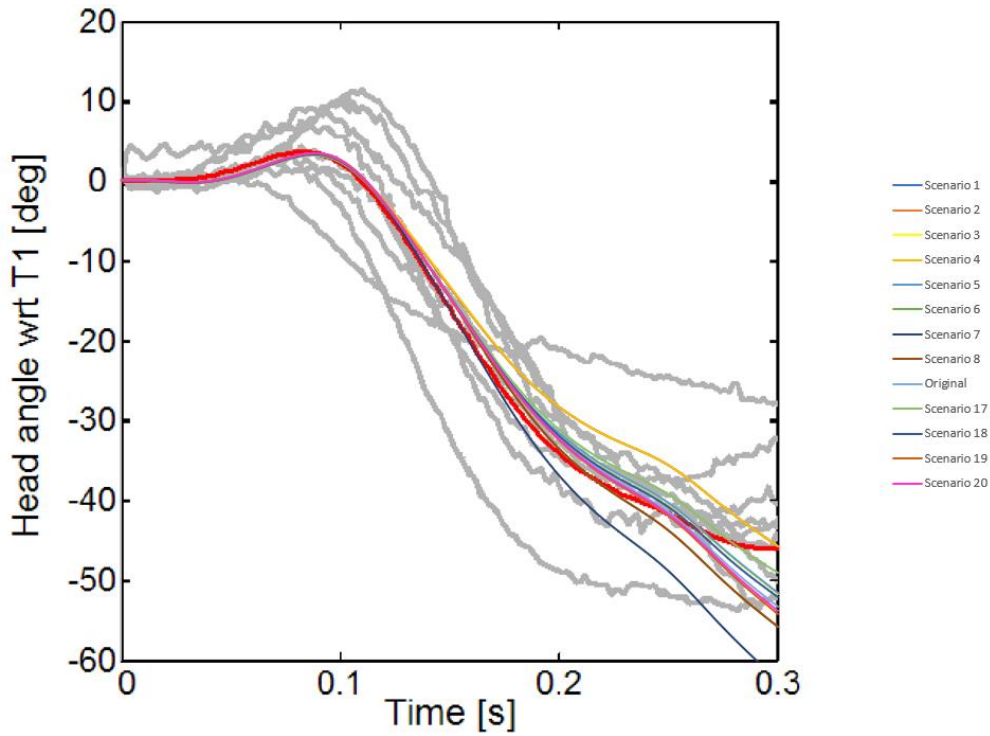
Figure 5.15 Comparison head angle with respect to T1 values of head and neck model between scenarios 1 through 8, scenarios 17 through 20, original and volunteer experiment data in Himmetoglu [23] .
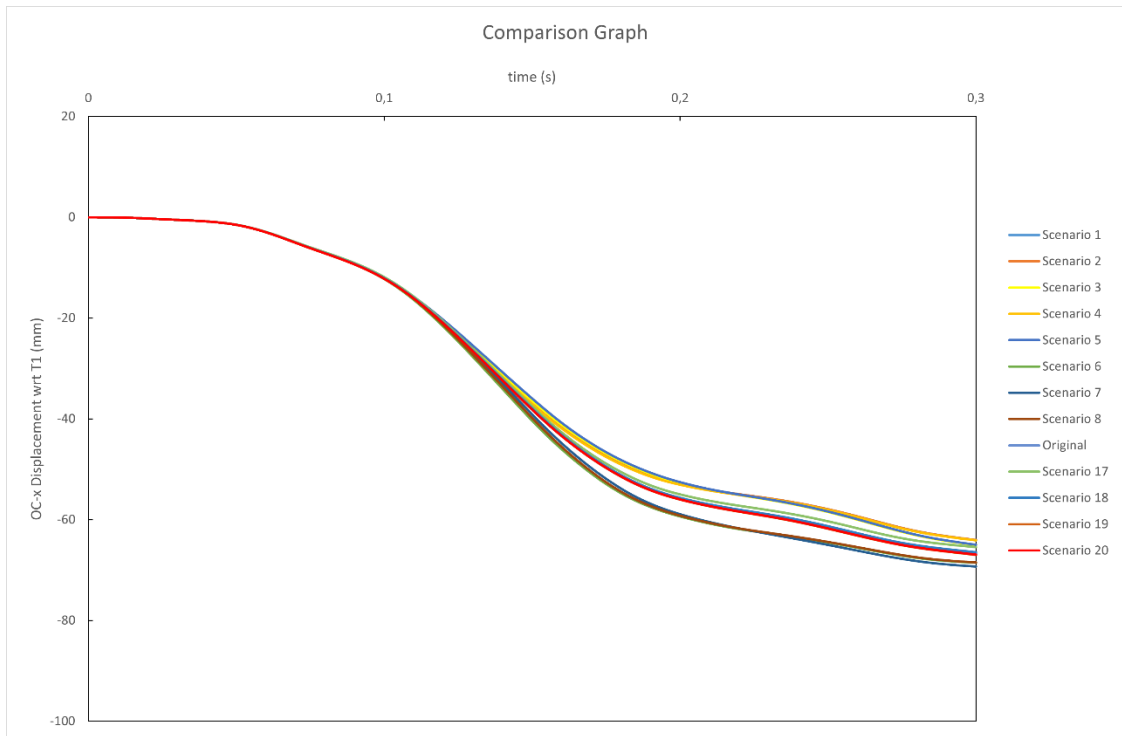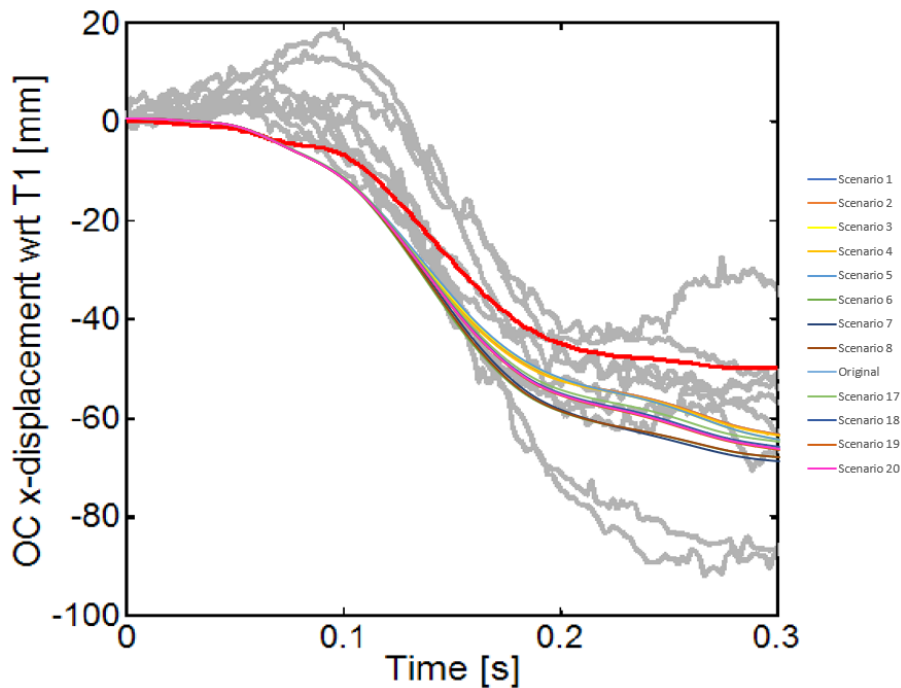

Figure 5.16 Comparison O.C. x displacement with respect to T1 values of head and neck model between scenarios 1 through 8, scenarios 17 through 20, original and volunteer experiment data in Himmetoglu [23] .
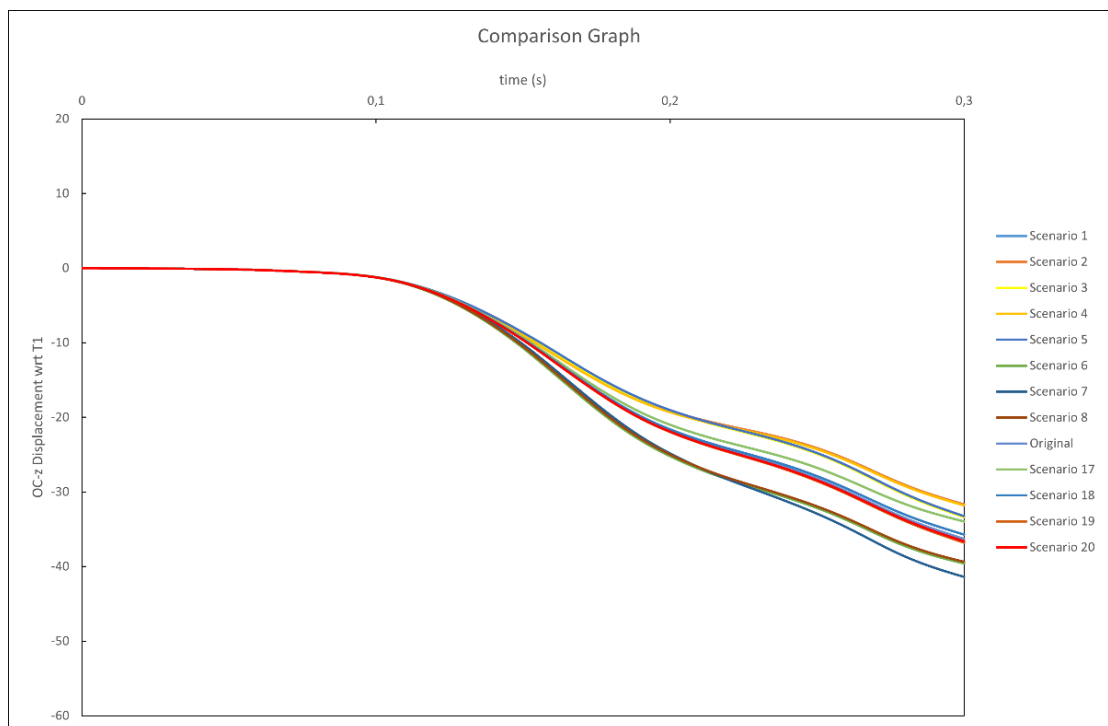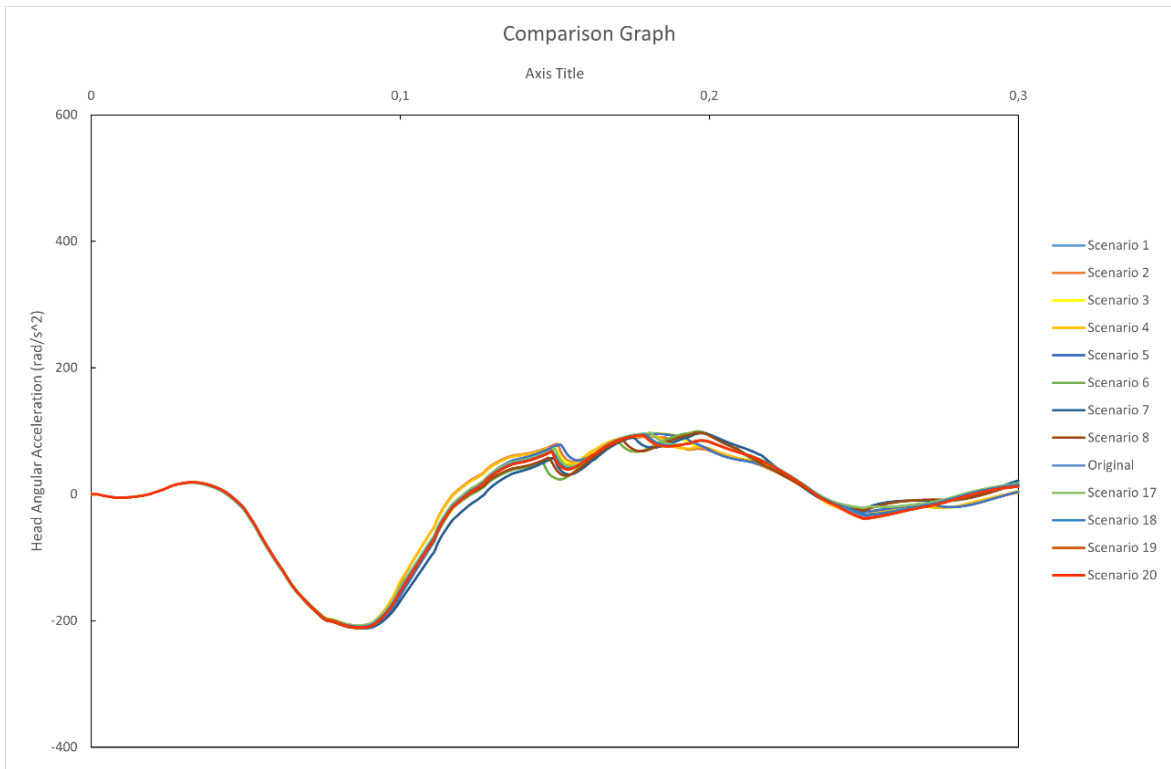
Figure 5.17 Comparison O.C. z displacement with respect to T1 values of head and neck model between scenarios 1 through 8, scenarios 17 through 20, original and volunteer experiment data in Himmetoglu [23] .

Figure 5.18 Comparison head angular acceleration values of head and neck model between scenarios 1 through 8, scenarios 17 through 20, original and volunteer experiment data in Himmetoglu [23] .
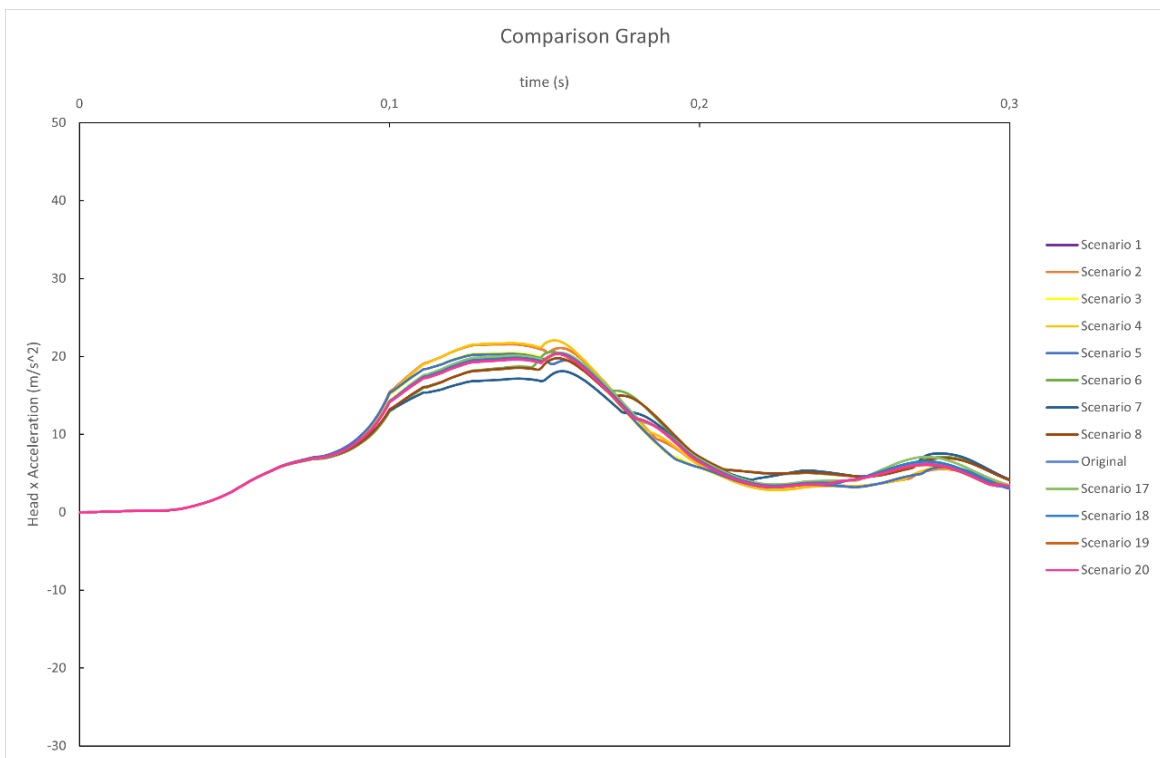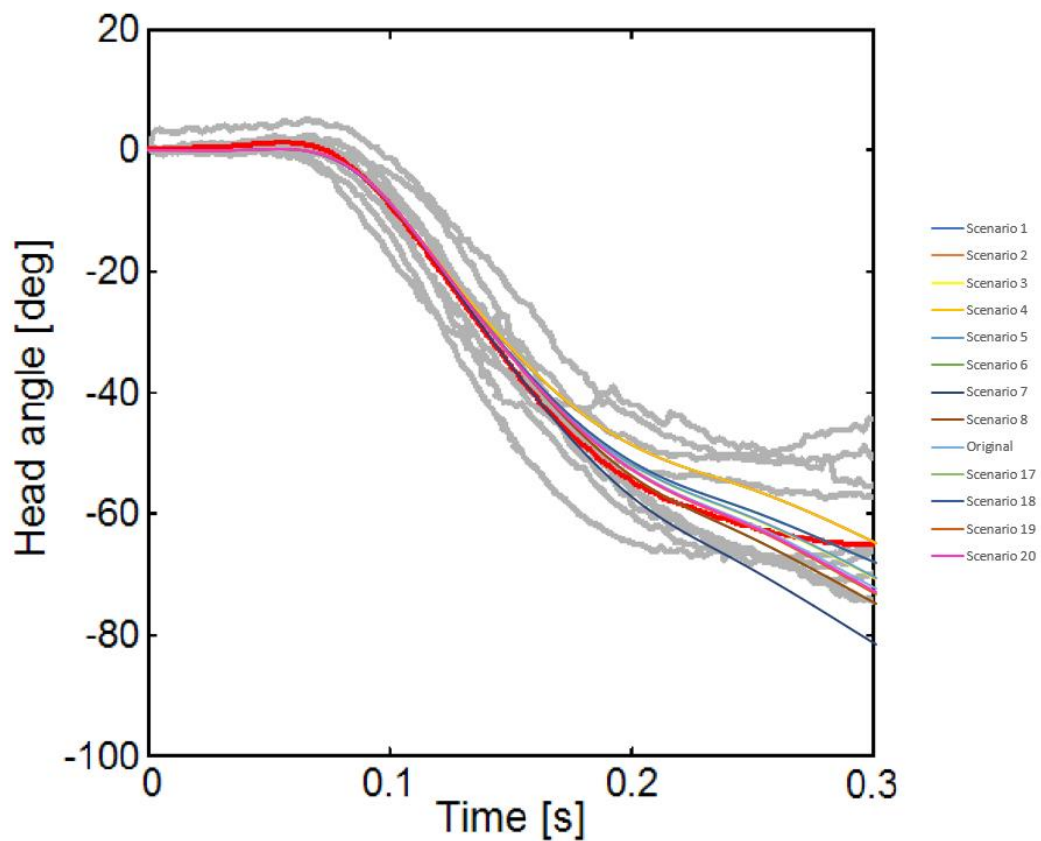
Figure 5.19 Comparison head acceleration values of head and neck model between scenarios 1 through 8, scenarios 17 through 20, original and volunteer experiment data in Himmetoglu [23] .
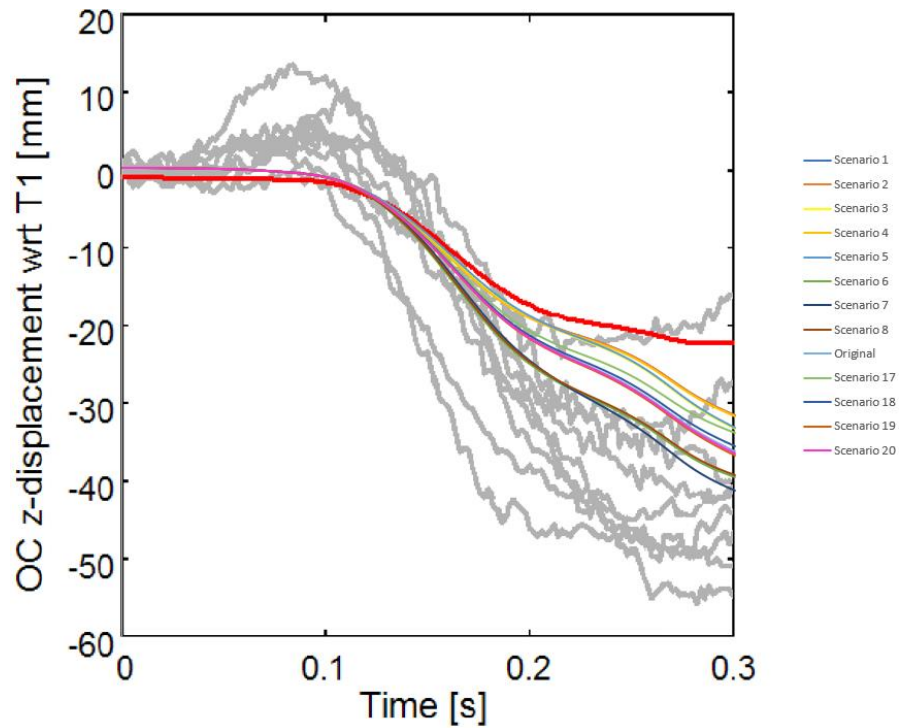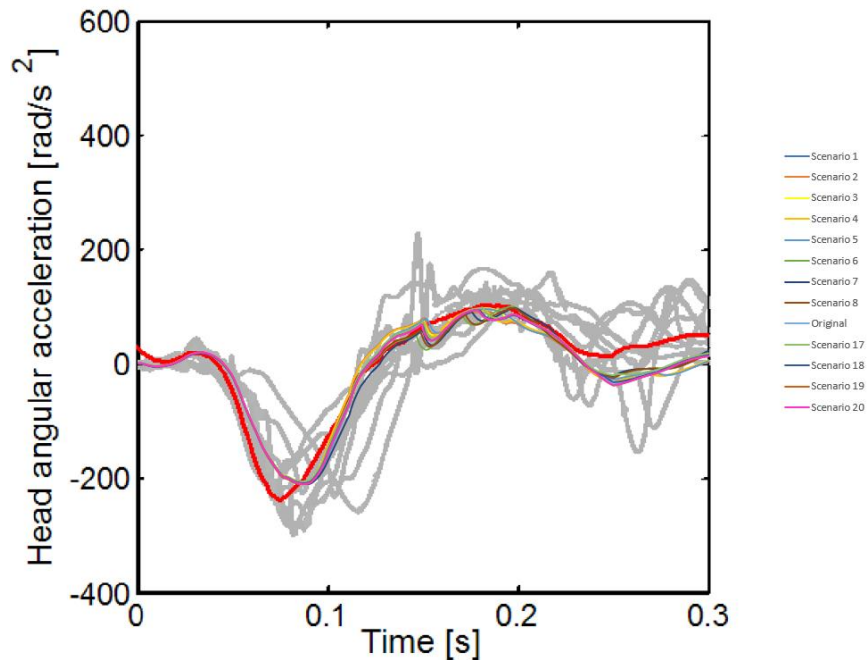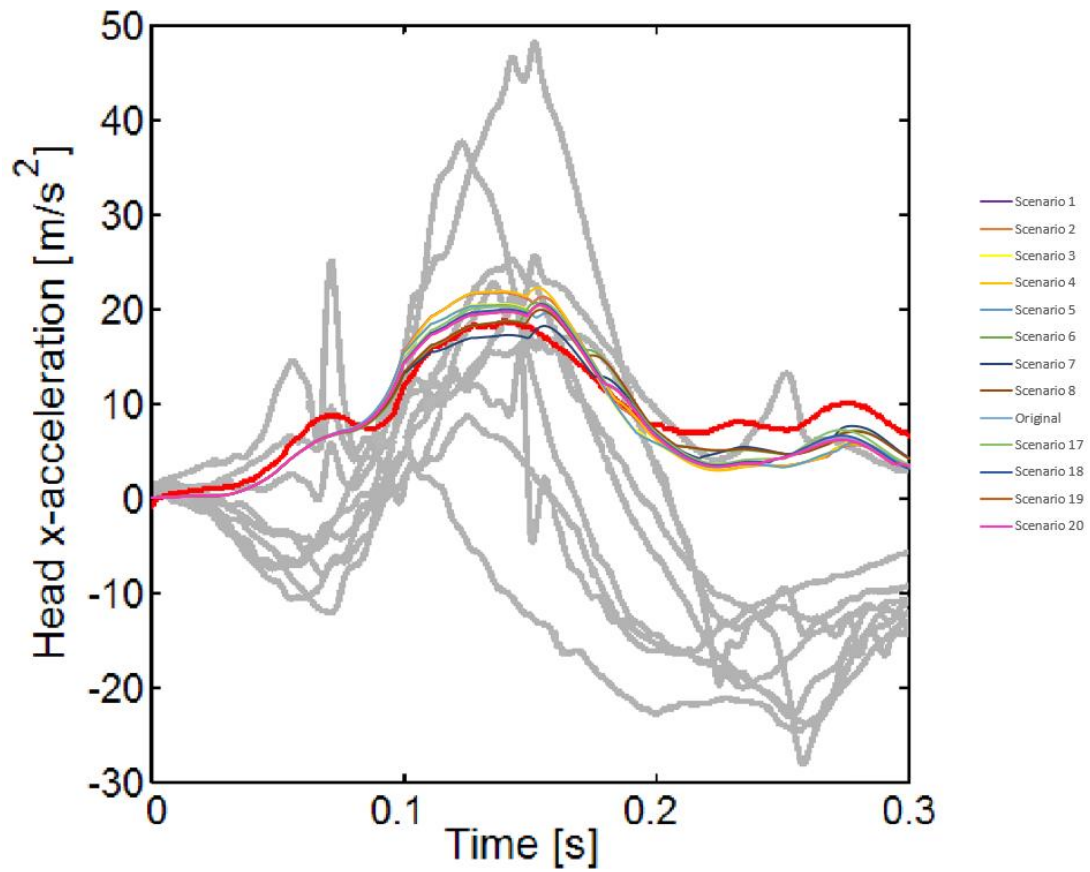
6. RESULTS AND DISCUSSION

The equations necessary for the head and neck model to achieve static equilibrium, which is the first aim of the thesis, were derived and applied to the head and neck model in simulation. As a result, it was seen that the head and neck model could not stand in static equilibrium and by correcting the error caused by the working environment of the model, the head and neck model achieved static equilibrium.

The other aim of the thesis was to add muscles to the head and neck model and as a result, to find the forces that will move these muscles by giving data from volunteer experiments as input to the head and neck model. To do this, the necessary equations were derived with the help of the inverse dynamics method and the results were obtained by running these equations appropriately in MATLAB. To give the input motion, data were collected from the reference [7] and these data were digitized and interpolated to make them usable. The muscles that needed to be implemented were implemented by using the information in the reference [17] and the head and neck model was completed with the muscles and became ready for simulation.

It has already been mentioned that the revolute joints connecting the vertebrae in the head and neck model have a damper and rotational spring. When muscle forces are obtained, these forces depend on the damper, i.e., the damping coefficient plots. Because force and velocity are used when obtaining damping coefficient plots, the obtained forces are the damper forces.

Since the head and neck model was created in the MSC VisualNastran 4D program, the simulation was run here and when the results were considered, it was seen that it exhibited movements close to the movements of the volunteer experiments and in this sense, it can be said that this study was successful. In addition, a simulation matrix was created, and scenarios were created by making changes in the damping coefficient and applied to the model and results were obtained. These results were compared with the responses of the volunteers in the JARI experiments given in reference [23] data. The model developed before changing the damping coefficient was already showing behavior close to the movements of the volunteer experiments. After changing the damping coefficient,

Scenario 17 shows an improvement compared to the previous situation when compared to the volunteer experiments. This shows that the already good model can get better. Since the start and end points of the damping coefficient graphs were increased by a factor of 5 in Scenario 17, it can be said that the model has improved.

Figure 6.1 Comparison head acceleration values of head and neck model between scenario 17 and volunteer experiment data in Himmetoglu [23].

Figure 6.2 Comparison head angular acceleration values of model between scenario 17 and volunteer experiment data in Himmetoglu [23].
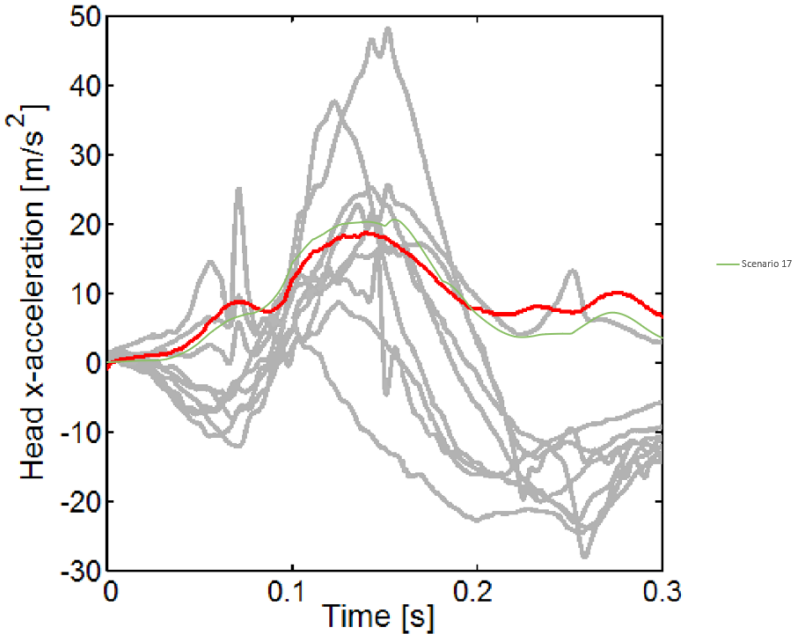
Figure 6.3 Comparison head angle values of head and neck model between scenario 17 and volunteer experiment data in Himmetoglu [23].
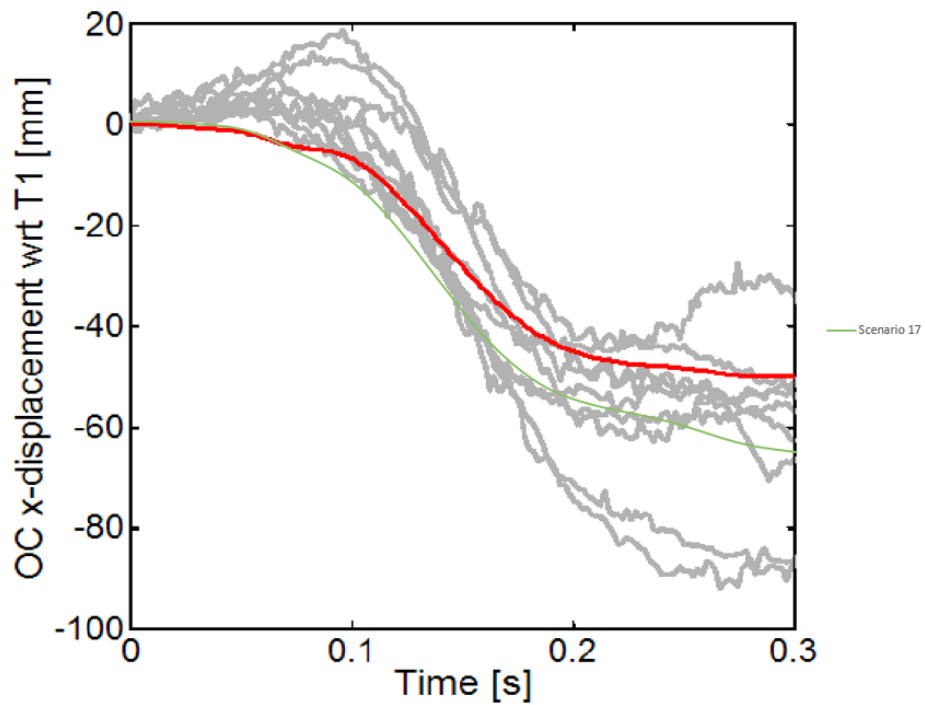
Figure 6.4 Comparison O.C. x displacement with respect to T1 values of head and neck model between scenario 17 and volunteer experiment data in Himmetoglu [23].
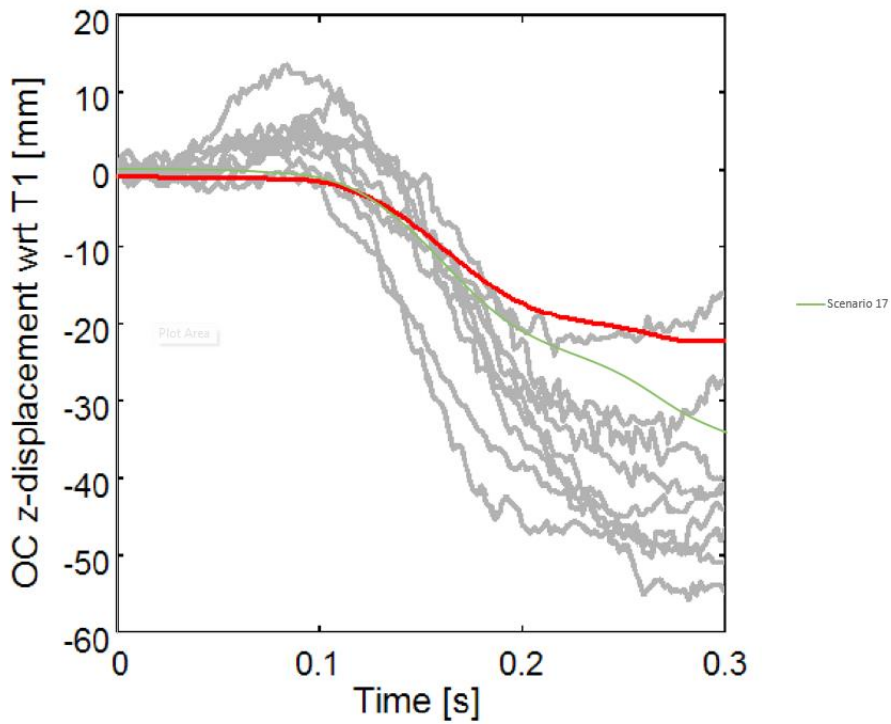
Figure 6.5 Comparison O.C. z displacement with respect to T1 values of head and neck
model between scenario 17 and volunteer experiment data in Himmetoglu [23]
.
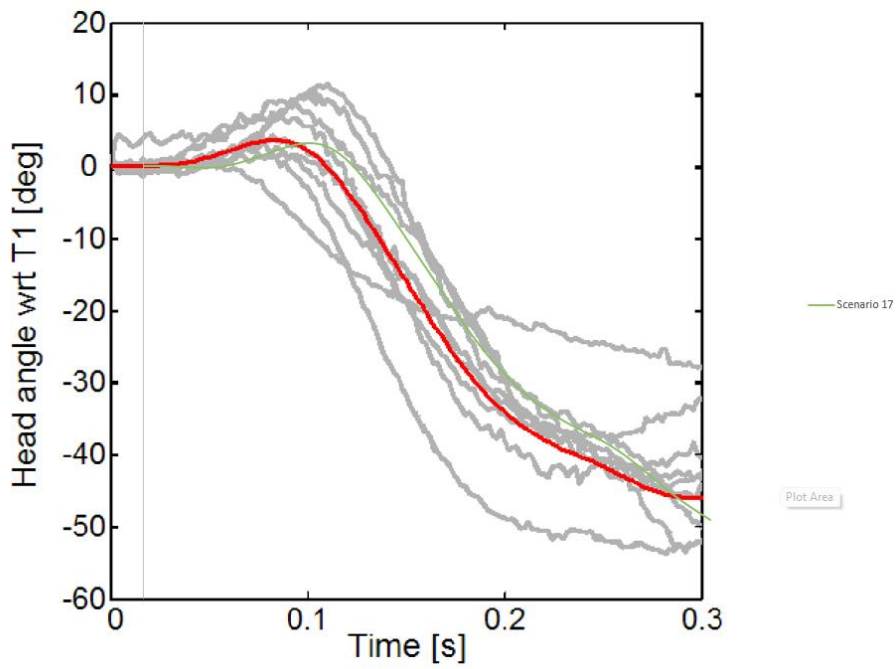
Figure 6.6 Comparison head angle with respect to T1 values of head and neck model
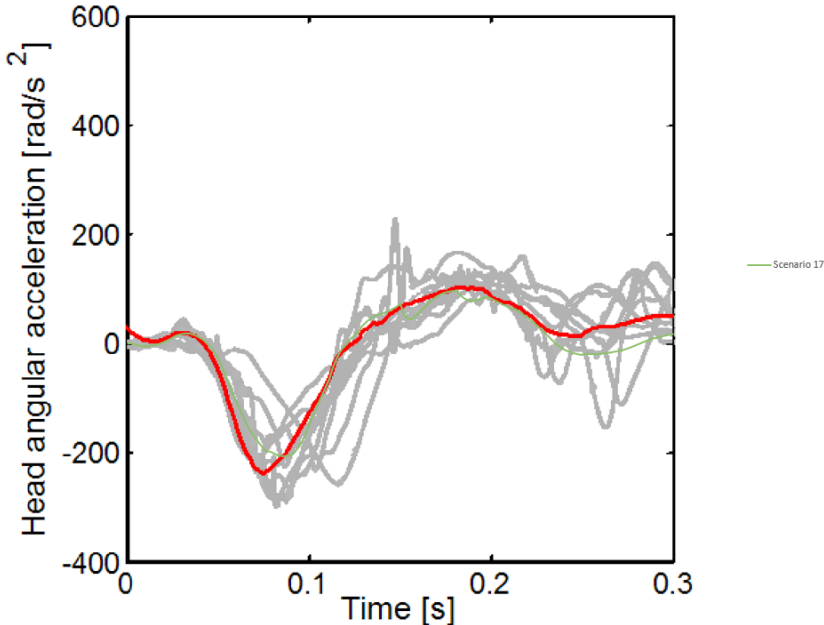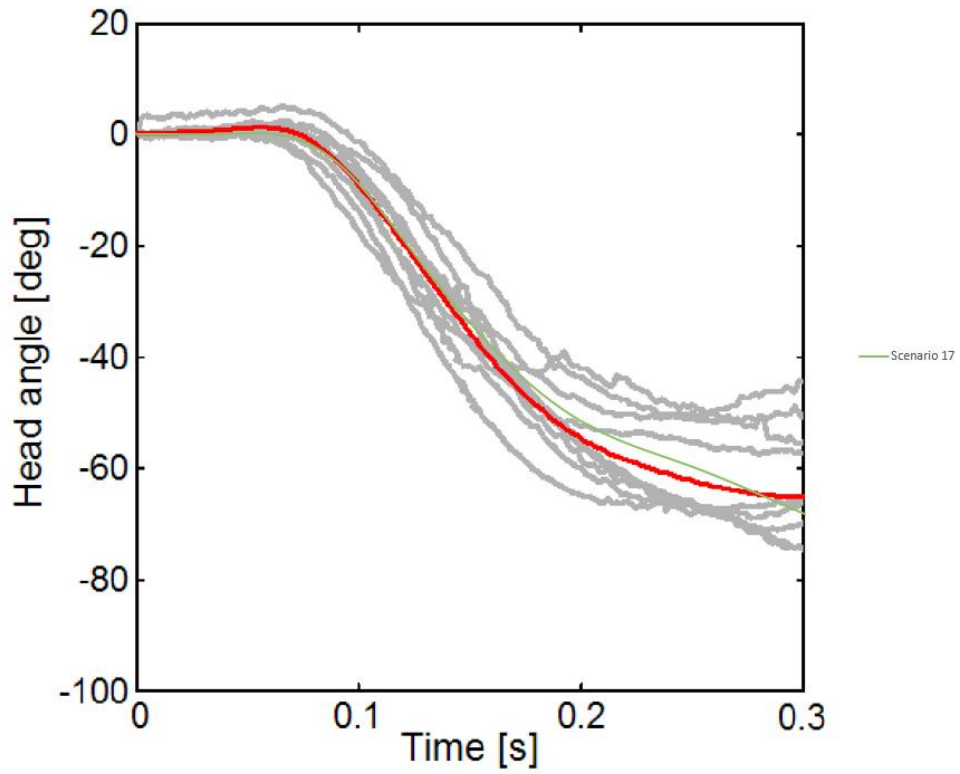between scenario 17 and volunteer experiment data in Himmetoglu [23].

After the improvement of the head and neck model, at this point, if a rear impact test dummy is to be produced using this thesis, the data in this thesis can be used because the physical production of the head and neck model was also taken into consideration when developing the head and neck model and implementing the muscles into the model.

Finally, the thesis study has successfully achieved all its objectives.

REFERENCES

[1] D. C. Viano, Role of the Seat in Rear Crash Safety, Society of Automotive Engineers, Warrendale, **2003**.

[2] R. W. Evans, Some observations on whiplash injuries, Neurol. Clin. 10 **(1992) 4.**

[3] J. L. Dieleman, R. Baral, M. Birger, A. L. Bui, A. Bulchis, A. Chapin, H. Hamavid, C. Horst, E. K. Johnson, J. Joseph, R. Lavado, L. Lomsadze, Alex Reynolds, E. Squires, M. Campbell, B. DeCenso, D. Dicker, A. D. Flaxman, R. Gabert, T. Highfill, M. Naghavi, N. Nightingale, T. Templin, M. I. Tobias, T. Vos, C. J. L. Murray, US spending on personal health care and public health, 1996-2013, JAMA - Journal of the American Medical Association, 316 **(2016)**.

[4] Cervical Spine Anatomy, https://www.spine-health.com/conditions/spine-anatomy/cervical-spine-anatomy, (Last accessed on, 15/01/2023).

[5] M. Darok, E.P. Leizinger, A. Eichberger, and H. Steffan. Neck injury criterion validation using humand subjects and dummies. In N. Yoganandan and F.A. Pintar, editors, Frontiers in Whiplash Trauma, Clinical and Biomechanical, IOS Press, Amsterdam, 409–434, **2000**.

[6] BioRID-II, https://www.humaneticsgroup.com/products/anthropomorphic-test-devices/rear-impact/biorid-ii, (Last accessed on, 05/12/2022).

[7] J. Davidsson, P. Lövsund, K. Ono, M. Y. Svensson, And S. Inami, A Comparison between Volunteer, BioRID P3 and Hybrid III performance in Rear Impacts, Ircobi Conference, Sitges, Spain, **1999**, p. 165-178.

[8] S. Himmetoglu, M. Acar, A. J. Taylor, and K. Bouazza-Marouf, A multi-body head-and-neck model for simulation of rear impact in cars, IMechE Part D Journal of Automobile Engineering, 221 **(2007)** 5,

[9] J. Östh, M. Mendoza-Vazquez, F. Sato, M. Y. Svensson, A. Linder, and K. Brolin, A female head–neck model for rear impact simulations, J Biomech, 51 **(2017)**.

[10] L. Jakobsson, H. Norin, C. Jernstroem, S-E. Svensson, P. Johnsen, I. I. Isaksson-Hellman and M. Y. Svensson, Analysis of Different Head and Neck Responses in Rear-End Car Collisions using a New Humanlike Mathematical Model," IRCOBI Conference, Lyon, France, **1994**, p. 109–125**.**

[11] M. de Jager, Mathematical Head-Neck Models for Acceleration Impacts, PhD Thesis, Eindhoven University of Technology, Eindhoven, **1996**.

[12] A. van den Kroonenberg, J. Thunnissen, and J. Wismans, A Human Model for Low-Severity Rear-Impacts, IRCOBI Conference, Hannover, Germany, **1997**, p. 117–132.

[13] K. Yamazaki, K. Ono, and K. Kaneoka, A simulation analysis of human cervical spine motion during low speed rear-end impacts, SAE Technical Papers, **(2000)**.

[14] A. Linder, A new mathematical neck model for a low-velocity rear-end impact dummy: Evaluation of components influencing head kinematics, Accid Anal Prev, 32 **(2000)** 2.

[15] M. J. van der Horst, "Human Head Neck Response in Frontal, Lateral and Rear End Impact Loading - modelling and validation, PhD Thesis, Eindhoven University of Technology, Eindhoven, Holland, **2002**.

[16] D. W. van Lopik, A computational model of the human head and cervical spine for dynamic impact simulation, PhD Thesis, Loughborough University, Loughborough, UK, **2004**.

[17] J. Borst, P. A. Forbes, R. Happee, and D. Veeger, "Muscle parameters for musculoskeletal modelling of the human neck, Clinical Biomechanics, 26 **(2011)** 4.

[18] D. C. Viano, W. N. HARDY, and A. I. KING, Response of the Head, Neck and Torso to Pendulum Impacts on the Back, Journal of Crash Prevention and Injury Control, 2 **(2001)** 4.

[19] Energy as a tool for mechanics problem solving, http://hyperphysics.phy-astr.gsu.edu/hbase/flobj.html, (Last accessed on, 16/12/2022).

[20] Lagrangian Mechanics for Dummies: An Intuitive Introduction, https://profoundphysics.com/lagrangian-mechanics-for-beginners/, (Last accessed on, 20/12/2022).

[21] Chapter 6 The Lagrangian Method, https://scholar.harvard.edu/files/david-morin/files/cmchap6.pdf, (Last accessed on, 21/12/2022).

[22] M. Yazji, M. Raison, C-É. Aubin, H. Labelle, C. Detrembleur, P. Mahaudens & M. Mousny, Are the mediolateral joint forces in the lower limbs different between scoliotic and healthy subjects during gait?, Scoliosis, 10 **(2015)** S3.

[23]   S. Himmetoğlu, Integration of muscle tone into a multi-body head-and-neck model for crash applications, 26th International Scientific Conference Transport Means 2022, Kaunas, Lithuania, **2022**, p.27-32.

[24]   Splenius cervicis muscle, https://en.wikipedia.org/wiki/Splenius_cervicis_muscle, (Last accessed on, 08/01/2023).

[25]   Sternohyoid   Muscle,   https://en.wikipedia.org/wiki/Sternohyoid_muscle,   (Last accessed on, 08/01/2023).

[26]   Sternocleidomastoid Muscle,
https://en.wikipedia.org/wiki/Sternocleidomastoid_muscle, (Last accessed on, 08/01/2023).